NASA CR-66841-1
October 1969

EXPERIMENTAL INVESTIGATION OF THE INTERACTION OF A PLANE, OBLIQUE, INCIDENT-REFLECTING SHOCK WAVE WITH A TURBULENT BOUNDARY LAYER ON A COOLED SURFACE

VOLUME 1: TEST DESCRIPTION AND DATA SUMMARY

GENERAL DYNAMICS
Fort Worth Division

Prepared under Contract No. NAS1-6588

for

NATIONAL AERONAUTICS AND SPACE ADMINISTRATION

NASA CR-66841-1
October 1969

EXPERIMENTAL INVESTIGATION OF THE INTERACTION OF A PLANE, OBLIQUE, INCIDENT-REFLECTING SHOCK WAVE WITH A TURBULENT BOUNDARY LAYER ON A COOLED SURFACE

VOLUME 1: TEST DESCRIPTION AND DATA SUMMARY

By

Richard F. Kilburg and Donald R. Kotansky

Prepared under Contract No. NAS1-6588 by
Fort Worth Division of General Dynamics
Fort Worth, Texas

for

NATIONAL AERONAUTICS AND SPACE ADMINISTRATION

Page intentionally left blank

FOREWORD

This document is Volume 1 of three volumes reporting an experimental investigation of the two-dimensional interaction of an incident-reflecting shock wave with a turbulent boundary layer on a cooled surface.

The three volumes are:

Volume 1: Test Description and Data Summary (CR-66841-1)

Volume 2: Basic Plotted Data (CR-66841-2)

Volume 3: Tabulated Data (CR-66841-3)

This volume describes the test apparatus and procedure used during testing, instrumentation calibration, and data reduction. Nondimensional data descriptive of the flow in the interaction region are presented in summary form. These data include wall pressure distributions, shock-wave locations, and nondimensional boundary-layer velocity and stagnation temperature profiles.

Volume 2 contains the plotted data obtained during conduct of the test program and the nondimensional data that does not logically fit the data summary of Volume 1.

Volume 3 contains all the primary tabulated data generated during testing and the nondimensional data subsequently calculated.

Page intentionally left blank

TABLE OF CONTENTS

	Page
FOREWORD	iii
LIST OF TABLES AND FIGURES	vi
NOMENCLATURE	vii
SUMMARY	1
INTRODUCTION	1
MODEL AND TEST INFORMATION	3
Model Description	3
Facility Description	6
Test Conditions	6
Sequence of Testing Operations	7
Data Processing	9
RESULTS	9
Data Presentation	9
Data Accuracy	11
APPENDIX A: INSTRUMENTATION CALIBRATION	12
APPENDIX B: DATA REDUCTION	20
REFERENCES	25

LIST OF TABLES AND FIGURES

Table		Page
I	Shock-Generator Wedge Position and Theoretical Wave-Pattern Data	26
II	Test Conditions and Manual Input for Final Data Reduction	27

Figure		
1	2-D Boundary Layer Model General Arrangement	28
2	Model Installed in Tunnel	29
3	Pressure Orifice and Thermocouple Locations	30
4	Plate-Instrumentation Details	31
5	Total Pressure/Total Temperature Probe	32
6-20	Plate Static Pressure and Shock-Wave Pattern in the Interaction Region	33
21-47	Non-Dimensional Velocity and Temperature Profiles	48

NOMENCLATURE

C_p	Pressure coefficient
M	Mach number
P	Absolute pressure
q	Dynamic pressure
RE/l	Unit Reynolds number (per foot)
T	Absolute temperature
XP(n)	Probe position, where n designates position code
δ	Boundary layer thickness
Y	Vertical distance referenced to plate surface
V	Velocity
W_k^m	Wedge location and incidence-angle code as shown in Table I
X_I	Horizontal distance from plate leading edge to shock interaction with plate surface
X	Horizontal distance from plate leading edge to wedge leading edge
Z	Vertical distance from plate surface to wedge leading edge
C	Horizontal distance from shock intersection with plate surface to expansion-wave intersection with plate surface
ρ	Mass density
θ	Wedge shock wave angle referenced to freestream flow direction
μ	Absolute Viscosity

Subscripts and Superscripts

e	Boundary layer edge
I	Incident
k	Geometric wedge incidence-angle code
m	Wedge position code
R	Reflected
t	Total
w	Wall
o	Freestream
'(prime)	Data measured by the boundary layer probe

EXPERIMENTAL INVESTIGATION OF THE INTERACTION OF A PLANE, OBLIQUE, INCIDENT-REFLECTING SHOCK WAVE WITH A TURBULENT BOUNDARY LAYER ON A COOLED SURFACE

By

Richard F. Kilburg and Donald R. Kotansky
Fort Worth Division of General Dynamics

SUMMARY

A test was conducted to obtain measurements of the boundary layer total temperature and velocity profiles in the region of the interaction of a two-dimensional, incident, reflecting, oblique shock wave with the turbulent boundary layer on a cryogenically cooled flat plate. Data were taken at Mach numbers of 2.0, 3.2, and 4.2 at unit Reynolds numbers of from 6.4 to 20.2 million per foot. The ratio of wall surface to stagnation temperature was 0.3 for most data. Adiabatic data were taken at a Mach number of 3.2. Incident shock strength was varied by testing with shock generator wedge angles of 6° and 8°. Data presented include the plate surface-pressure distribution, incident and reflected shock locations, and the boundary layer velocity and stagnation temperature profiles.

INTRODUCTION

The performance of supersonic and hypersonic airbreathing propulsion systems is dependent to a large extent on the design of the air induction system. As the flight Mach number increases, the aerodynamic design and the resulting performance of the inlet become primarily a function of the behavior of boundary layers in adverse pressure gradients due to oblique and normal shock interactions and continuous compression fields. Inlet system designs normally employ the use of flow diverters and bleeds to control the growth of the boundary layer on wetted surfaces. These methods simply remove the boundary layer, or the low-energy portion of the boundary layer, such that the inlet operates in a flow field less influenced by viscous flow effects. Improvements

in inlet performance achieved through the use of these methods have more than offset the drag and weight penalties involved in ducting the undesired mass flow overboard.

As vehicle speeds increase, the exposed inlet surfaces must be cooled in order to maintain the structural temperatures within design limits. The heat transfer from the boundary layer to the cooled walls results in a reduction of the total temperature of the boundary layer fluid and has a stabilizing effect on the boundary layer. Although under these conditions the bleed flow may be relatively cool, the bleed ducts may also require cooling. The additional weight and complexity of a bleed system, combined with inlet surface cooling, reduces the desirability of bleed as a means of boundary layer control with cooling.

It has been found experimentally (Reference 1) that cooling the boundary layer in an adverse pressure gradient yields a considerable improvement in boundary layer characteristics. The cooled boundary layer (1) negotiates higher adverse pressure gradients without separation, and (2) is thinner and contains a more desirable Mach number distribution than the uncooled boundary layer. Thus, cooling the boundary layer is, in itself, a means of control. Calculation of hypersonic inlet performance by methods which properly account for these changes in boundary layer characteristics with wall cooling (for example, the method of Reference 2) would indicate that wall cooling will improve the total pressure recovery.

The above emphasizes the importance of boundary layer behavior in high Mach number inlets. The detailed characteristics of the turbulent boundary layer under representative adverse conditions must be known in order to properly design and assess the performance of current and future high-speed air induction systems. Toward this end, the experimental research program reported here was designed to provide data for a compressible turbulent boundary layer on a flat plate with an oblique shock wave interaction, where the history of the boundary layer preceding the region of interaction is controlled and well defined. Data were to be acquired at stations upstream of the interaction, in the immediate region of interaction, and well downstream of the interaction. Implicit in the program plan was the independence of the test variables: Mach number, Reynolds number, shock-wave strength, and heat transfer as described by the ratio of wall surface to stagnation temperature.

MODEL AND TEST DESCRIPTION

Model Description

The components used in accomplishing this research program are: (1) the model with installed instrumentation, (2) a combination boundary layer probe and traverse mechanism, and (3) a coolant supply system with monitoring instruments and recording devices.

The model is a flat plate, bounded by side walls and supported from the wind tunnel ceiling by four legs. The plate surface is aligned with the flow. The side walls provide shielding of the plate from edge effects and also serve to support the shock-generator wedge and boundary layer probe traverse mechanism. Windows are installed in the sidewalls for schlieren and shadowgraph photography of the boundary layer and the shock wave. A general arrangement drawing of the model is shown in Figure 1. Photographs of the installation are shown in Figure 2. The configuration of the model is such that it operates essentially as a two-dimensional inlet. Therefore, the shock generator is remotely actuated such that its incidence angle is low during the starting process. After starting, the wedge is rotated to a preselected incidence angle. Actuation is accomplished using a double-acting hydraulic actuator. The wedge support is manually positioned prior to each run so that the shock wave generated impinges on the plate at approximately the same longitudinal location for all test conditions.

The flat plate is a built-up assembly of four major parts: a lower portion of nickel-plated copper, a core of stainless steel, and inlet and outlet plenums near the plate centerline and outside edges, respectively. Attachment of the stainless-steel upper plate, ported for inlet distribution and recovery of coolant, forms a flat pressure vessel. Coolant passages are 0.015 inch high and span the plate transversely from 3.68 inches behind the leading edge to the trailing edge. The passage height is established by narrow ridges on the steel core. The coolant flows laterally from the center to both outboard edges and then into the outlet plenum. A sharpened wedge-shaped stainless-steel leading edge completes the assembly. A distributor and inlet header for each side of the plate completes the inlet plumbing.

A nominal ratio of wall temperature to stagnation temperature of 0.3 was achieved by pumping liquid nitrogen directly through the plate-surface cooling passages. Four thermocouples are installed in the inlet and outlet connections to the model. These thermocouples, with appropriate reference junctions, are connected to a strip-chart recorder through a switching arrangement so that inlet and outlet coolant temperature may be monitored. Thus, an adequate amount of coolant flow is assured.

The lower surface of the flat plate assembly is ground flat within 0.005 inch over the 12- by 38-inch surface. A deflection analysis and inspection of a test specimen under maximum internal static pressure indicated that the waviness increase due to internal pressure during testing would not be more than 0.001 inch in a 3-inch length. This is a result of the close spacing of the plate supports provided by the design.

Ice formation on the side wall windows presented a testing difficulty. This was, to some extent, prevented by keeping the side wall temperature well above the plate temperature. A passageway was provided between the cooled plate assembly and the side walls. The side walls were insulated from the plate in this region by a 0.060- to 0.080-inch-thick teflon strip. Hot (650 to 700^{o}R), dry nitrogen flow through this passageway provided the thermal isolation needed to keep ice formation on the walls to an acceptable level.

The plate instrumentation consists of 60 static pressure orifices connected pneumatically to transducers located on top of the tunnel test section and 53 chromel-alumel thermocouple assemblies with reference junctions in the inlet coolant line at the top of the test section. A single chromel-alumel thermocouple located among the reference junctions was used with a reference thermocouple in a liquid nitrogen bath to obtain the reference junction temperature so that incremental plate temperatures could be correlated to an absolute temperature reference.

Fifty-six static pressure taps on the plate centerline are numbered serially from 1 to 56, starting from the plate forward end. Four static pressure taps, located 2.925 inches off centerline, laterally, are numbered 57 through 60. The index 61 is reserved for the static pressure read by the traversing probe. The 53 thermocouples are numbered serially from the plate forward end. The plate instrumentation locations are shown in Figure 3. Thermocouple and static tap installation details are shown in Figure 4.

Each pressure tube is connected to a helium gas supply manifold as well as to the transducer. The helium gas is allowed to flow through the pressure tube to the plate orifice during the period between runs to prevent formation of ice in the tubing due to moisture condensation. During the run, these connections to the helium manifold are closed with a control valve so that each pressure tube and transducer is isolated from all others. With the control valve in the open position, helium gas is continuously discharged through the pressure orifice and provides a helium blanket on the plate surface. Helium is used for this purpose primarily because the plate surface is inverted (Figures 1 and 2); the low-density helium then forms a blanket over the instrumented surface. This system reduces the ice formation on the plate and effectively provides anti-icing for the static pressure tubes.

Measurements of stagnation pressure, stagnation temperature, and static pressure in the boundary layer are made simultaneously with a multi-purpose probe. The stagnation pressure and total temperature probes are mounted adjacent to each other as shown in Figure 5. The static pressure probe is displaced laterally a distance sufficient to assure no interference with the stagnation probes.

The probe is supported on a vertical traverse mechanism supported by a blade spanning the side walls at the aft end of the model. The vertical traverse mechanism drives the probe at a selected constant velocity through a maximum distance of 1.0 inch. A probe velocity of 0.06 inch per second was selected because it permits completion of all data acquisition in the available run time. The minimum distance of closure with the plate surface is set to 0.015 inch to prevent damage to the probe. The longitudinal position of the probe is manually set prior to each run.

The total pressure and static pressure tubes are connected pneumatically to differential transducers mounted in the probe support. The total temperature thermocouple reference is in the liquid nitrogen bath at the top of the test section.

The total temperature probe was especially developed to optimize the response characteristics. The development is described in Reference 3. Probe response and recovery factor data are presented in Appendix A.

Facility Description

The General Dynamics High Speed Wind Tunnel, located at San Diego, California, is a 4- by 4-foot pressure-driven intermittent wind tunnel which operates over a Mach number range from approximately 0.5 to 5.0. The duration of stable flow in the test section is from 30 to 40 seconds, depending upon test Mach number.

The experimental program was run at Mach numbers of 2.0, 3.2, and 4.2, with unit Reynolds numbers ranging from 6 to 20.5 x 10^6 per foot. Test section temperature was maintained constant (within $\pm$ 5°R) during a run by a storage heater. Storage heater temperature varied from 530°R to 575°R, depending on the frequency of tunnel operation and ambient conditions.

Data acquisition, using installed high-speed data handling and processing equipment, is limited to 20 channels of high-level and 120 channels of low-level signals. Low-level signals come from sources such as transducers, strain-gage bridges, and related balancing and conditioning circuitry. Data channels are serially selected, amplified, digitized, and transferred to storage within an IBM 1800 Computer System through high-speed electronic scanning equipment. The scan rate and the number of channels per scan are normally pre-set but may be altered during a run.

Test Conditions

Test variables were the freestream Mach number, M_o; unit Reynolds number, RE/1; ratio of plate temperature to freestream stagnation temperature, T_w/T_{t_o}; wedge shock-generator configuration, W_k^m, and the boundary layer survey station, XP(n), where n = 0, 1, or 2. The wedge configuration is denoted by its longitudinal location position code, m, and the incidence angle code in the run position, k. The wedge angle is determined by using a bubble-type clinometer with vernier markings to 1 minute of arc. The angle is set by adjusting the stop mechanism, with the hydraulic actuator holding the wedge in the run position. The wedge incidence angle is then verified after at least one cycle from the start to the run position.

The boundary layer survey stations, XP(n) are defined as follows:

Station 0, XP(0): A station upstream of the shock interaction region selected so that the characteristics of the boundary layer approaching the wave are defined.

Station 1, XP(1): A station in the region of interaction selected at the point of maximum plate surface static pressure or where the reflected shock wave leaves the boundary layer, whichever is farther downstream.

Station 2, XP(2): A station well downstream of the interaction based on predicted wave patterns, where the boundary layer will be unaffected by the intersecting expansion fan from the aft end of the wedge.

The boundary layer probe is positioned longitudinally to the selected survey station before each run. Measurements of the position location are made with a vernier caliper.

Data were first acquired with the probe at Station 2 for each combination of Mach number, Reynolds number, and wedge angle. Selection of the most aft probe position, XP(2), was based on the predicted intersections of the oblique wave and the expansion fan with the plate surface (Table I). Plate station 36.00 was selected for Mach numbers of 2.0 and 3.2, while station 33.00 was selected for a Mach number of 4.2.

The plate static pressure distribution and the schlieren and shadowgraph photographs of shock location provided sufficient data from which to select XP(0) and XP(1). For most runs, the point of maximum plate static pressure proved to be the selected XP(1) location.

Sequence of Testing Operations

When model cooling is required, a typical run sequence is as follows:

1. Model shrouds, a probe protective cover, and excessive ice accumulations are removed just prior to closing the tunnel.
2. The warm nitrogen anti-icing flow is stopped and the plate temperature brought under control by allowing some liquid

nitrogen through the plate while monitoring inlet and outlet temperature.

3. With the data system in the manual mode, air-off data from all signal sources are recorded.
4. Data system controls are switched to run positions with interface connections to the computer system for data storage.
5. The control valve is moved to the run position, shutting off the helium flow through the static pressure tubing.
6. The maximum coolant flow rate is established anticipating wind tunnel starting within 10 seconds.
7. The wind tunnel is started. Stable flow in the test section is normally indicated within 5 seconds.
8. The shock generator is moved to the run position while wedge action is monitored on closed circuit television.
9. Three consecutive scans of all data channels are made.
10. The data system is changed to a continuous sampling mode. Only those channels essential to the boundary layer survey are sampled.
11. The probe drive is actuated and the probe moved toward the plate surface from a preselected position away from the plate. The data system is coupled with the probe drive controls so that data are taken only while the probe is in motion.
12. Schlieren and shadowgraph photos are taken just prior to the completion of the probe traverse.
13. Data system controls are switched back to manual and three consecutive scans of all data channels are again made.
14. The probe is moved away from the plate surface and the tunnel flow terminated.
15. Coolant flow through the plate is reduced to the minimum amount that will maintain temperature control.
16. The wedge is moved to the start position and final air-off data are acquired.
17. The control valve is moved to the off position, re-establishing the helium flow through the static pressure tubes, and hot nitrogen anti-icing is begun before the test section is opened.

Although actual run time is only 30 to 40 seconds in duration, 3 to 5 minutes are required for the above sequence of operations to complete a run. Steps 5, 15, and 17 are omitted during test sequences which do not require model cooling.

Data Processing

Measured plate static pressures are reduced to pressure coefficients, Cp, and the plate temperature data are reduced to ratios of wall surface to freestream total temperature, T_w/T_{t_o}. These computations and the development of the negatives of the shock wave photographs constitute the primary data reduction requirements for each run.

Boundary layer data measured by the combination probe are reduced to a static pressure coefficient $C_{P_{61}}$; probe total temperature ratio, T_t'/T_{t_o}; and the probe stagnation pressure ratio, P_{t_1}/P_{t_o}. Local Mach number is computed from probe static pressure and probe stagnation pressure. The Rayleigh pitot formula is used for supersonic Mach numbers ($P_{61}/P_t' \leq .5283$) and isentropic relations for subsonic Mach numbers ($P_{61}/P_t' > .5283$). These boundary layer data are machine-plotted versus probe position, Y. All test variables are tabulated. These plots and tables constitute the basic test data.

Boundary layer thickness, δ, and edge conditions are determined from analysis of the basic data plots. The criterion for selection of edge conditions is that the basic variable becomes invariant with increasing distance from the plate surface. When M_e is determined, the boundary layer thickness is defined as that Y value where $M = 0.99\ M_e$. Boundary layer edge conditions are tabulated and transmitted to the wind tunnel for final data reduction. These data, P_e, M_e, T'_{t_o}, and δ, are shown in Table II. Final data reduction produces the non-dimensional variables V/V_e, $T_t'/T_t'_e$, and Y/δ, which are the final plotted data. A complete list of data reduction equations is given in Appendix B.

RESULTS

Data Presentation

Plate surface data and shock-wave patterns in the region of interaction with the boundary layer are presented in Figures 6 through 20. The data presented are:

1. The measured plate static pressure distribution presented as pressure coefficients compared with the pressure increase through the double shock-wave pattern computed

from theory.

2. The locations of the incident and reflected shock waves as measured from shadowgraphs compared with the wave locations as determined from theory.
3. The Mach number, M_2, as measured and as computed from theory at survey station 2 (downstream of the interaction).
4. The boundary layer thickness from Table II.
5. The shadowgraph of the interaction region.

The tables and charts of Reference 4 were used to compute the theoretical wave positions and Mach numbers.

In many of the shadowgraphs, data quality was degraded because of ice accumulations on the window. This occurred in spite of preventive design efforts and preventive measures taken during the test. An extraneous, rather weak wave sometimes appears running diagonally across the picture. This was determined to be a reflected wave originating at the plate leading edge.

The static pressure coefficients obtained at orifices located off the centerline are shown. They are not found to be in good agreement with centerline data, nor does the probe static pressure data agree exactly with centerline data. It is to be noted, however, that no sizeable pressure gradient is measured preceding the interaction. The reason for this lack of agreement is not known. The accuracy of the centerline data may therefore be subject to question due to the indicated lack of two-dimensional flow off centerline. The plate surface temperature variation from an isothermal condition was insignificant except for a short distance downstream of the uncooled leading edge.

Boundary layer velocity and temperature profiles, normalized to boundary layer edge conditions, are presented in Figures 21 through 47. Data are shown preceding the interaction (Survey Station 0), in the region of interaction (Survey Station 1), and downstream of the interaction (Survey Station 2). Complete sets of boundary layer data are presented only for those runs where plate summary data are shown. An index to these data and the boundary layer edge conditions is presented in Table II.

Data Accuracy

The accuracy with which quantities were measured have been estimated on the basis of calibrations, examination of incremental changes in initial and final air-off data, and the types of instruments used for these measurements. The error in any single data point cannot be quoted. The probable error and the possible error in measured quantities are as follows:

Measurement	Probable Error	Possible Error
P_t' (psia)	$\pm$ 0.75	$\pm$ 1.5
P_{61} (psia)	$\pm$ 0.15	$\pm$ 1.0 Note (1)
P_{1-60} (psia)	$\pm$ 0.15	$\pm$ 0.15 Note (2)
T_t''' (^oR)	$\pm$ 2	--
T' (^oR)	$\pm$ 5	$\pm$ 5 Note (3)
T_{1-53} (^oR)	$\pm$ 4	$\pm$ 8
Y (inches)	$\pm$ 0.005	$\pm$ 0.005 Note (4)

Notes: (1) This large possible error is based on a significant zero shift with plate cooling. A two-point calibration at the low temperature indicated no change in sensitivity. The transducer was thermally isolated, but since thermal variation could not be measured during a run this error must be assumed possible.

(2) Except for the cases where the pressure orifices were plugged with ice while cooling, the probable error will not be exceeded.

(3) Temperature measurement errors assume that absolute calibration data are valid and that probe temperature corrections for lag and recovery factor will yield results as predicted in Reference 2.

(4) No increase above the probable error is likely, since this parameter was continually being calibrated during normal conduct of test procedures.

APPENDIX A

INSTRUMENTATION CALIBRATION

Thermocouples and Thermocouple Assemblies

Thermocouple assemblies were manufactured according to Fort Worth Division specifications for use in plate surface instrumentation. All assemblies used the same mill run of chromel and alumel wires and should exhibit identical characteristics.

Three thermocouple assemblies were calibrated by the Fort Worth Division Standards Laboratories for use during preliminary design studies and in the model assembly. These assemblies yielded data accurate to within + 4°R of the published standards for chromel-alumel (K type) thermocouples over a temperature range from 140° to 530°R.

One thermocouple assembly was selected at random from the group installed in the plate temperature reference junction to be the junction-absolute-temperature measuring instrument. A sample of the 0.004-inch-diameter K-type thermocouple, prepared for use in probe manufacture and mounted on a 0.005-inch-thick fiberglass base, was also selected for absolute temperature calibration. These two couples were calibrated against reference junctions prepared and furnished by the High Speed Wind Tunnel.

Calibration data given in Table AI show that agreement with standard data is excellent from 140° to 450°R, but, from 450°R to the maximum calibration temperature of 532°R, these couples have outputs just under 1% higher than published standards. These calibration data were input to an IBM third-order curve-fit procedure and the resulting constants were used in all data reduction.

Boundary Layer Probe Calibrations

Two probes were manufactured to support this research program. Both probes were calibrated at Mach 4.02, and probe number 2 was checked at Mach 2.86. These calibrations were made in the Fort Worth Division 6- by 6-inch free jet facility.

The method of calibration and the details of probe development are contained in Reference 3 along with a detailed discussion of the theory leading to a correction for thermal lag and the development of the equations.

Briefly, a thermocouple in a moving fluid may be considered as a simple first-order system with an absence of large radiation and conduction losses. Assuming a constant velocity of probe motion through a thermal gradient with the fluid flow results in an expression for the heat transfer energy balance expressed as

$$h A_e (T_t'' - T_t''') = C_e m_e \dot{Y} \frac{d T_t'''}{d Y} \qquad (1A)$$

where

h is the convective heat transfer coefficient
A_e is the thermocouple heat transfer area
C_e is the specific heat of the thermocouple materials
m_e is the mass of the thermocouple element
T_t'' is the equilibrium temperature without thermal lag
T_t''' is the indicated transient measured temperature
$\dot{Y}$ is the probe velocity dY/dt.

It is reasonable to expect that h will not be constant since the probe is exposed to continuously changing external flow characteristics. Differentiation of equation (1A) with respect to Y yields

$$\frac{d T_t''}{d Y} = \left[1 - \frac{C_e m_e}{A_e h^2} \frac{dh}{dY}\right] \frac{d T_t'''}{dY} + \frac{C_e m_e}{A_e h} \frac{d^2 T_t'''}{dY^2} \qquad (2A)$$

or

$$\frac{d T_t''}{dY} = A \frac{d T_t'''}{dY} + B \frac{d^2 T_t'''}{dY^2} \qquad (3A)$$

where A and B are variable coefficients.

If part of the data within the boundary layer is linear or can be linearized, a comparison of steady measured data with

transient measured data yields a value for the coefficient A, since

$$A = \frac{d\ T_t''/dY}{d\ T_t'''/dY} \qquad \text{when} \qquad \frac{d^2 T_t'''}{dY^2} = 0 \tag{4A}$$

The coefficient B can be determined if in the data either of the first derivatives becomes zero, for, when

$$\frac{d\ T_t''}{dY} = 0, \text{ then } B = -\ \frac{A\ d\ T_t''/dY}{\frac{d^2\ T_t''}{dY^2}} \tag{5A}$$

or, when $\frac{d\ T_t'''}{dY} = 0$, then $B = \frac{d\ T_t''/dY}{d^2 T_t'''/dY^2}$ (6A)

and if both first derivatives are zero at the same Y position, B equals zero.

Attempts to determine values for the coefficient B from the experimental data produced inconclusive results. This was due to difficulties in establishing a numerical value for the second derivative and in determining the Y position when one of the first derivatives is zero. The effect of the second-derivative correction is sufficiently small so that it can be ignored.

The coefficient A is presented as a function of stream unit Reynolds number in Figure A1. Since calibration data were taken only to RE/1 = 6 x 10^6 per foot, the extrapolation of these data into the test range is shown.

The probe recovery factor, R, was determined from data taken outside the boundary layer. The recovery factor by definition is

$$R = (T_t'' - T)/(T_t' - T) \tag{7A}$$

where T_t'' is the indicated steady state local temperature
T_t' is the local total temperature
T is the static temperature

During calibration, T_t'' is the measured probe temperature outside the boundary layer, T_t' is the stagnation temperature measured in the stilling chamber (V = 0), and T, the static temperature, is computed from the Mach number.

Probe recovery factor as a function of unit Reynolds number and the extrapolation of calibration data into the test range are shown in Figure A2.

The data reduction methods discussed in Appendix B were used to obtain the corrected temperature data shown in Figure A3. Good agreement is shown for the cases of steady measured data corrected for recovery factor and transient measured data corrected for lag and recovery factor.

TABLE AI

THERMOCOUPLE CALIBRATIONS

Temperature ^{o}R	Thermocouple Output (mv)		
	Probe T/C	T/C Assembly	Standards
140	0.0	0.0	0.0
150	0.10	0.09	0.09
175	0.33	--	0.32
183	0.40	--	0.39
201	0.60	--	0.60
224	--	0.90	0.89
230	0.98	--	0.98
240	--	1.12	1.12
244	1.15	--	1.15
272	1.60	--	1.60
291	--	1.90	1.90
300	2.05	--	2.05
325	--	2.45	2.41
329	2.50	--	2.49
360	3.00	--	3.00
365	--	3.10	3.10
402	--	3.87	3.85
436	--	4.55	4.54
450	4.83	4.87	4.83
482	5.55	--	5.50
530	6.60	--	6.56
532	--	6.65	6.60

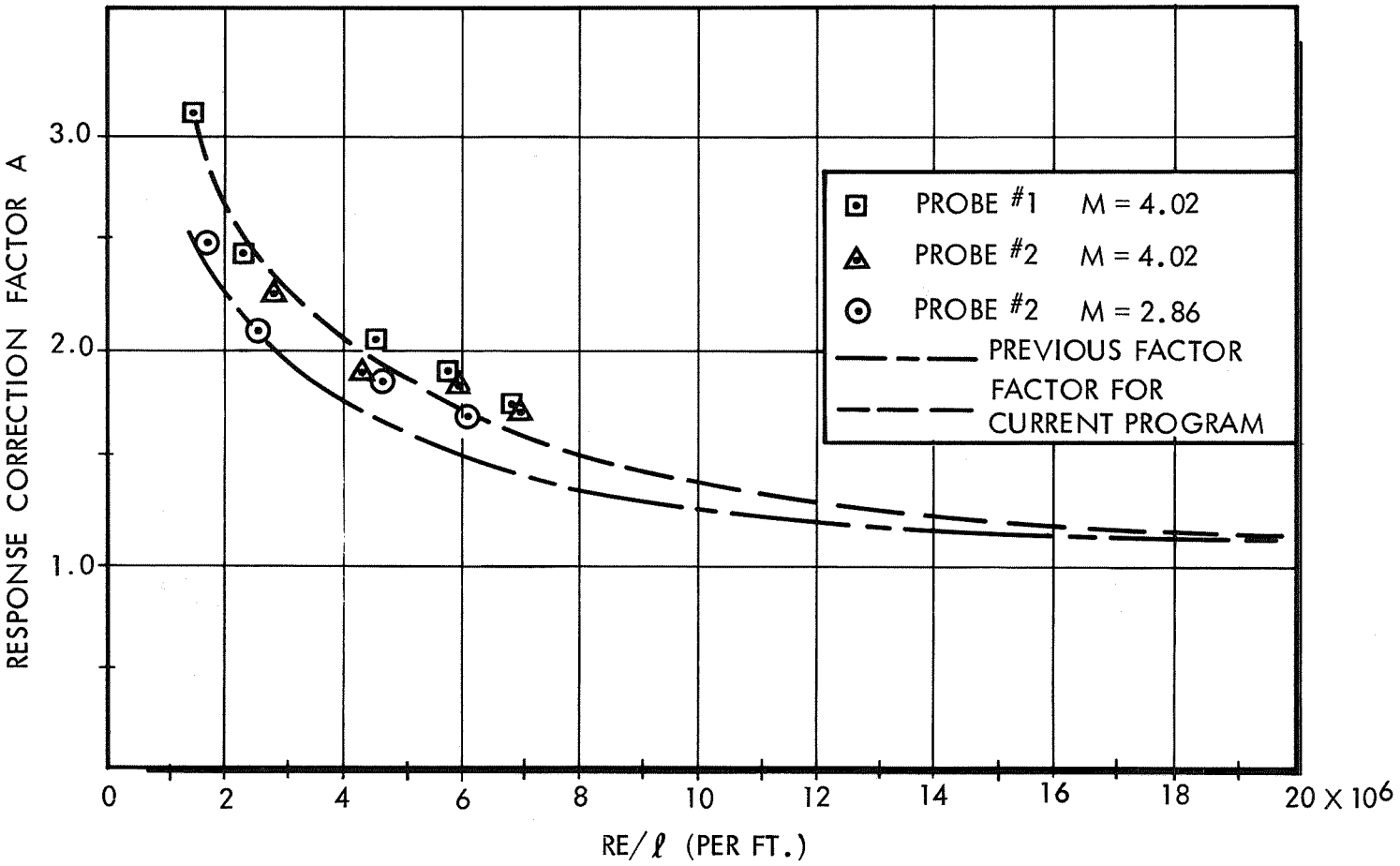

Figure A1 EMPIRICAL RESPONSE CORRECTION FACTOR

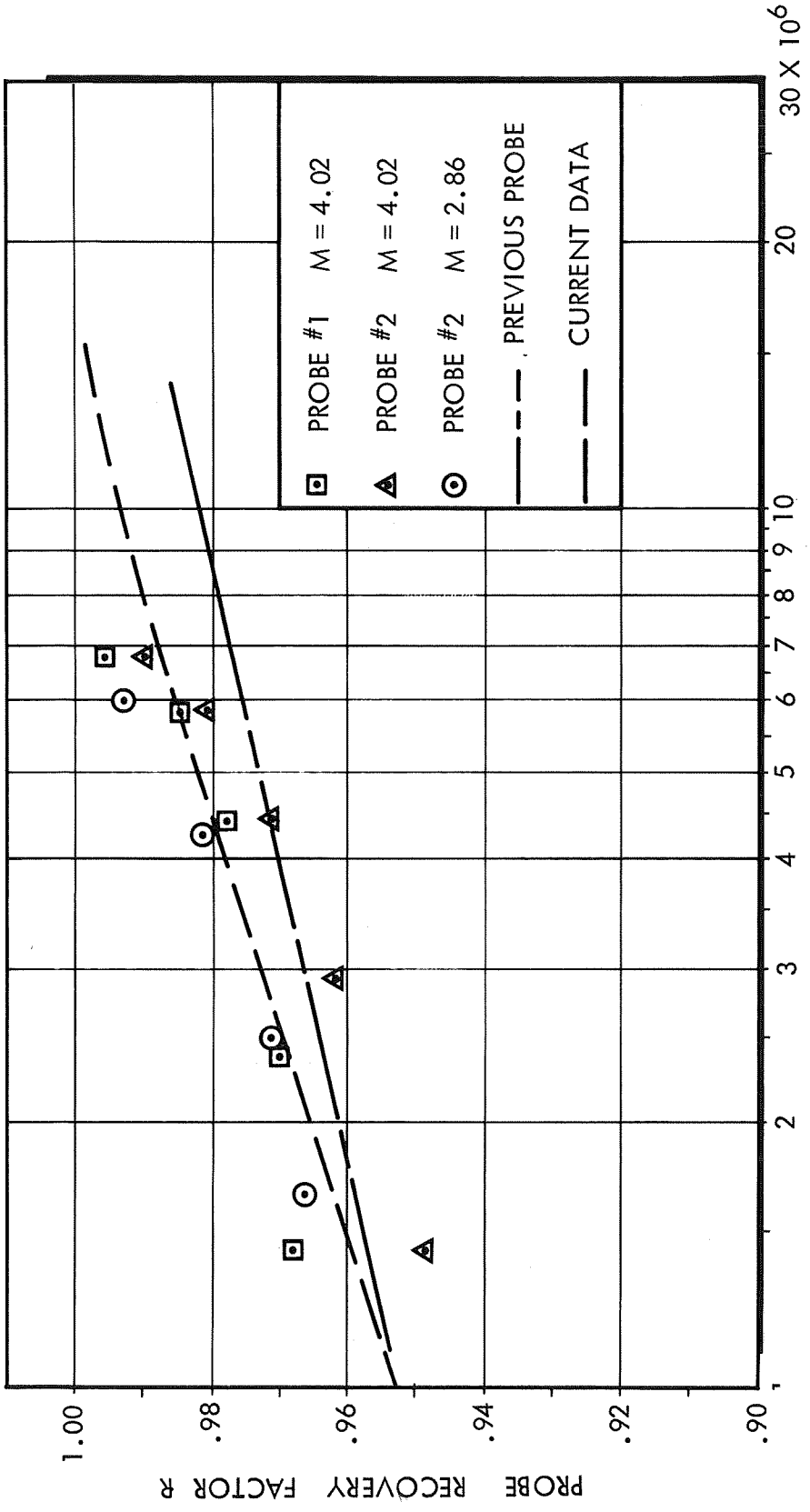

Figure A2 VARIATION OF RECOVERY FACTORY WITH UNIT REYNOLDS NUMBER

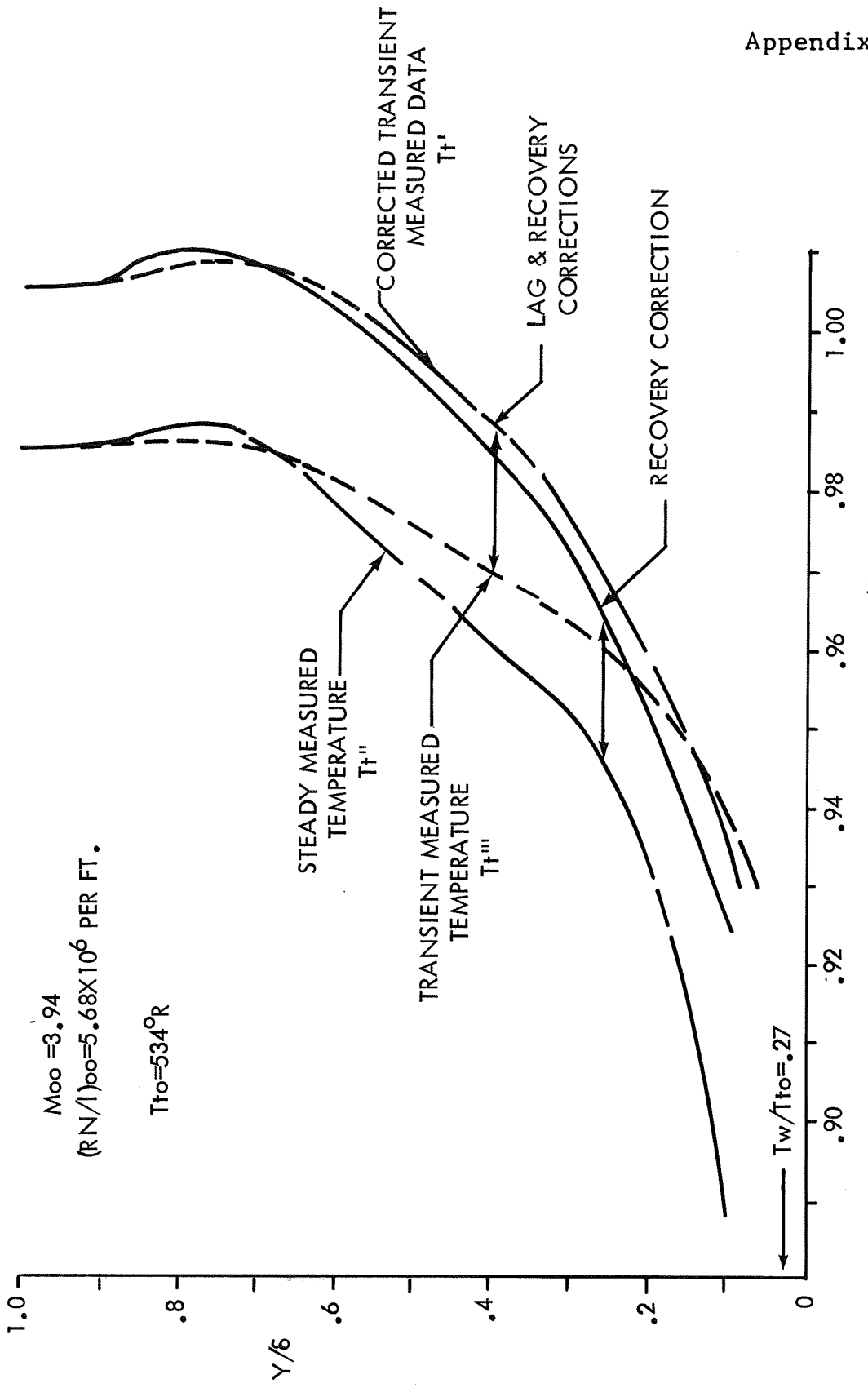

Figure A3 TYPICAL LAG AND RECOVERY FACTORY CORRECTIONS

APPENDIX B

DATA REDUCTION

General

Basic data were reduced from raw data inputs and are tabulated and plotted. Boundary layer edge conditions and the boundary layer thickness were extracted from the basic data to compute normalized boundary layer variables. Only two normalized variables were plotted: the velocity and temperature ratios, V/V_e and $T_t'/T_t'_e$, versus the non-dimensional probe location Y/δ.

Basic Data

Basic data were reduced during testing. The following equations were used:

Pressure Data

$$P_t' = A_t + B_t\,(R1) + C_t\,(R1)^2 \tag{B1}$$

$$P_i = B_i\,(RS_i) + C_i\,(RS_i)^2 \tag{B2}$$

$$P_{61} = A + B_{61}\,(RS_{61}) + C_{61}\,(RS_{61})^2 \tag{B3}$$

where

A is barometric pressure
B and C are calibration constants associated with each transducer
i is location index
R1 and RS are raw data for total and static pressures, respectively.

$$CP_i = (P_i - P_o)/q_o \tag{B4}$$

The static pressure used for local Mach number computations was normally taken from probe P_{61}.

Temperature Data

$$T_t''' = D_t + E_t\,(R2) + F_t\,(R2)^2 + G_t\,(R2)^3 \qquad (B5)$$

$$T_j = T_J + E_j\,(RT_j) + F_j\,(RT_j)^2 + G_j\,(RT_j)^3 \qquad (B6)$$

$$T_J = D_J + E_J\,(R_J) + F_J\,(R_J)^2 + G_J\,(R_J)^3 \qquad (B7)$$

where

D is the reference junction temperature

D_t and D_J = $140^{\circ}R$

E, F, and G are calibration constants for the thermocouples used in the various locations

R2, RT_j, R_J are raw data for the probe total temperature, the plate temperature, and the plate-installed reference junction temperature, respectively

j is a location index

Lag Correction to Probe Temperature

$$(T_t'')_n = (T_t''')_o + \sum_n (\Delta T_t'')_n \qquad (B8)$$

where

$(T_t''')_o$ is the probe indicated temperature before traverse begins

$$(\Delta T_t'')_n = A\,(T_t'''_n - T_t'''_{n-1}) \qquad (B9)$$

where

A is computed by linear interpolation from tabulated input of A vs RE/l using freestream unit Reynolds number as the argument

n is index internal to computer program monotonically increasing for each data point after probe traverse begins

Local Mach Number

$$M = \left[\frac{5}{(P_{61}/P_t')^{2/7}} - 5\right]^{\frac{1}{2}} \quad \text{for } P_{61}/P_t' \geq 0.5283 \text{ (subsonic flow)} \qquad \text{(B10)}$$

A series approximation to the inversion of the Rayleigh pitot formula was used to compute M when

$P_{61}/P'_t < 0.5283$ (supersonic flow)

Local Unit Reynolds Number

Local unit Reynolds number computations for each data point required this order of equations:

$$T/T_t = 1/(1 + M^2/5) \qquad \text{(B11)}$$

$$P_t = P_{61}\ (1 + M^2/5)^{7/2} \qquad \text{(B12)}$$

$$\mu = 2.270 \left[\frac{(T_t'')^{3/2}}{T_t'' + 198.6}\right] \times 10^8 \text{ lbs-sec/ft}^2 \qquad \text{(B13)}$$

$$RE/1 = \frac{144\ P_t M}{\mu} \left[\frac{3.5}{4290(T_t'')}\right]^{\frac{1}{2}} \left[\frac{T}{T_t}\right] \left[\frac{\frac{T}{T_t} + \frac{198.6}{T_t''}}{1 + \frac{198.6}{T_t''}}\right]^{1.5} \qquad \text{(B14)}$$

Probe Temperature Corrected for Recovery Factor

$$T_t' = T_t''\ (T_t'/T_t'') \qquad \text{(B15)}$$

where

$$T_t'/T_t'' = \frac{1}{R + (1 - R)(T/T_t)} \qquad \text{(B16)}$$

R is computed by linear interpolation from tabular input of R vs RE/1 using local unit Reynolds number as the argument.

Probe Position

Probe vertical position, Y, with respect to the plate surface was computed as:

$$Y = H_1 (\Delta R_3) + H_2 (\Delta R_3)^2 + H_4 (\Delta R_4) + Y_I \qquad (B17)$$

where

Y_I is a set distance, probe to plate, normally 0.80 inch, and the initial output of R_3 and R_4 are recorded

H_1, H_2, and H_4 are the calibration constants associated with the particular potentiometer in use

ΔR_3 is output of the potentiometer indicating change in position of probe with respect to the actuator

ΔR_4 is output of the potentiometer indicating change in position of actuator with respect to the plate.

Manual Input Data

XP (inches) - Probe Station

PX_i (inches) - Pressure tap locations according to index, i.

TX_j (inches) - Thermocouple locations according to index, j.

Basic Plotted Data

Data which were plotted are as follows:

$$CP_i \text{ vs } PX_i$$

$$T_j/T_{t_o} \text{ vs } TX_j$$

$$T_t'/T_{t_o},\ P_t'/P_{t_o},\ CP_{61},\ M \text{ vs } Y$$

Normalized Boundary Layer Variables

These data were reduced from basic boundary layer data, the boundary layer thickness, and select boundary layer edge conditions. All variables are tabulated. Reduction equations and variable descriptions are as follows:

M/M_e = Mach number ratio

$T_t'/T_t'_e$ = Total temperature ratio

T/T_e = Static temperature ratio, where

$$T/T_e = T_t'/T_t'_e \left[\frac{1.0 + 0.2\ M_e^2}{1.0 + 0.2\ M^2}\right] \tag{B18}$$

V/V_e = Velocity ratio, where

$$V/V_e = M/M_e\ (T/T_e)^{\frac{1}{2}} \tag{B19}$$

ρ/ρ_e = Mass density ratio, where

$$\rho/\rho_e = (T_e/T)(P_{61}/P_{61_e}) \tag{B20}$$

Y/δ = Nondimensional probe location

Plotted Normalized Data

Only two variables were plotted:

T_t'/T_{t_e} and V/V_e vs Y/δ.

REFERENCES

1. Kepler, C. E., O'Brien, R. L., Supersonic Turbulent Boundary Layer Growth Over Cooled Walls in Adverse Pressure Gradients, Aeronautical Systems Division Report ASD TDR-62-87, October 1962.

2. Kepler, C. E., Crossen, J. W., and Demarest, P. E., Hypersonic Inlet Investigations, Including Tests to Mach 8.7 and Theoretical Analyses to Mach 15, ASD Technical Report 61-137.

3. Kilburg, R. F., A High Response Probe for Measurement of Total Temperature and Total Pressure Profiles Through A Turbulent Boundary Layer With High Heat Transfer In Supersonic Flow, AIAA Paper No. 68-374, AIAA 3rd Aerodynamic Testing Conference, San Francisco, California, 8-10 April 1968.

4. Ames Research Staff, Equations, Tables and Charts for Compressible Flow, NACA Report 1135, 1953.

5. Howell, G. A., Shock-Boundary Layer Interaction and Survey Test, General Dynamics/Astronautics Report GD/A ERR-AN-509, June 1964.

TABLE I
SHOCK GENERATOR WEDGE POSITION AND
THEORETICAL WAVE PATTERN DATA

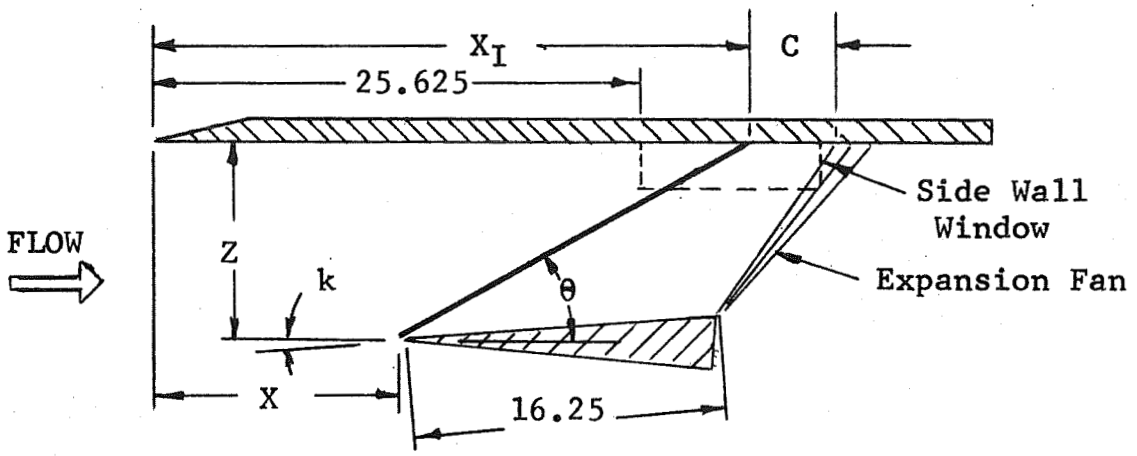

Mach No.	ANGLES - DEGREE			POSITION - INCHES				
	Incidence k	Turning *	Wave θ	Code m	X	Z	X_I	C
2.0	6	6.3	35.6	7	18.25	8.00	29.43	12.20
	8	8.5	37.7	8	18.85	8.17	29.42	11.48
3.2	6	6.6	23.1	5	10.29	8.00	29.05	9.50
	8	8.6	24.9	6	11.39	8.17	28.98	8.59
4.2	6	6.7	18.5	2	5.46	8.00	29.37	7.56
	8	8.7	20.2	3	7.07	8.17	29.27	6.56

* Turning angle includes the effective increase in deflection due to boundary layer growth on the wedge surface. This was obtained from measurements of shock wave angles in test data taken at the same Mach numbers and Reynolds numbers (Reference 5).

TABLE II

TEST CONDITIONS AND MANUAL INPUT FOR FINAL DATA REDUCTION

MACH NO. M_o	PLATE TEMP. RATIO T_w/T_{t_o}	RE/1 x 10^{-6} (ft.)	WEDGE CONFIG.	SURVEY STATION CODE	SURVEY STATION INCHES	RUN NO.	DATA FOR FINAL REDUCTION δ INCHES	M_e	T'_{t_e} ^oR	P_e PSIA
3.18	0.96	14.5	--	XP(0)	27.00	7	0.41175	3.083	519	2.429
			W_6^5	(1)	31.25	11	0.42231	2.677	527	5.966
			"	(2)	36.00	8	0.47340	2.640	531	5.359
			W_8^6	(1)	31.25	10	0.42425	2.400	522	7.512
			"	(2)	36.00	9	0.55171	2.433	527	6.984
3.18	0.30	14.5	--	XP(0)	27.00	22	0.40752	3.217	530	2.247
			W_6^5	(1)	31.25	29	0.37561	2.678	536	5.852
			"	(2)	36.00	21	0.46917	2.645	534	5.503
			W_8^6	(1)	31.25	28	0.38479	2.433	535	7.554
			"	(2)	36.00	20	0.52897	2.470	545	7.007
3.18	0.31	11.5	--	XP(0)	27.00	23	0.37772	3.368	536	1.611
			W_6^5	(1)	31.25	30	0.37407	2.640	535	4.800
			"	(2)	36.00	14	0.44643	2.606	523	4.446
			W_8^6	(1)	31.25	27	0.38099	2.430	535	5.997
			"	(2)	36.00	19	0.50882	2.421	541	5.752
3.18	0.31	10.3	--	XP(0)	27.00	25	0.40666	3.305	538	1.494
			W_6^5	(1)	31.25	31	0.35010	2.644	530	4.280
			"	(2)	36.00	17	0.44980	2.678	540	3.818
			W_8^6	(1)	31.25	26	0.36842	2.420	537	5.458
			"	(2)	36.00	18	0.50539	2.502	541	4.916
2.01	0.34	12.2	W_6^7	XP(2)	36.00	32	0.52773	1.578	521	11.625
			W_8^8	(2)	36.00	36	0.61342	1.407	526	14.330
2.01	0.32	6.4	W_6^7	XP(2)	36.00	33	0.53183	1.565	533	6.236
			W_8^8	(2)	36.00	34	0.61952	1.388	522	7.761
4.2	0.32	20.2	W_8^3	XP(2)	33.00	43	0.26848	3.081	504	5.938
4.2	0.32	14.5	W_6^2	XP(2)	33.00	46	0.36110	3.460	505	3.125
			W_8^3	(2)	33.00	44	0.31304	3.150	516	4.357

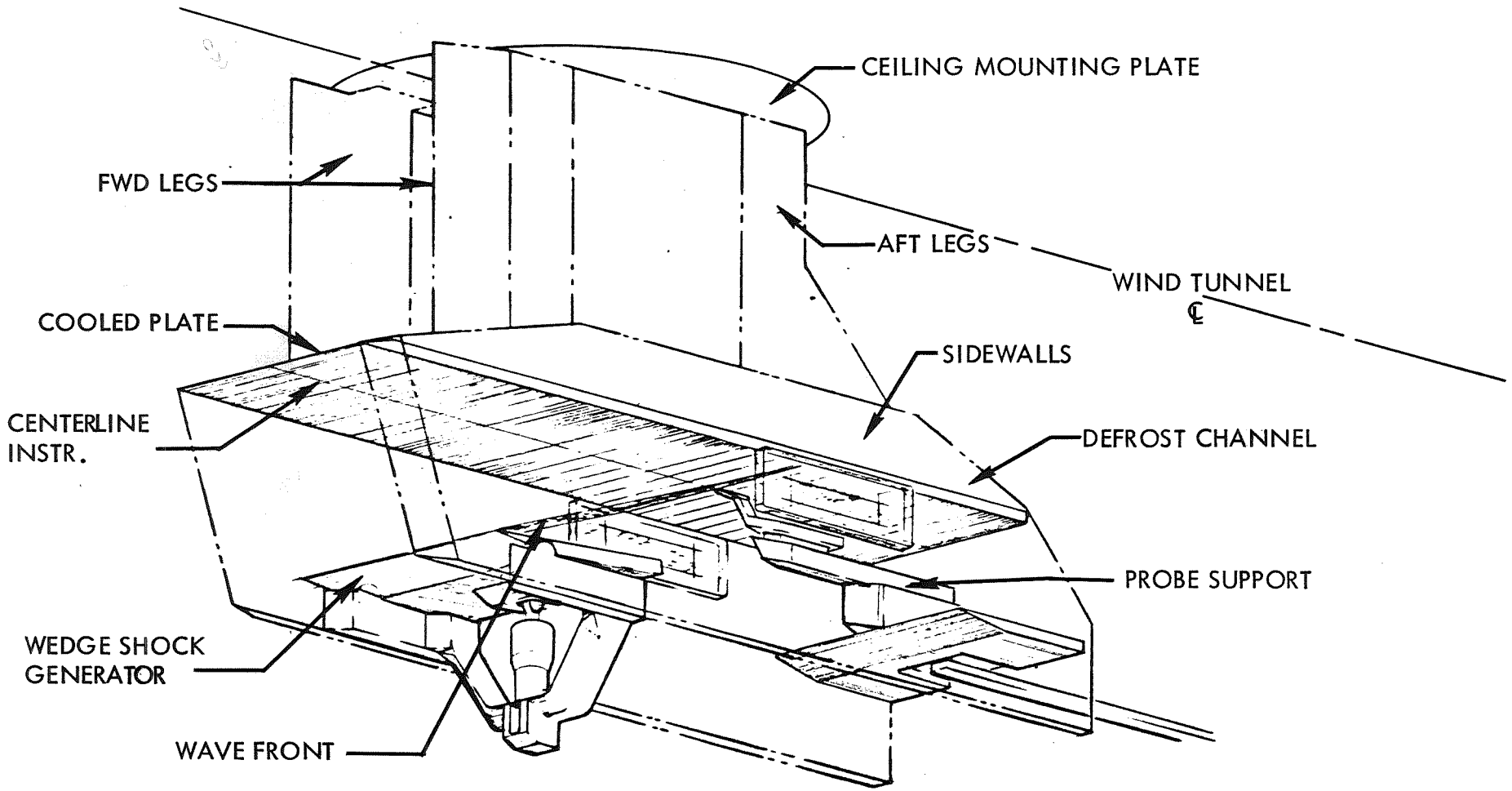

Figure 1 2-D BOUNDARY LAYER INTERACTION MODEL GENERAL ARRANGEMENT

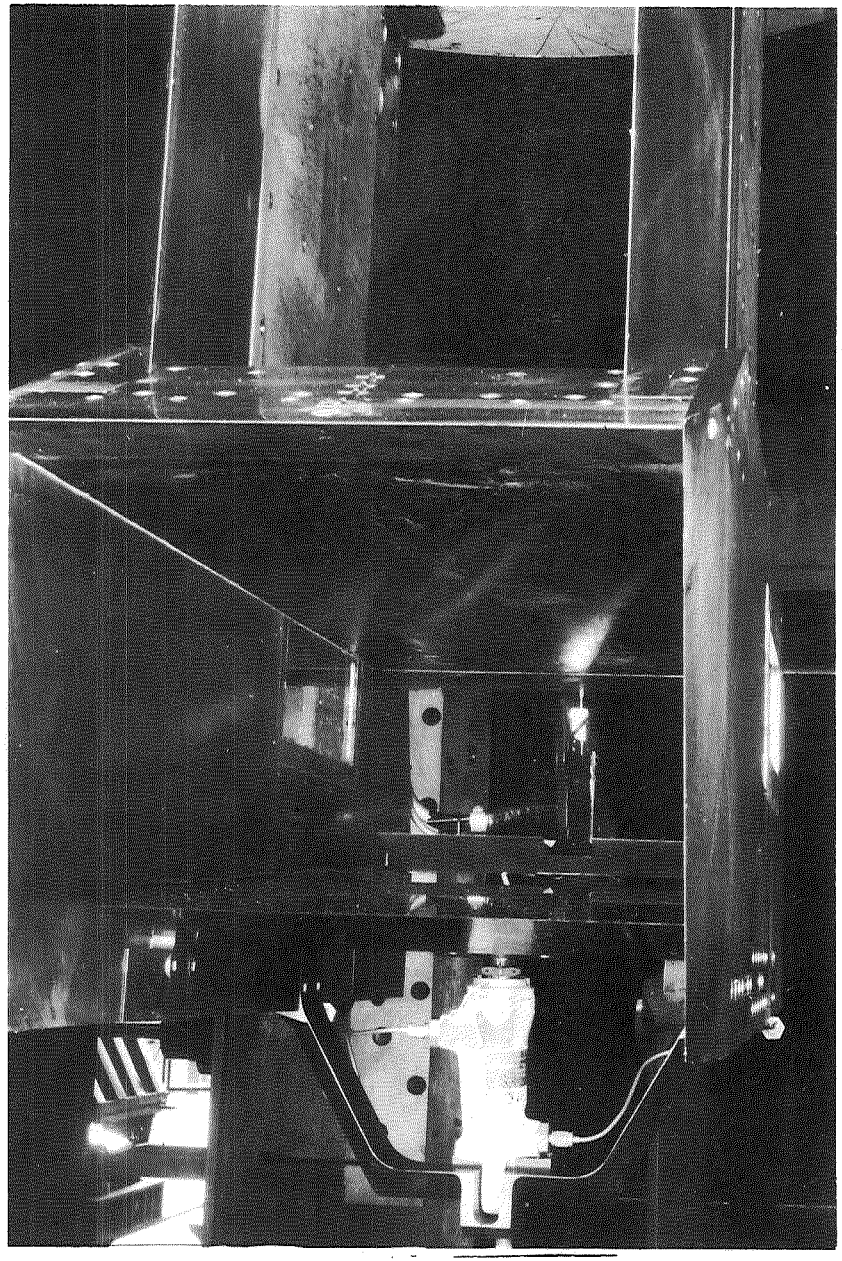

LOOKING DOWNSTREAM

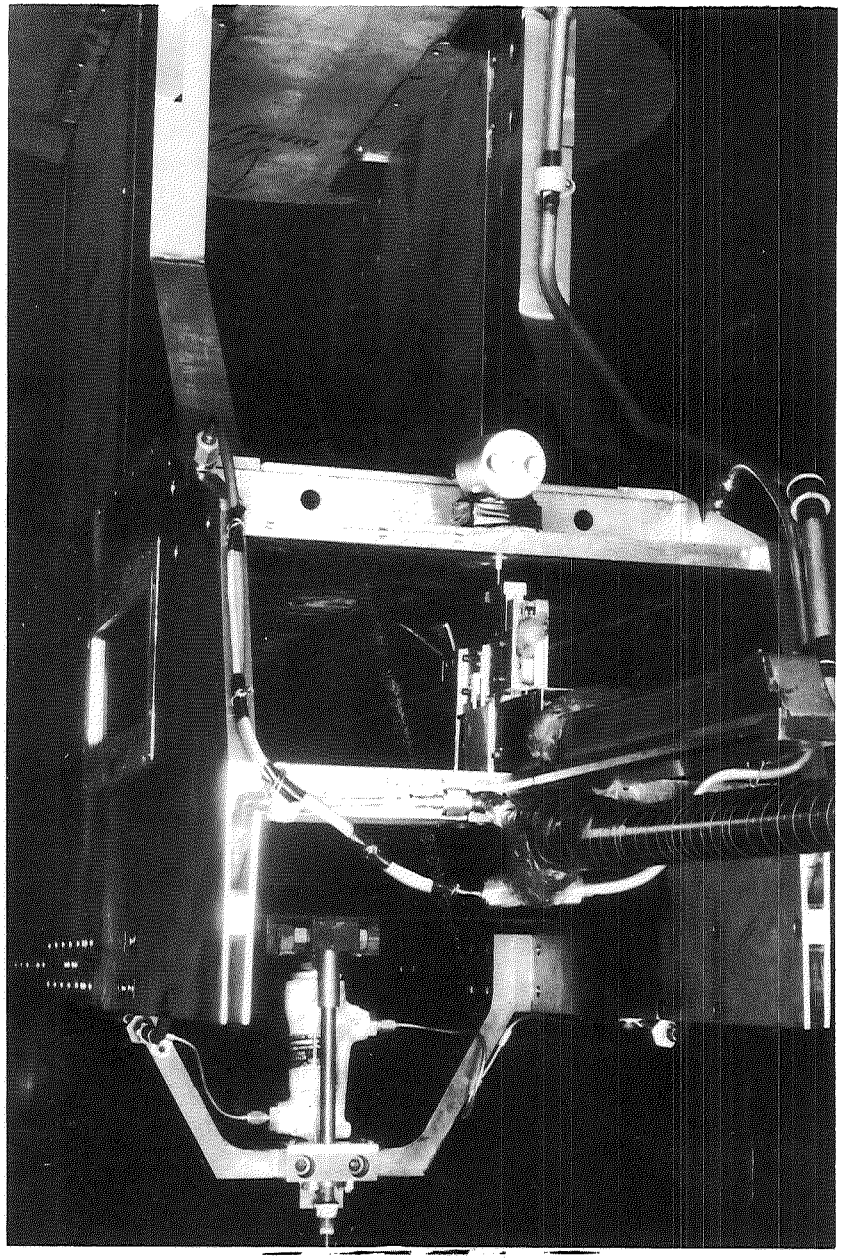

LOOKING UPSTREAM

Figure 2 MODEL INSTALLED IN TUNNEL

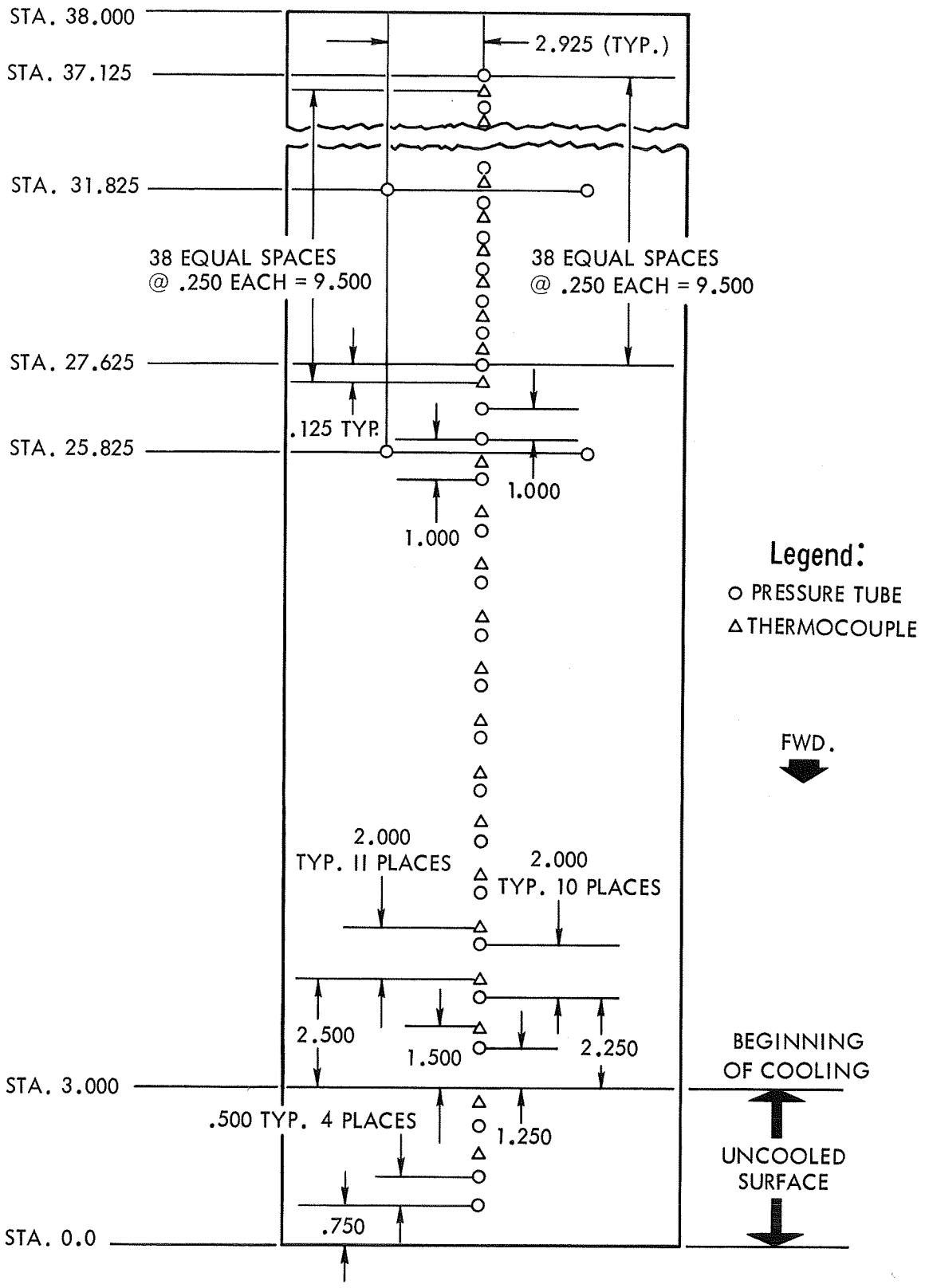

Figure 3 PRESSURE ORIFICE AND THEMOCOUPLE LOCATIONS

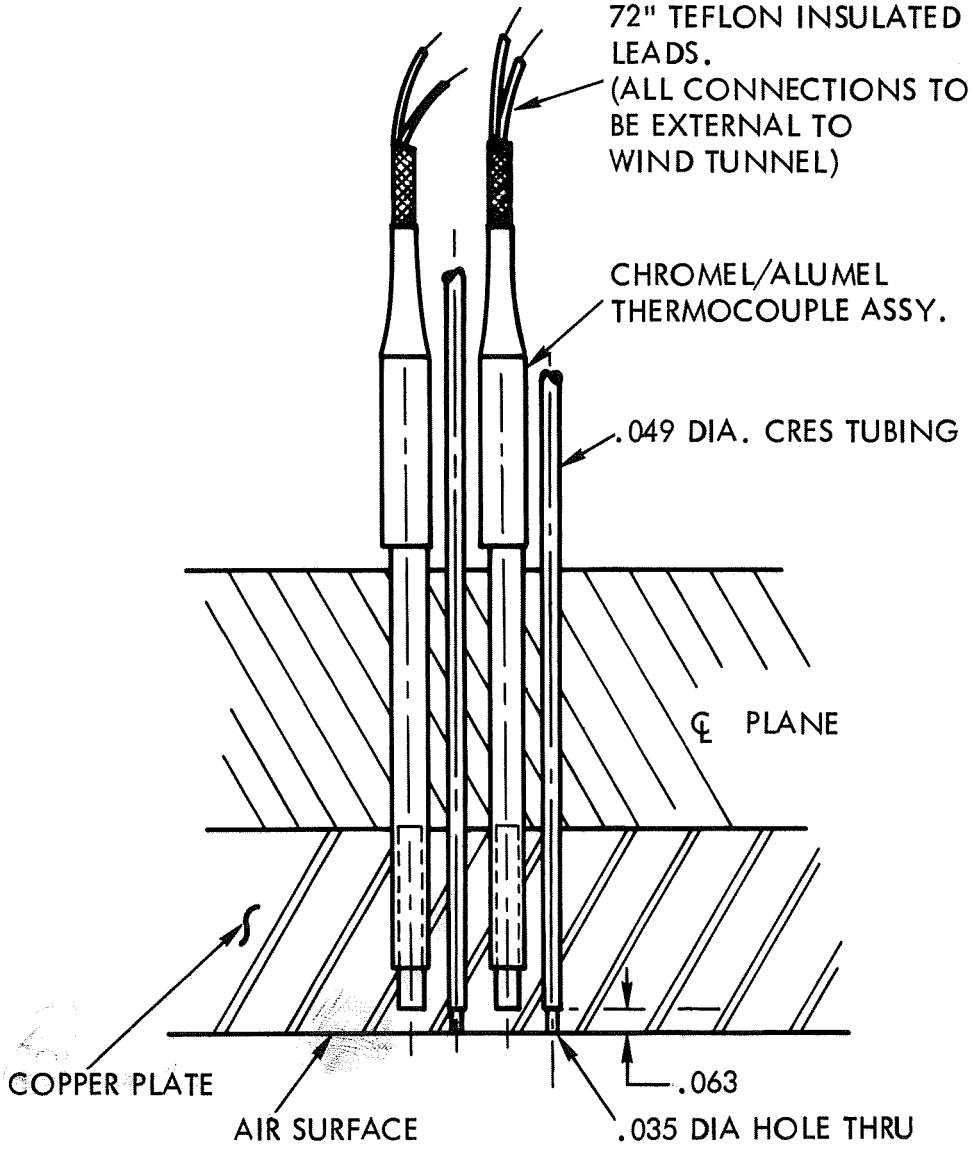

Figure 4 PLATE INSTRUMENTATION DETAILS

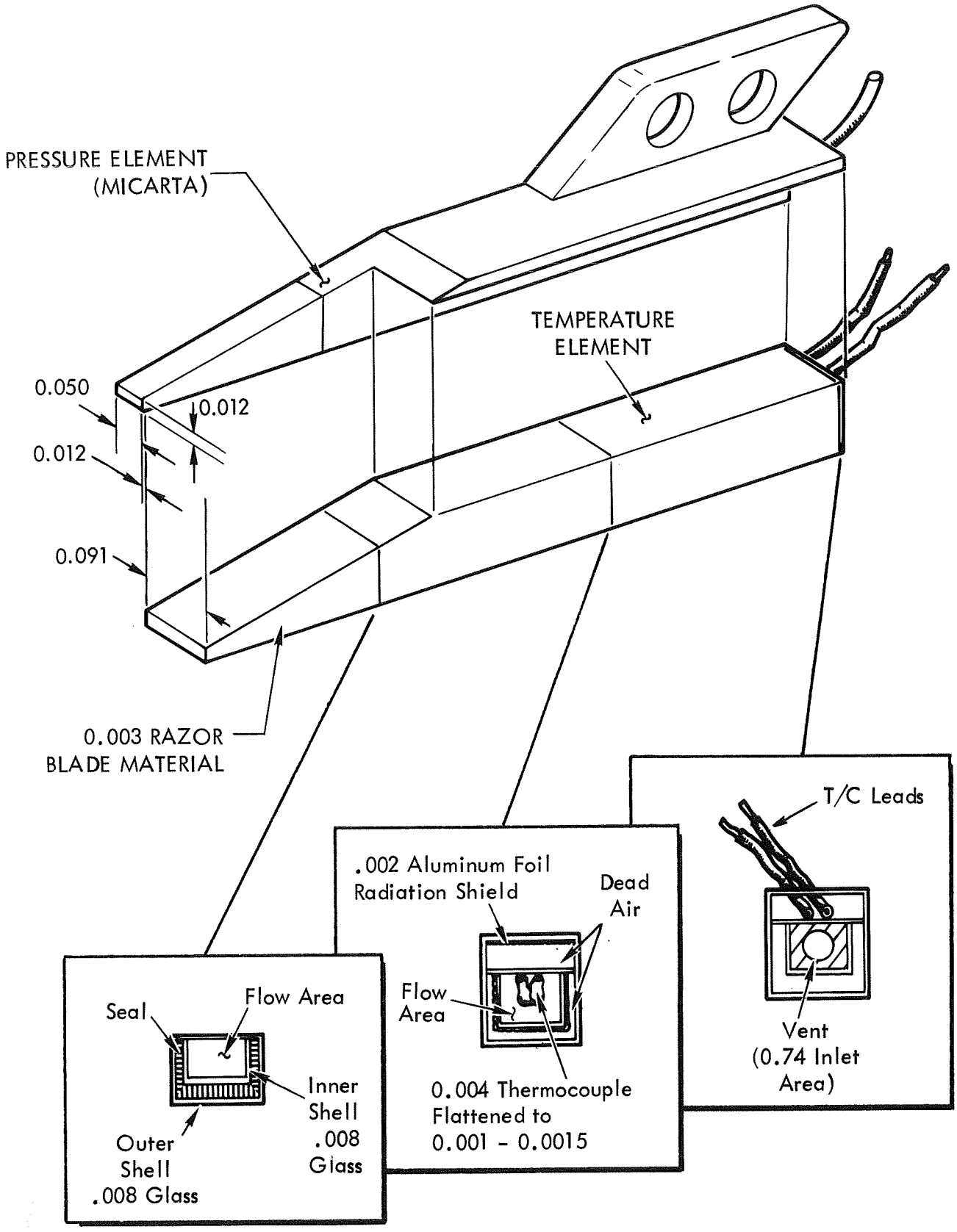

Figure 5 TOTAL PRESSURE/TOTAL TEMPERATURE PROBE

- M_o 3.18
- T_w/T_{to} 0.96
- Wedge Configuration W_6^5
- RE/ℓ 14.5×10^6 per ft.
- q_o 223$\bar{5}$ psf.

	M_2	θ_I	θ_R	C_P
Theory ------	2.63	23.1	18.9	0.234
Measure ———	2.64	23.8	21.3	⊙ Shown

Run No. 8 (Shadowgraph from Run 4)

Data Off ℄ ⊡ Left ■ Right

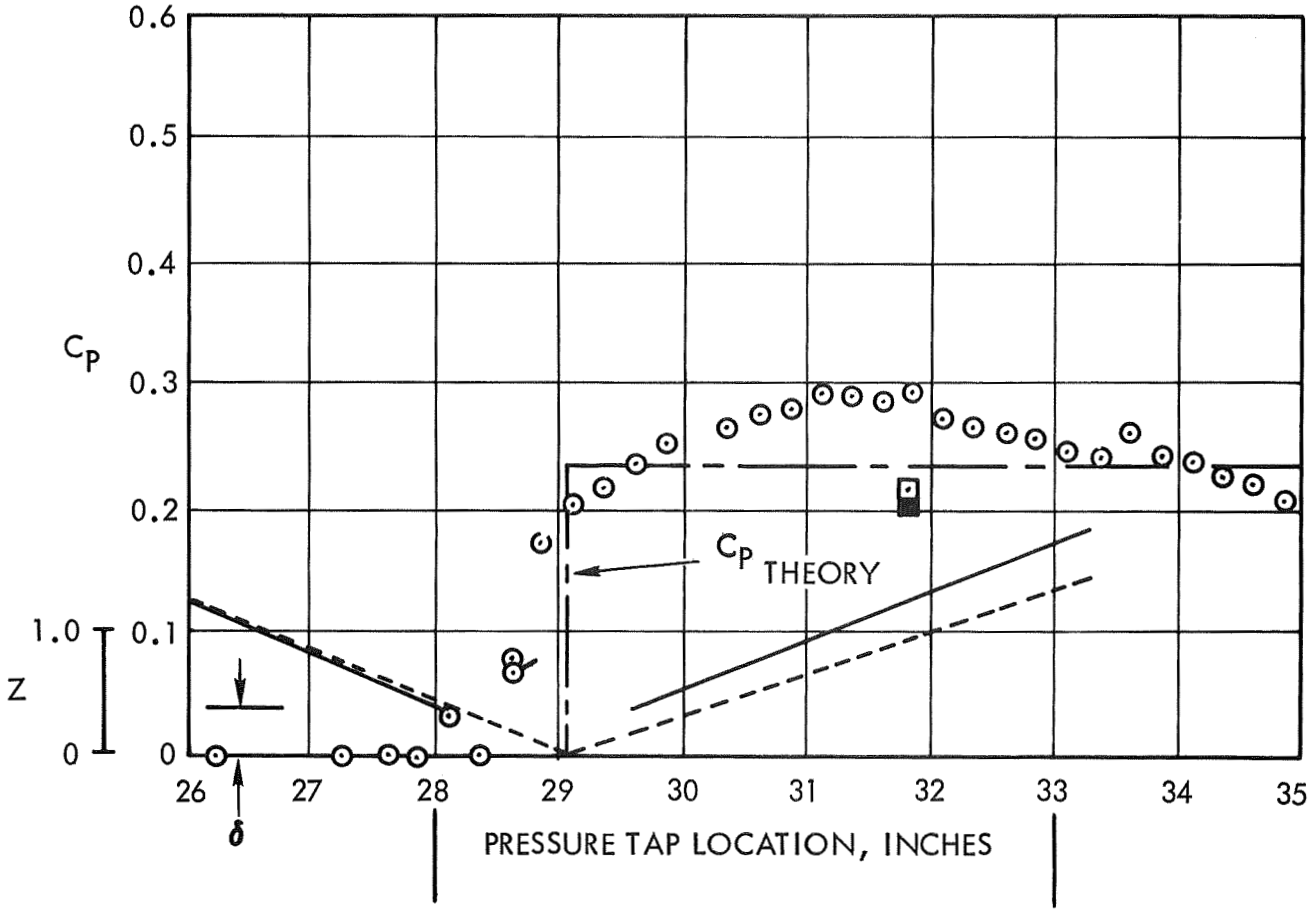

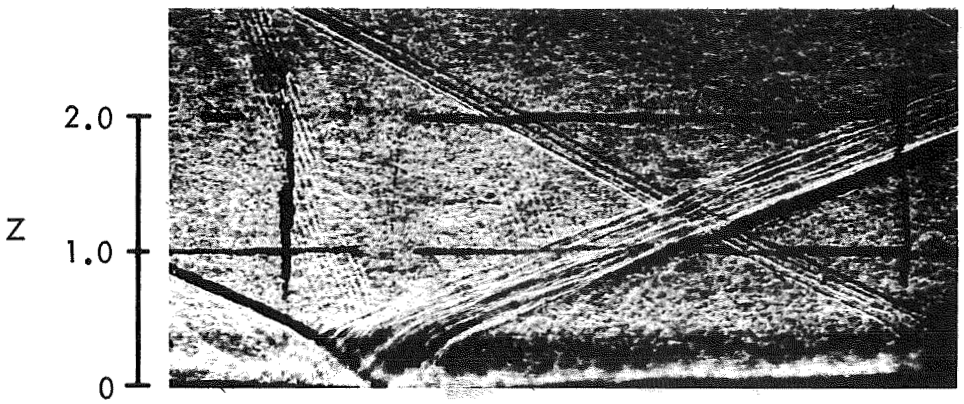

Figure 6 PLATE STATIC PRESSURE AND SHOCK WAVE PATTERN IN THE INTERACTION REGION.

- M_o 3.18
- T_w/T_{to} 0.97
- Wedge Configuration $W8^6$
- RE/ℓ 14.5×10^6 per ft.
- q_o 2232 psf.

	M_2	θ_I	θ_R	C_P
Theory - - - - -	2.38	24.9	19.6	0.342
Measure ———	2.43	25.0	21.6	⊙ Shown

Run No. 9

Data Off $\mathcal{L}$ ⊡ Left ■ Right

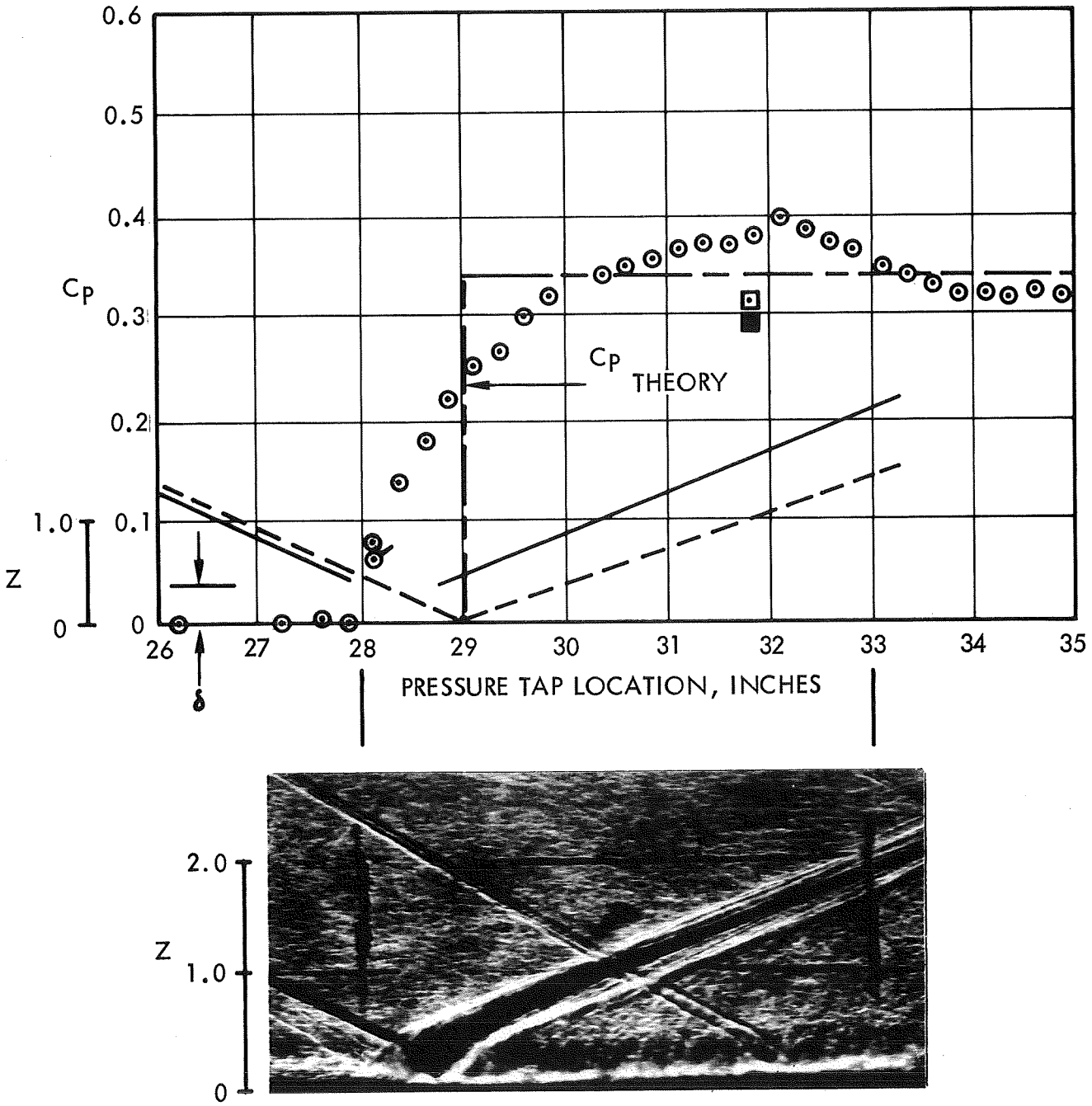

Figure 7 PLATE STATIC PRESSURE AND SHOCK WAVE PATTERN IN THE INTERACTION REGION.

- M_o 3.18
- T_w/T_{to} 0.29
- Wedge Configuration W_6^5
- RE/ℓ 14.4×10^6 per ft.
- q_o 2228 psf.

	M_2	θ_I	θ_R	C_P
Theory -----	2.63	23.1	18.9	0.234
Measure ———	2.63	24.0	20.0	◎ Shown

Run No. 21 (Shadowgraph from Run 12)
Data Off ℄ ◘ Left ■ Right

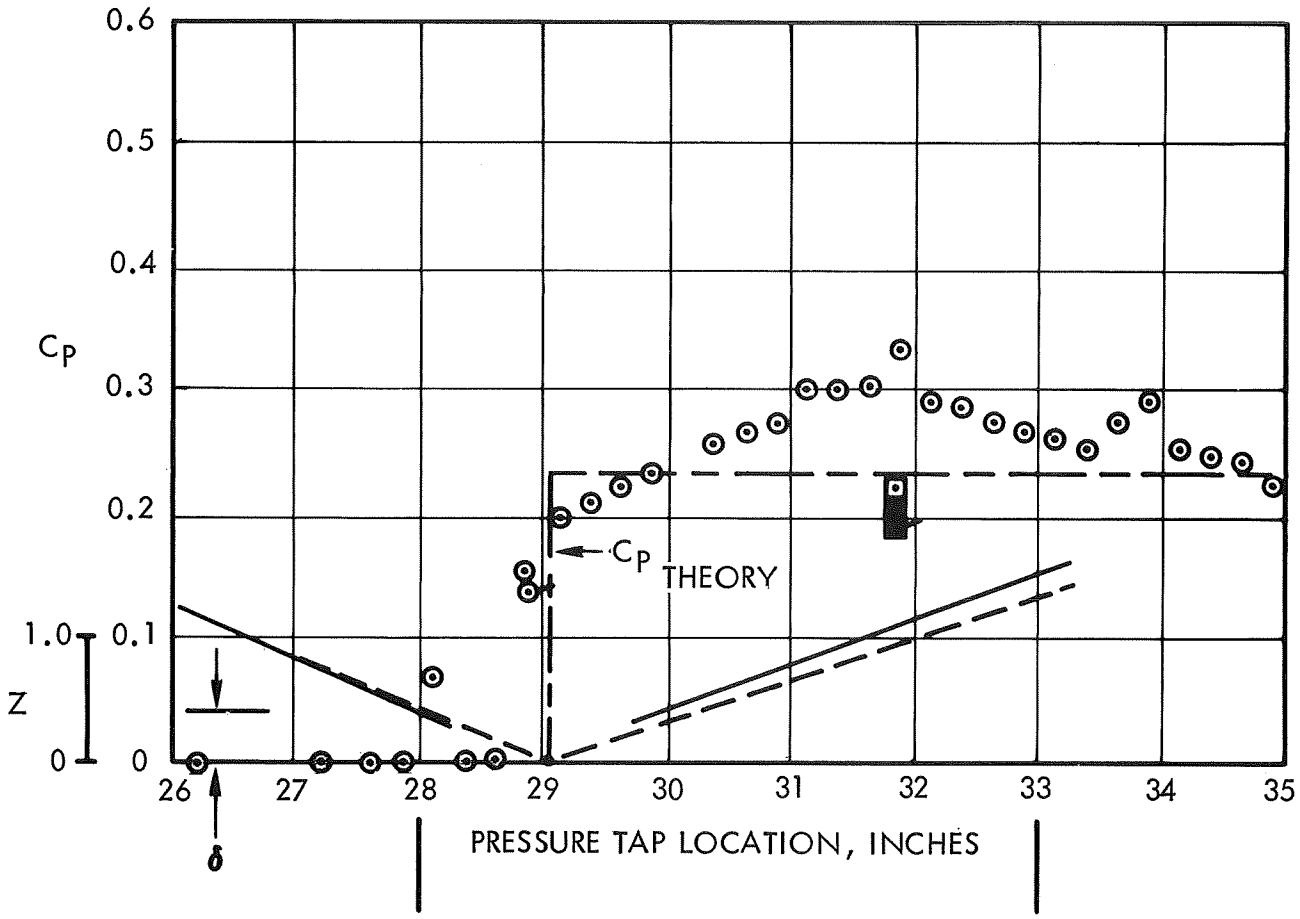

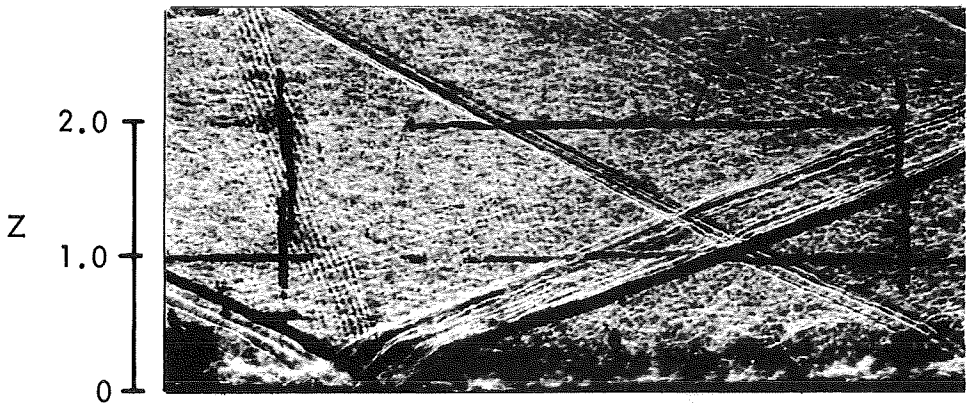

Figure 8 PLATE STATIC PRESSURE AND SHOCK WAVE PATTERN IN THE INTERACTION REGION.

- M_o 3.18
- T_w/T_{to} 0.31
- Wedge Configuration W_8^6
- RE/ℓ 14.5×10^6 per ft.
- q_o 2225 psf

	M_2	θ_l	θ_R	C_p
Theory -----	2.38	24.9	19.6	0.342
Measure ———	2.47	24.5	22.0	⊙ Shown

Run No. 20

Data Off ℄ ⊡ Left ■ Right

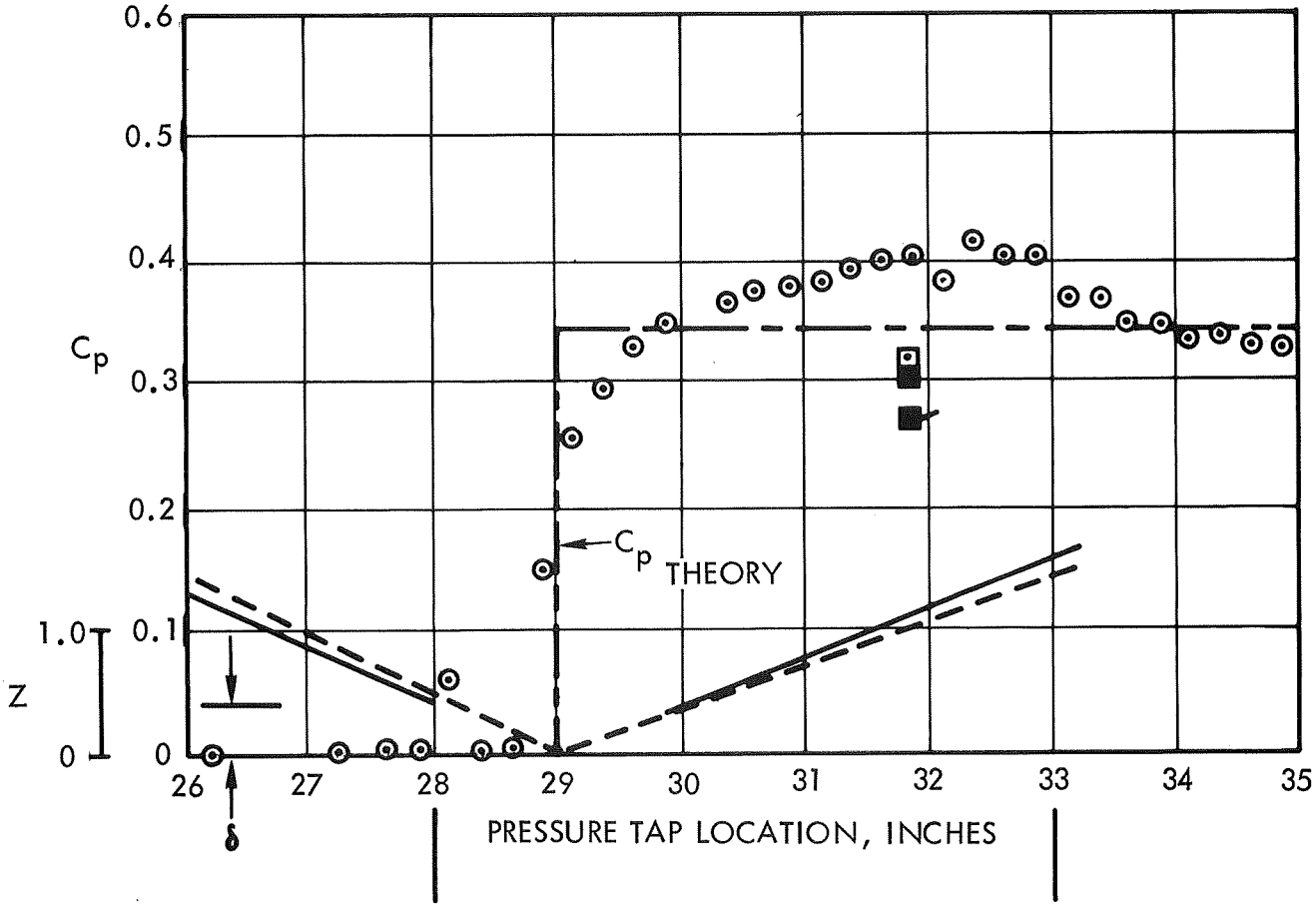

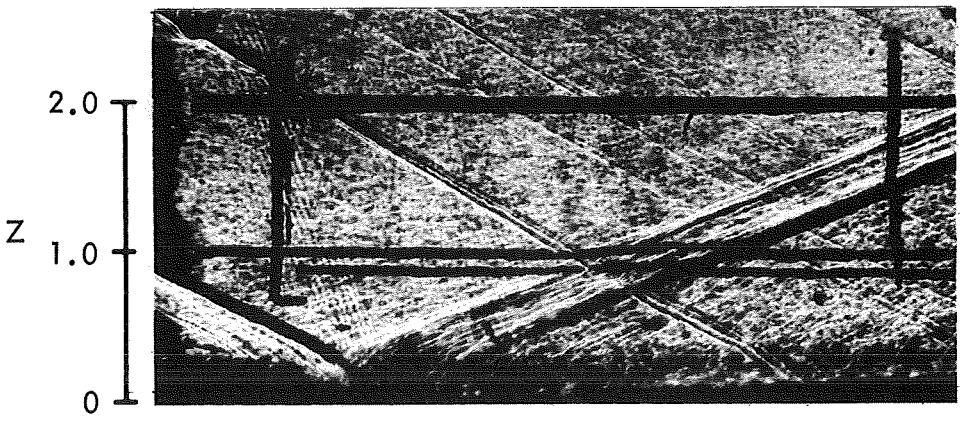

Figure 9 PLATE STATIC PRESSURE AND SHOCK WAVE PATTERN IN THE INTERACTION REGION.

- M_o 3.18
- T_w/T_{to} 0.31
- Wedge Configuration $W_6{}^5$
- RE/ℓ 11.5×10^6 per ft.
- q_o 1771 psf.

	M_2	θ_l	θ_R	C_P
Theory -----	2.63	23.1	18.9	0.234
Measure ———	2.61	24.0	21.0	⊙ Shown

Run No. 14

Data Off ℄ ⊡ Left ■ Right

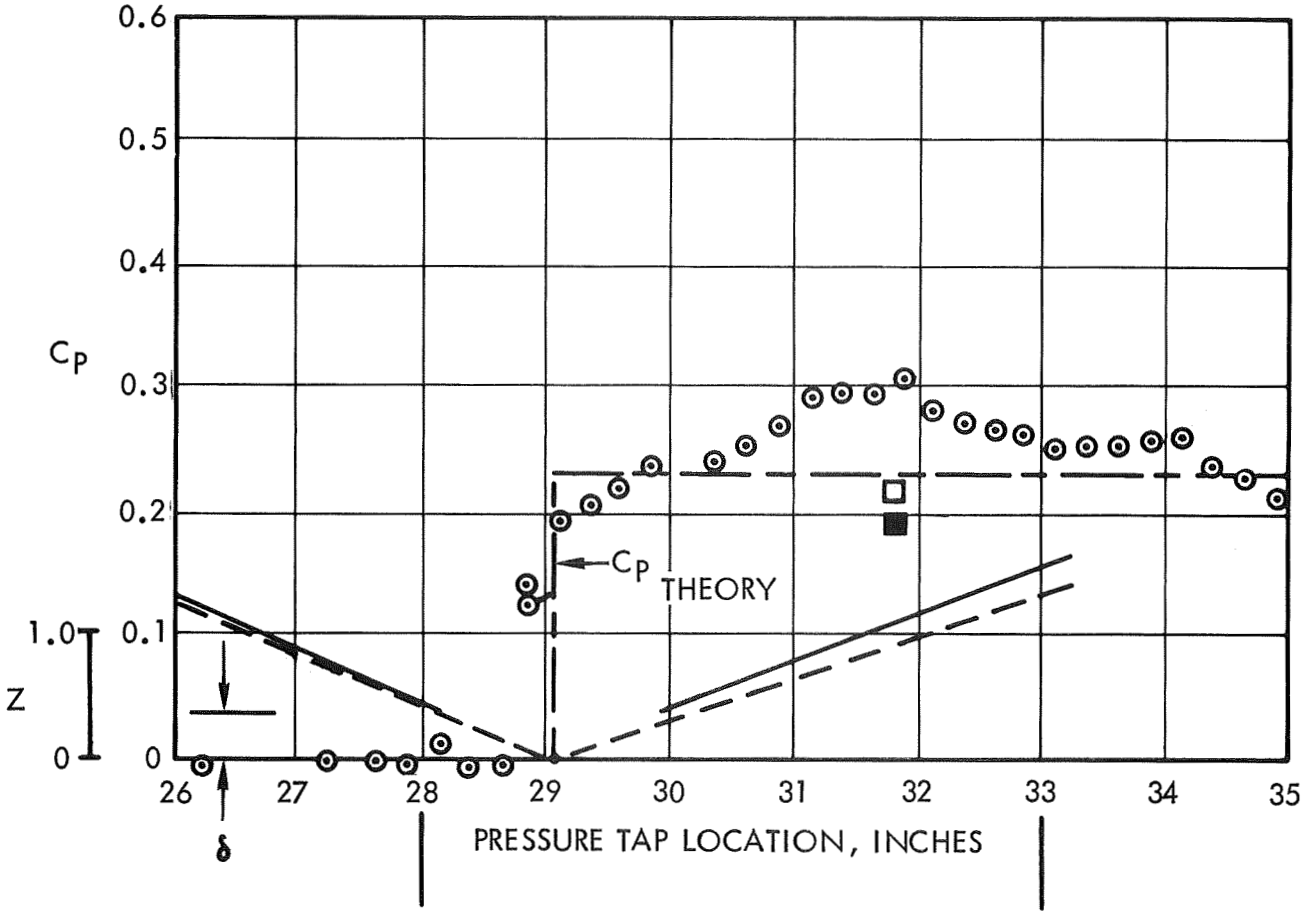

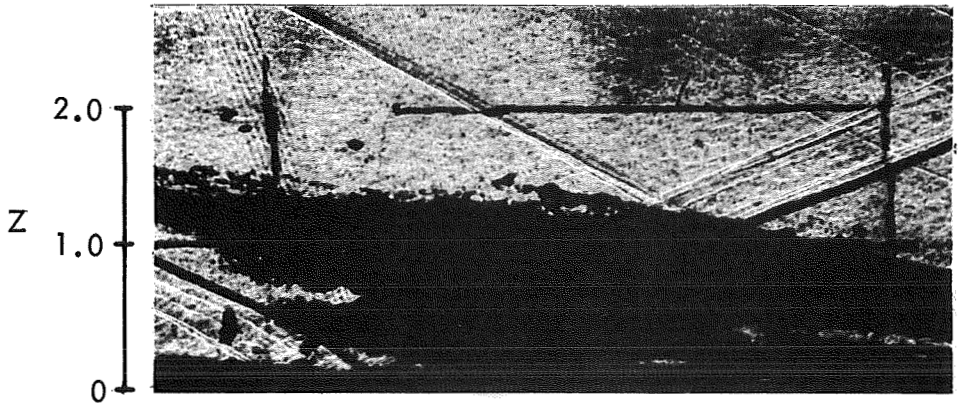

Figure 10 PLATE STATIC PRESSURE AND SHOCK WAVE PATTERN IN THE INTERACTION REGION.

- M_o 3.18
- T_w/T_{to} 0.31
- Wedge Configuration W_8^6
- RE/ℓ 11.5 x 10^6 per ft.
- q_o 1768 psf

	M_2	θ_I	θ_R	C_p
Theory - - - - -	2.38	24.9	19.6	0.342
Measure ———	2.42	26.0	23.0	Shown

Run No. 19
Data Off ℄ ⊡ Left ■ Right

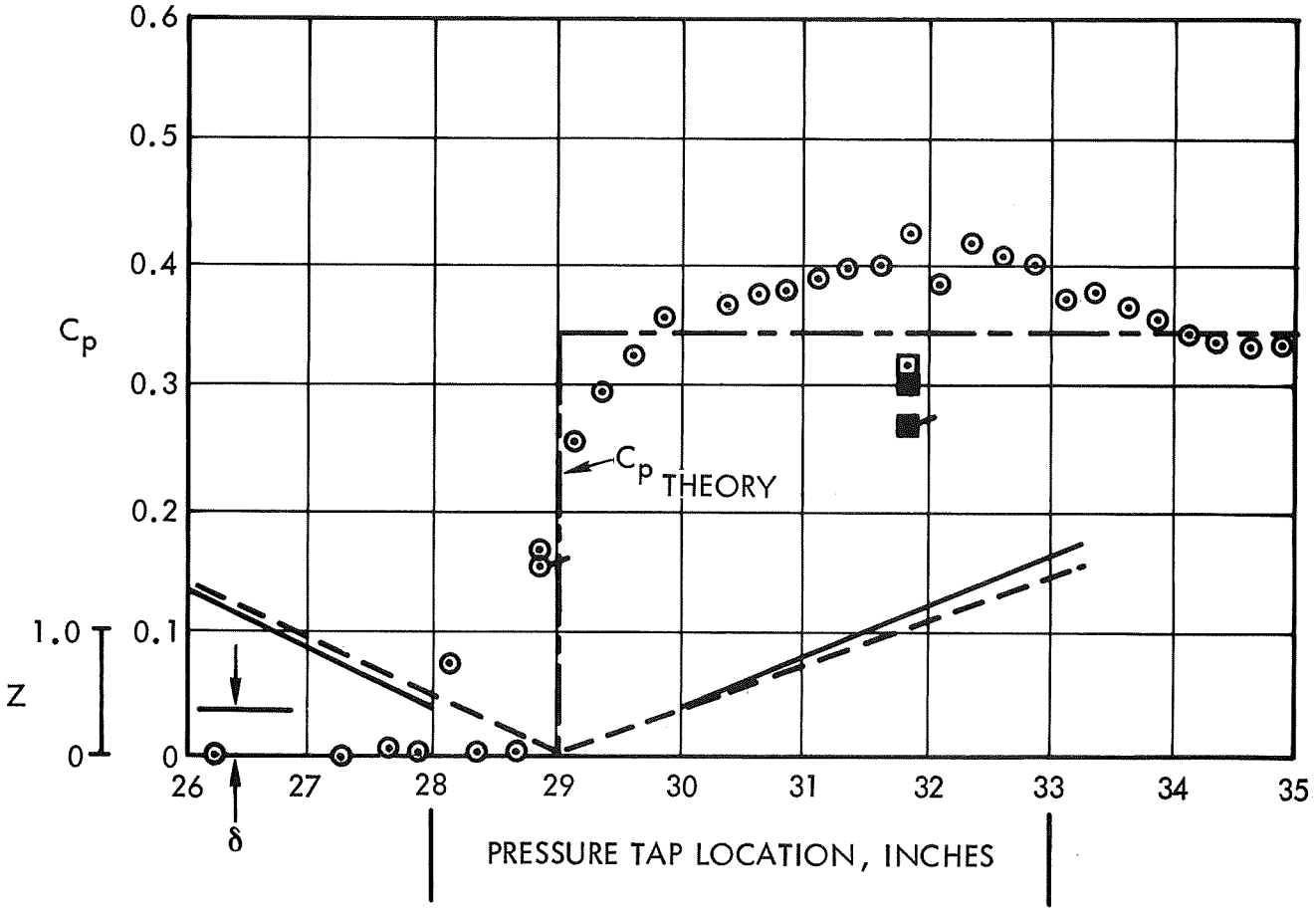

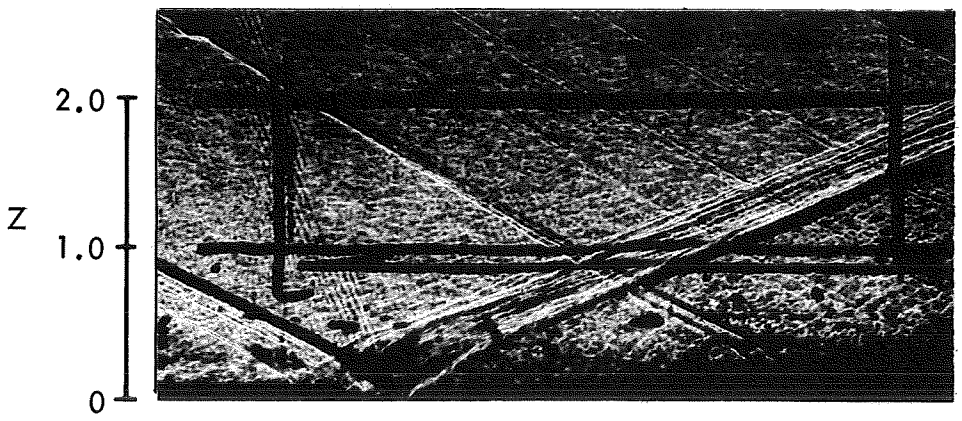

Figure 11 PLATE STATIC PRESSURE AND SHOCK WAVE PATTERN IN THE INTERACTION REGION.

- M_o 3.18
- T_w/T_{to} 0.30
- Wedge Configuration W_6^5
- RE/ℓ 10.3×10^6 per ft.
- q_o 1595 psf.

	M_2	θ_l	θ_R	C_P
Theory ------	2.63	23.1	18.9	0.234
Measure ———	2.68	25.0	20.0	⊙ Shown

Run No. 17
Data Off ℄ ⊡ Left ■ Right

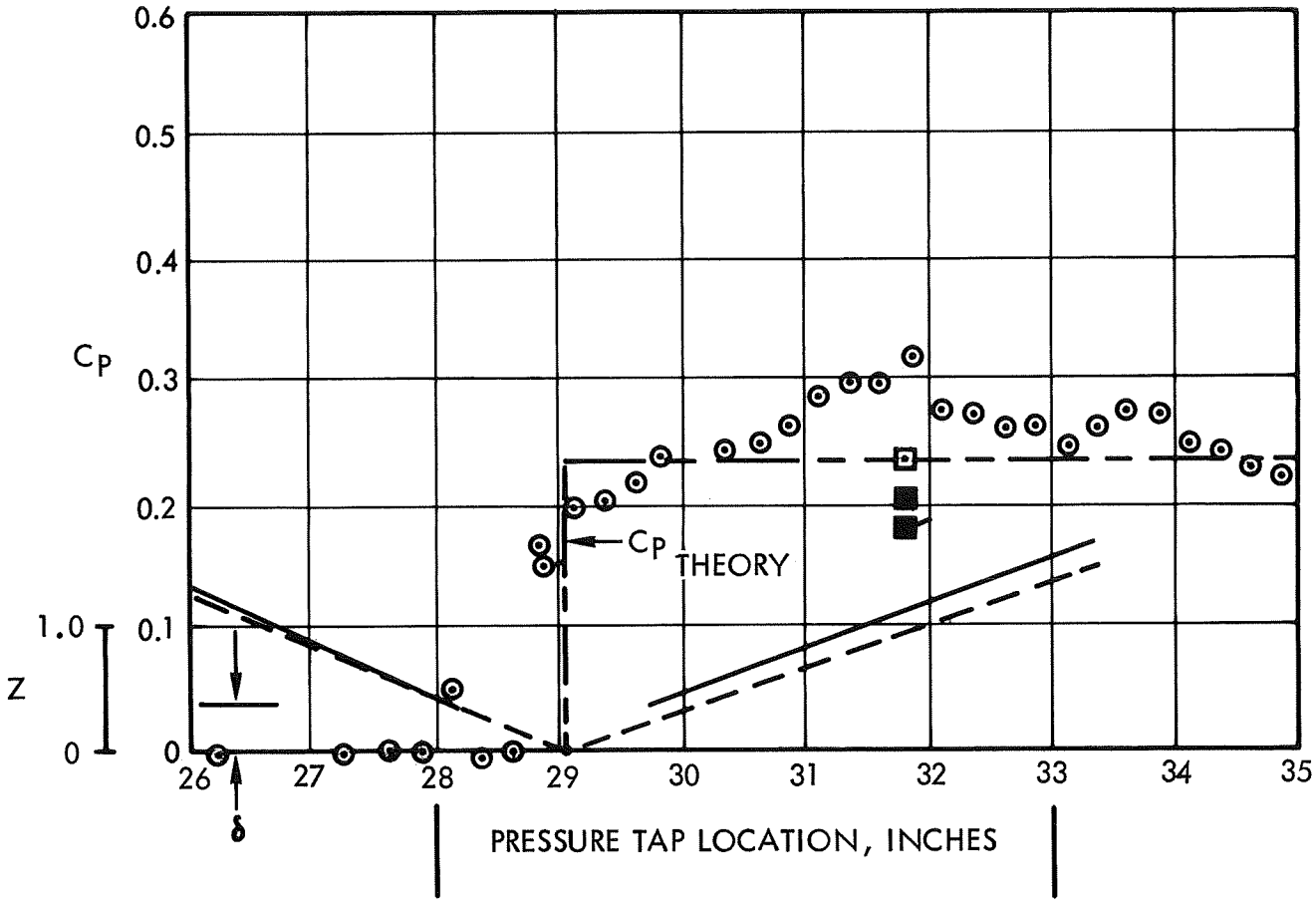

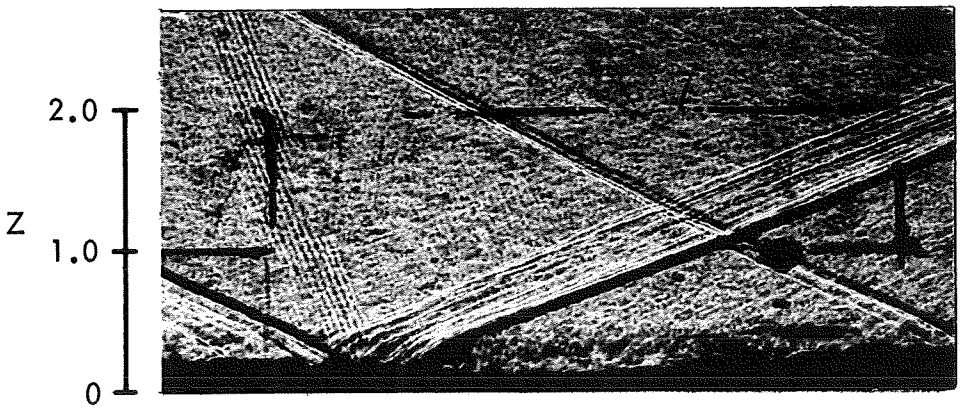

Figure 12 PLATE STATIC PRESSURE AND SHOCK WAVE PATTERN IN THE INTERACTION REGION.

- M_o 3.18
- T_w/T_{to} 0.31
- Wedge Configuration W_8^6
- RE/ℓ 10.3×10^6 per ft.
- q_o 1595 psf.

	M_2	θ_I	θ_R	C_P
Theory -----	2.38	24.9	19.6	0.342
Measure ———	2.50	25.0	23.0	⊙ Shown

Run No. 18

Data Off ℄ ⊡ Left ■ Right

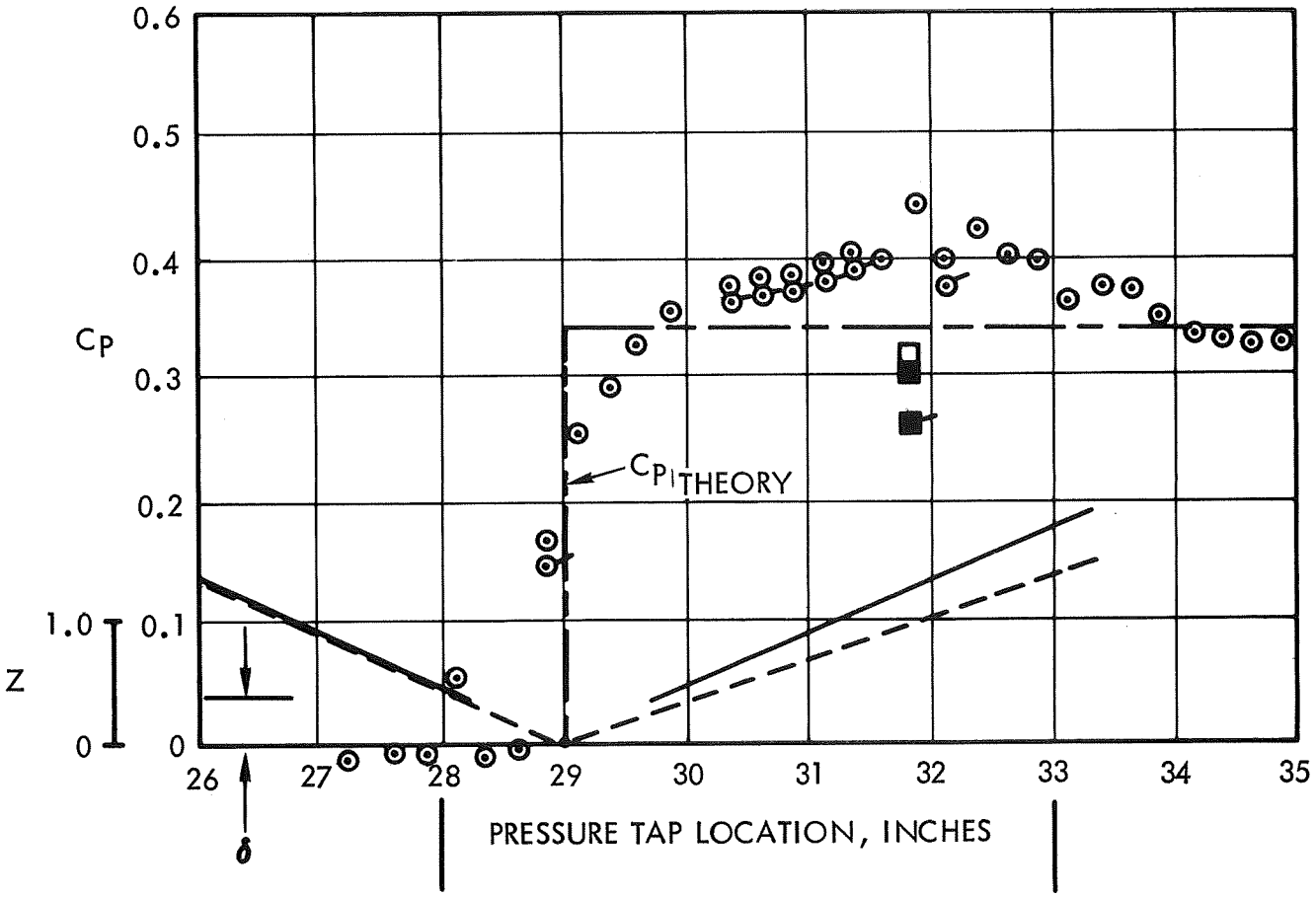

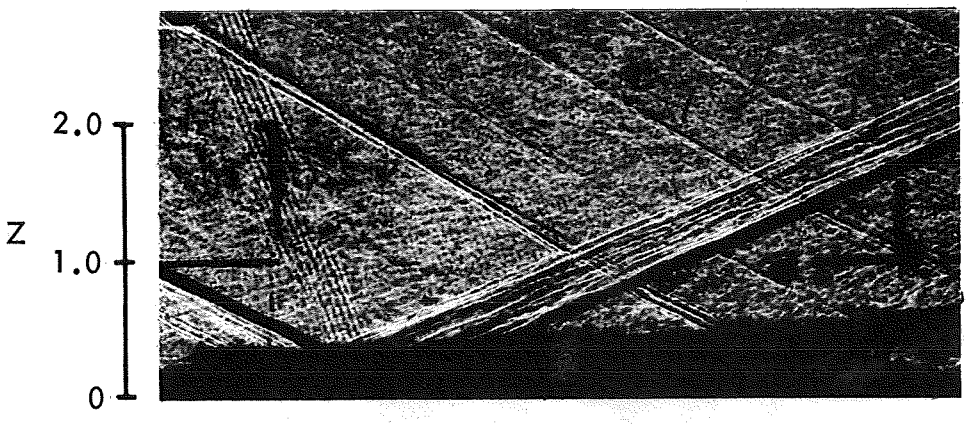

Figure 13 PLATE STATIC PRESSURE AND SHOCK WAVE PATTERN IN THE INTERACTION REGION.

- M_o 2.01
- T_w/T_{to} 0.34
- Wedge Configuration W_6^7
- RE/ℓ 12.2×10^6 per ft.
- q_o 2406 psf.

	M_2	θ_1	θ_R	C_P
Theory -----	1.55	35.6	34.2	0.332
Measure ———	1.58	37.0	38.0	⊙ Shown

Run No. 32

Data Off ℄ ⊡ Left ■ Right

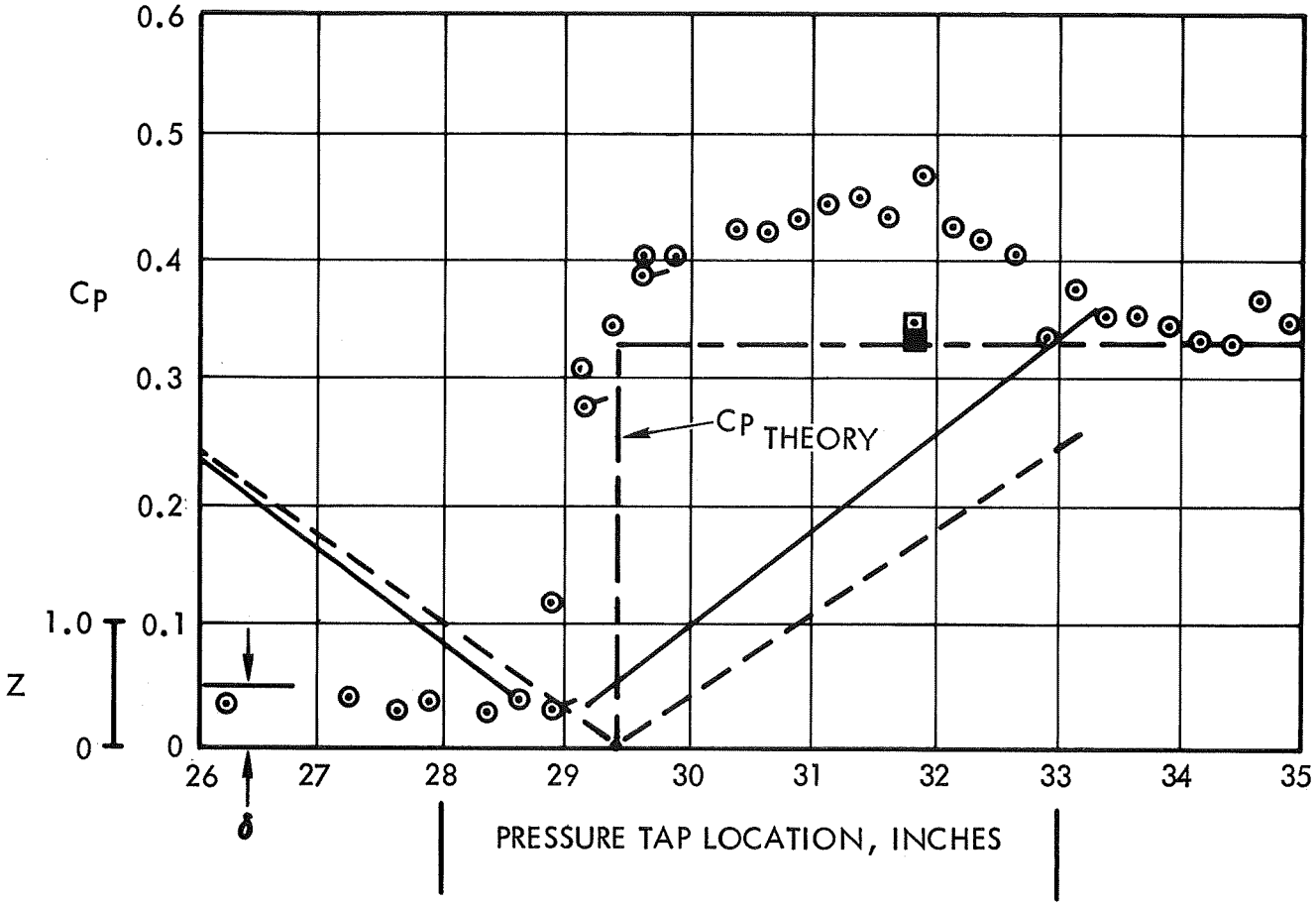

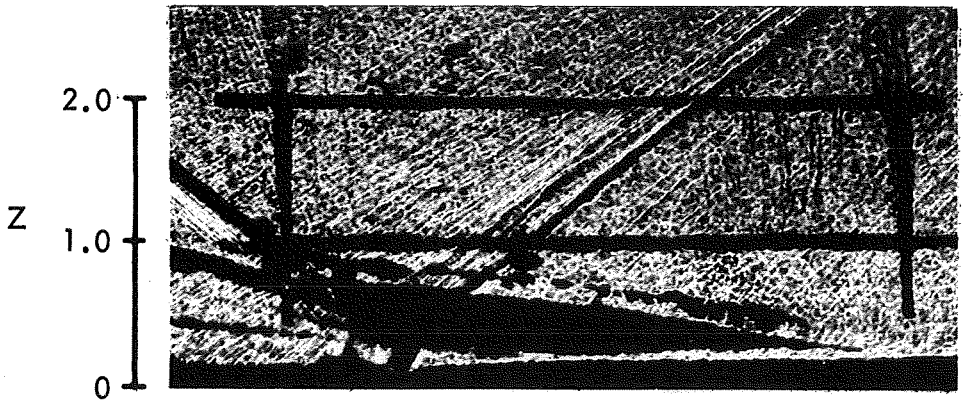

Figure 14 PLATE STATIC PRESSURE AND SHOCK WAVE PATTERN IN THE INTERACTION REGION.

- M_o 2.01
- T_w/T_{to} 0.34
- Wedge Configuration W_8^8
- RE/ℓ 12.2×10^6 per ft.
- q_o 2400 psf.

	M_2	θ_I	θ_R	C_P
Theory ------	1.40	37.7	36.5	0.491
Measure ———	1.41	40.0	42.0	Shown

Run No. 36

Data Off $\mathcal{L}$ ⊡ Left ■ Right

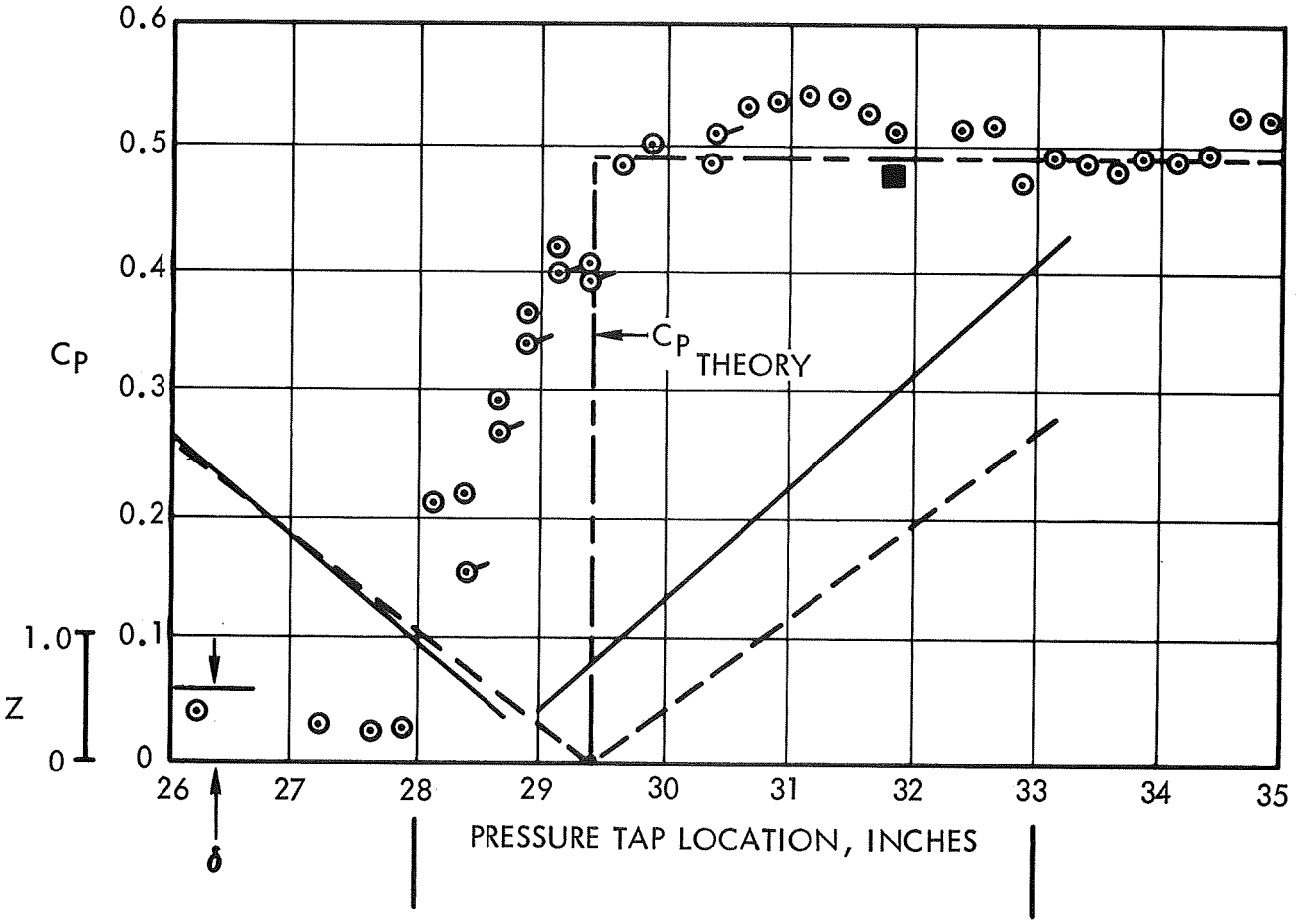

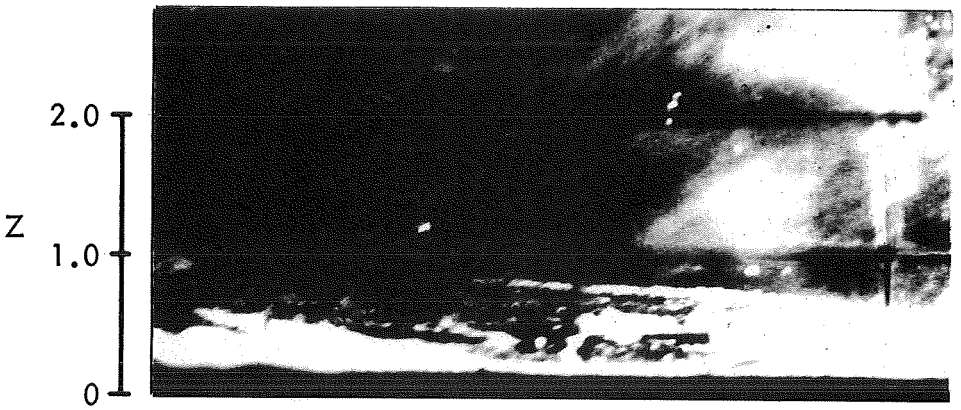

Figure 15 PLATE STATIC PRESSURE AND SHOCK WAVE PATTERN IN THE INTERACTION REGION.

- M_o 2.01
- T_w/T_{to} 0.32
- Wedge Configuration W_6^7
- RE/ℓ 6.4×10^6 per ft.
- q_o 1301 psf.

	M_2	θ_I	θ_R	C_P
Theory -----	1.55	35.6	34.2	0.332
Measure ———	1.57	36.0	38.0	⊙ Shown

Run No. 33
Data Off ℄ ⊡ Left ■ Right

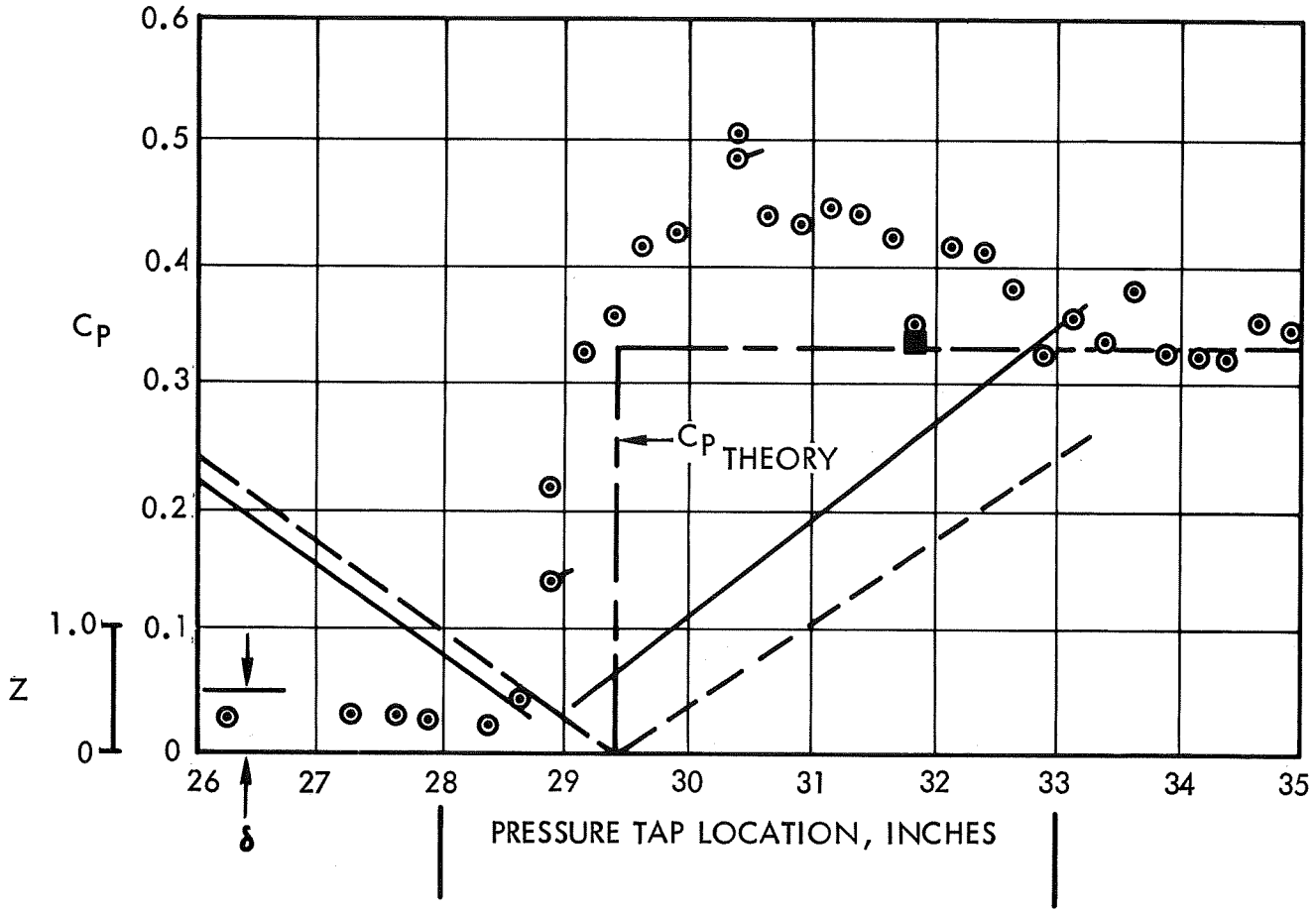

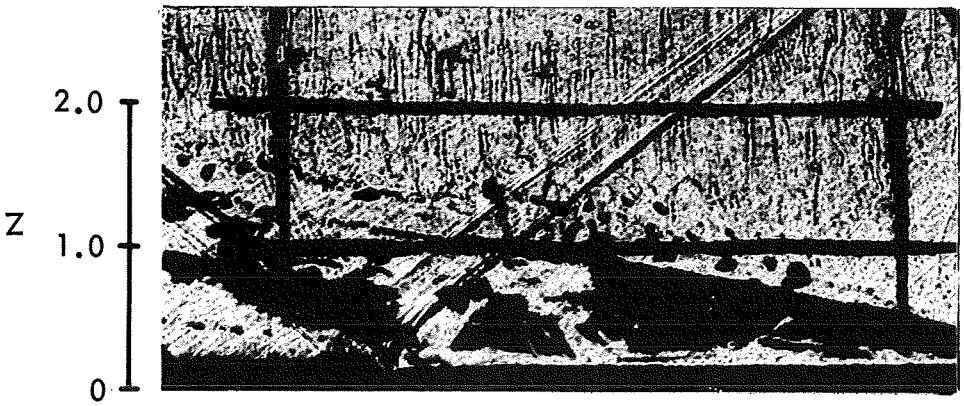

Figure 16 PLATE STATIC PRESSURE AND SHOCK WAVE PATTERN IN THE INTERACTION REGION.

- M_o 2.01
- T_w/T_{to} 0.33
- Wedge Configuration W_8^8
- RE/ℓ 6.4×10^6 per ft.
- q_o 1294 psf.

	M_2	θ_I	θ_R	C_P
Theory ------	1.40	37.7	36.5	0.491
Measure ———	1.39	40.0	40.0	Shown

Run No. 34 (Shadowgraph from Run 35)

Data Off ℄ ⊡ Left ■ Right

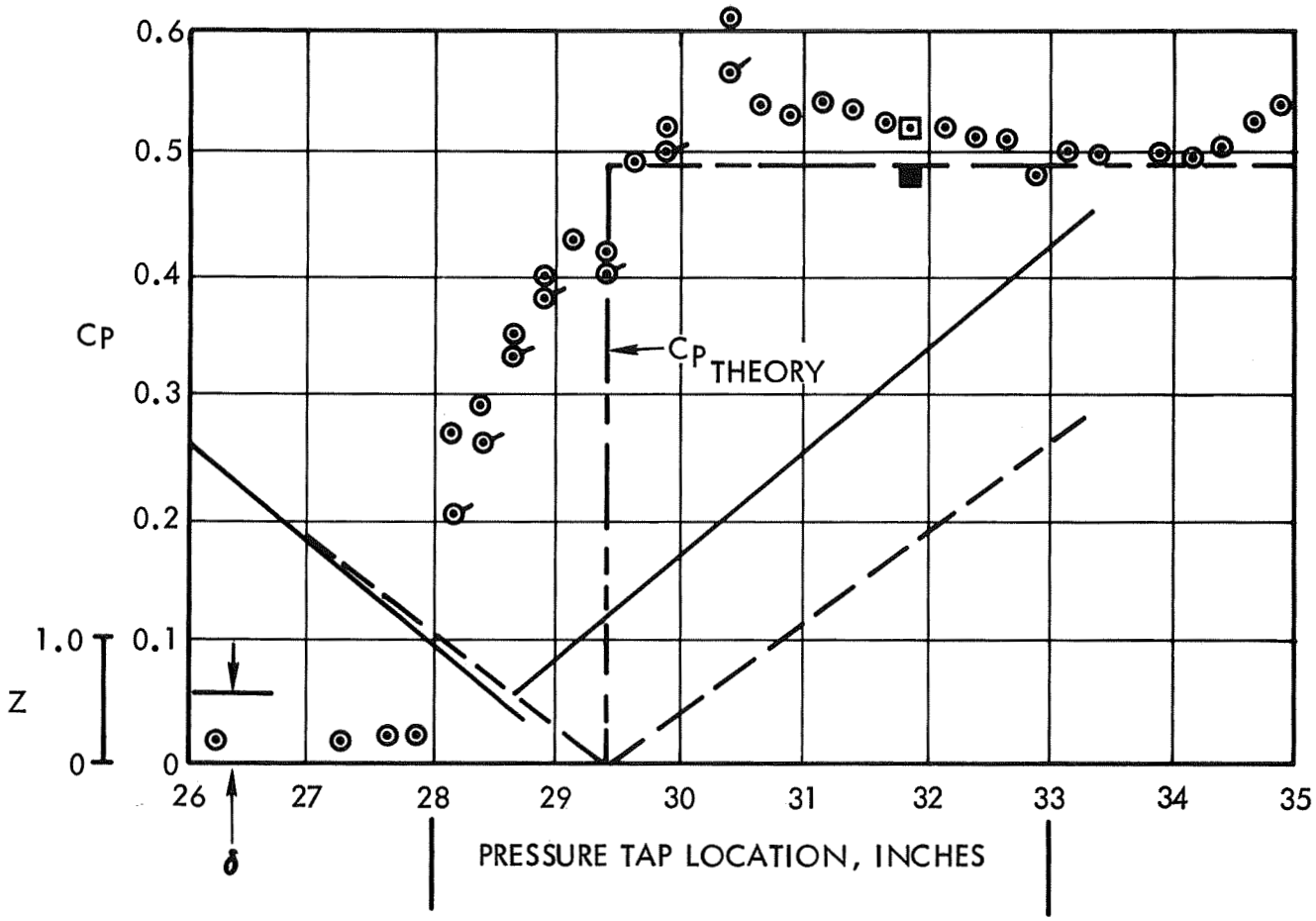

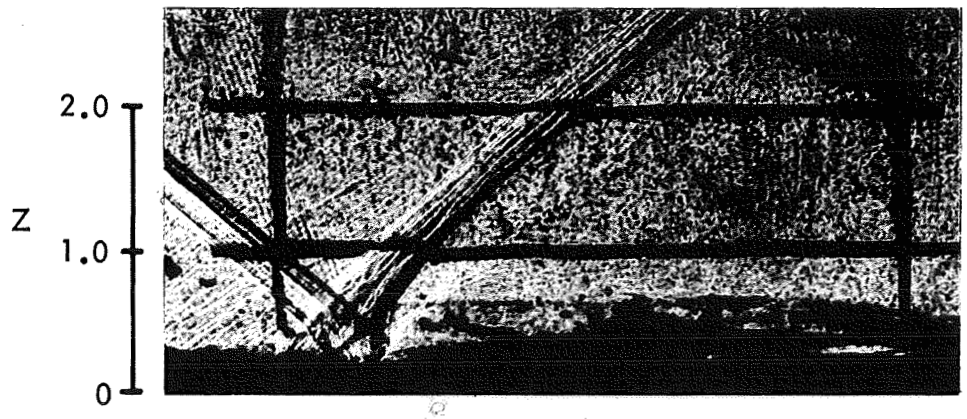

Figure 17 PLATE STATIC PRESSURE AND SHOCK WAVE PATTERN IN THE INTERACTION REGION.

- M_o 4.2
- T_w/T_{to} 0.32
- Wedge Configuration $W_8{}^3$
- RE/ℓ 20.2×10^6 per. ft.
- q_o 2147 psf

	M_2	θ_1	θ_R	C_P
Theory -----	3.10	20.2	14.5	.328
Measure ———	3.12	21.5	17.5	⊙ Shown

Run No. 43

Data Off ℄ ⊡ Left ■ Right

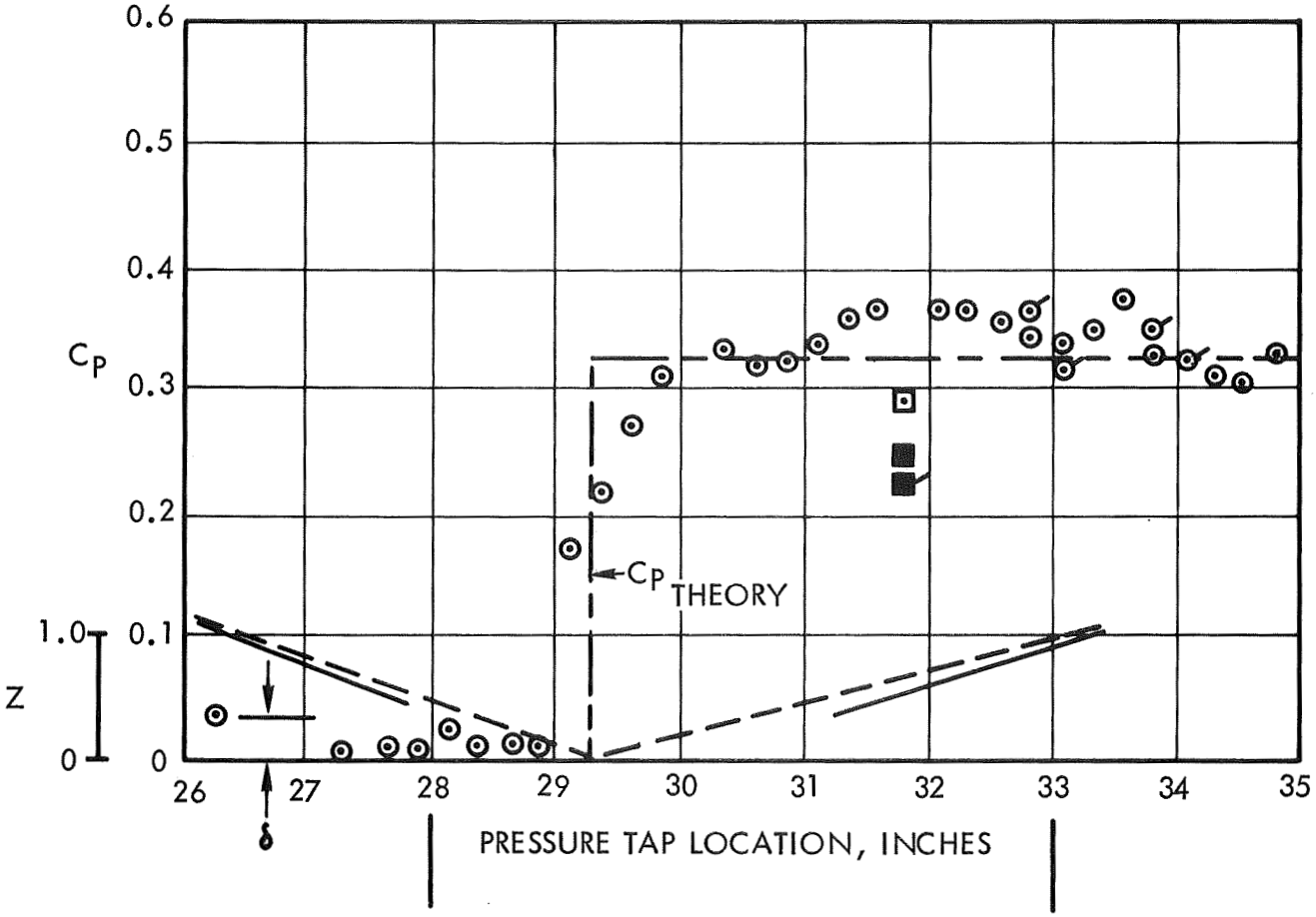

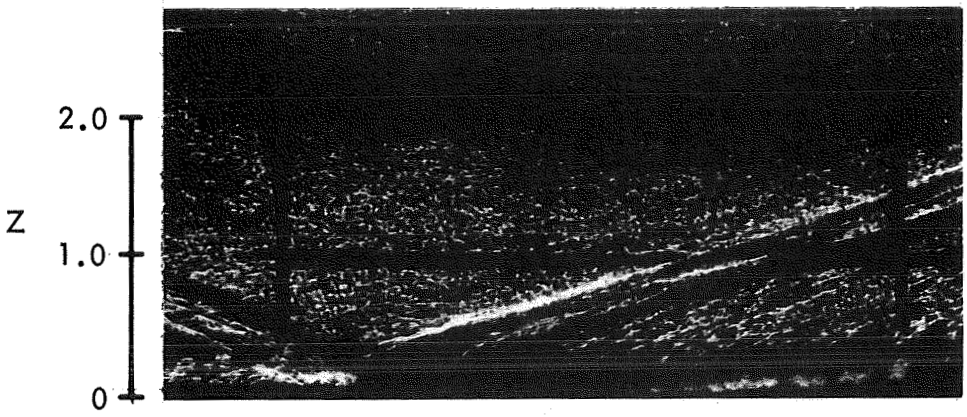

Figure 18 PLATE STATIC PRESSURE AND SHOCK WAVE PATTERN IN THE INTERACTION REGION.

- M_o 4.2
- T_w/T_{to} 0.32
- Wedge Configuration $W_6 2$
- RE/ℓ 14.5×10^6 per ft.
- q_o 1555 psf.

	M_2	θ_I	θ_R	C_P
Theory -----	3.30	18.5	13.8	0.207
Measure ———	3.46	21.0	15.0	⊙ Shown

Run No. 46

Data Off ℄ ⊡ Left ■ Right

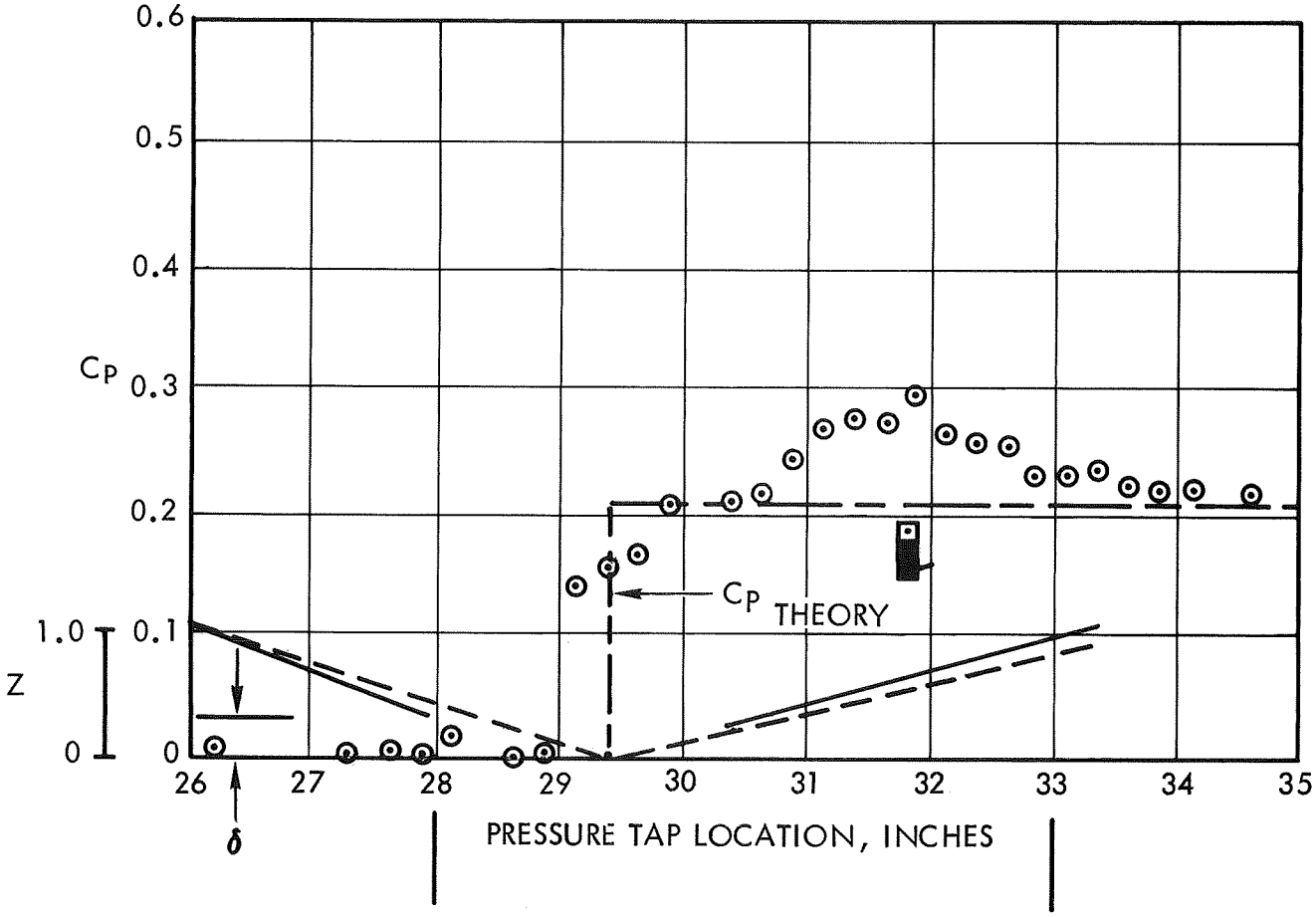

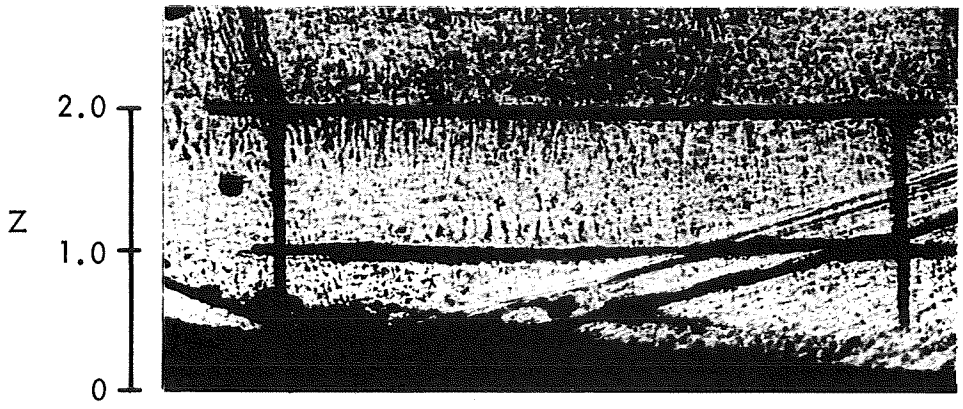

Figure 19 PLATE STATIC PRESSURE AND SHOCK WAVE PATTERN IN THE INTERACTION REGION.

- M_o 4.2
- T_w/T_{to} 0.32
- Wedge Configuration $W_8{}^3$
- RE/ℓ 14.5×10^6 per ft.
- q_o 1610

	M_2	θ_I	θ_R	C_P
Theory ------	3.10	20.2	14.5	0.328
Measure ———	3.15	27.0	17.0	⊙ Shown

Run No. 44

DATA OFF ℄ ⊡ LEFT ■ RIGHT

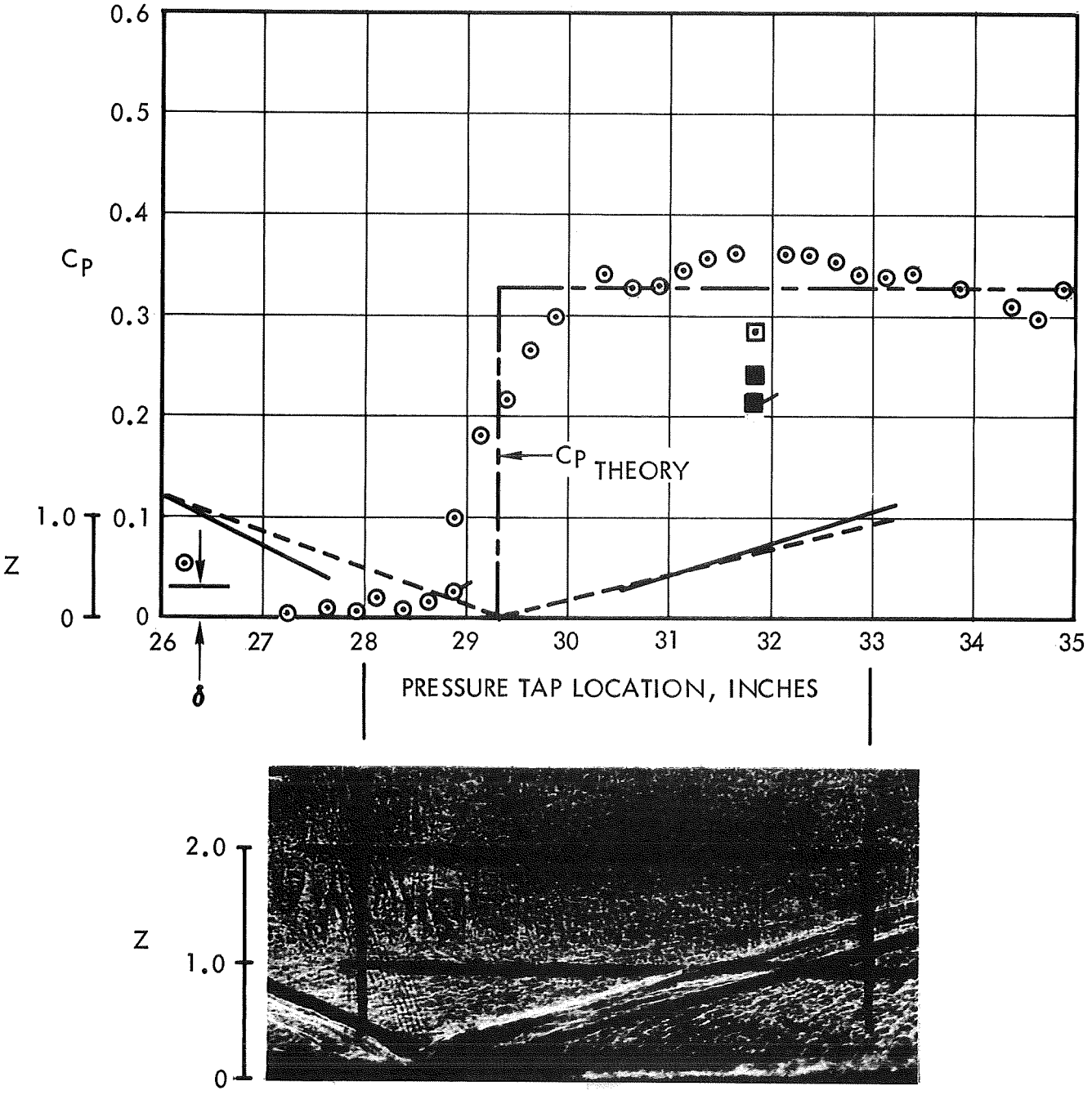

Figure 20 PLATE STATIC PRESSURE AND SHOCK WAVE PATTERN IN THE INTERACTION REGION.

M_o 3.18 RE/1 14.5×10^6 per ft. RUN 7

T_w/T_{to} 0.96 T_{to} 535 ^oR

Probe Station XP(0) = 27.00 inches

δ = 0.412 inches $T_{t'e}$ = 519 ^oR M_e = 3.08

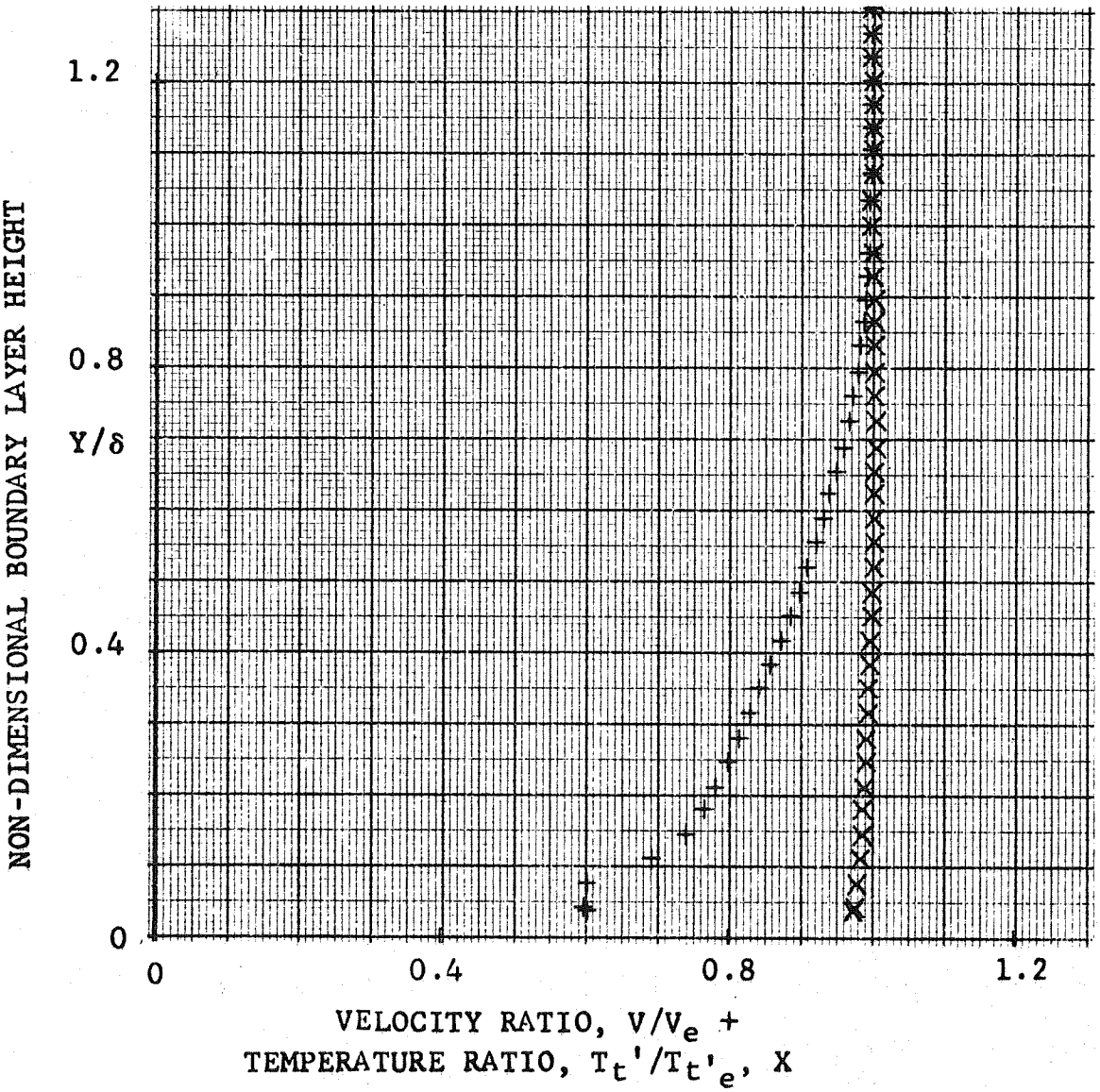

FIGURE 21.- NON-DIMENSIONAL VELOCITY AND TEMPERATURE PROFILES (UPSTREAM OF INTERACTION)

M_o 3.18 RE/1 14.5×10^6 per ft. RUN 11

T_w/T_{to} 0.96 T_{to} 541 ^oR

Wedge Configuration W_6^5

Probe Station XP(1) = 31.25 inches

δ = 0.422 inches $T_{t'_e}$ = 527 ^oR M_e = 2.68

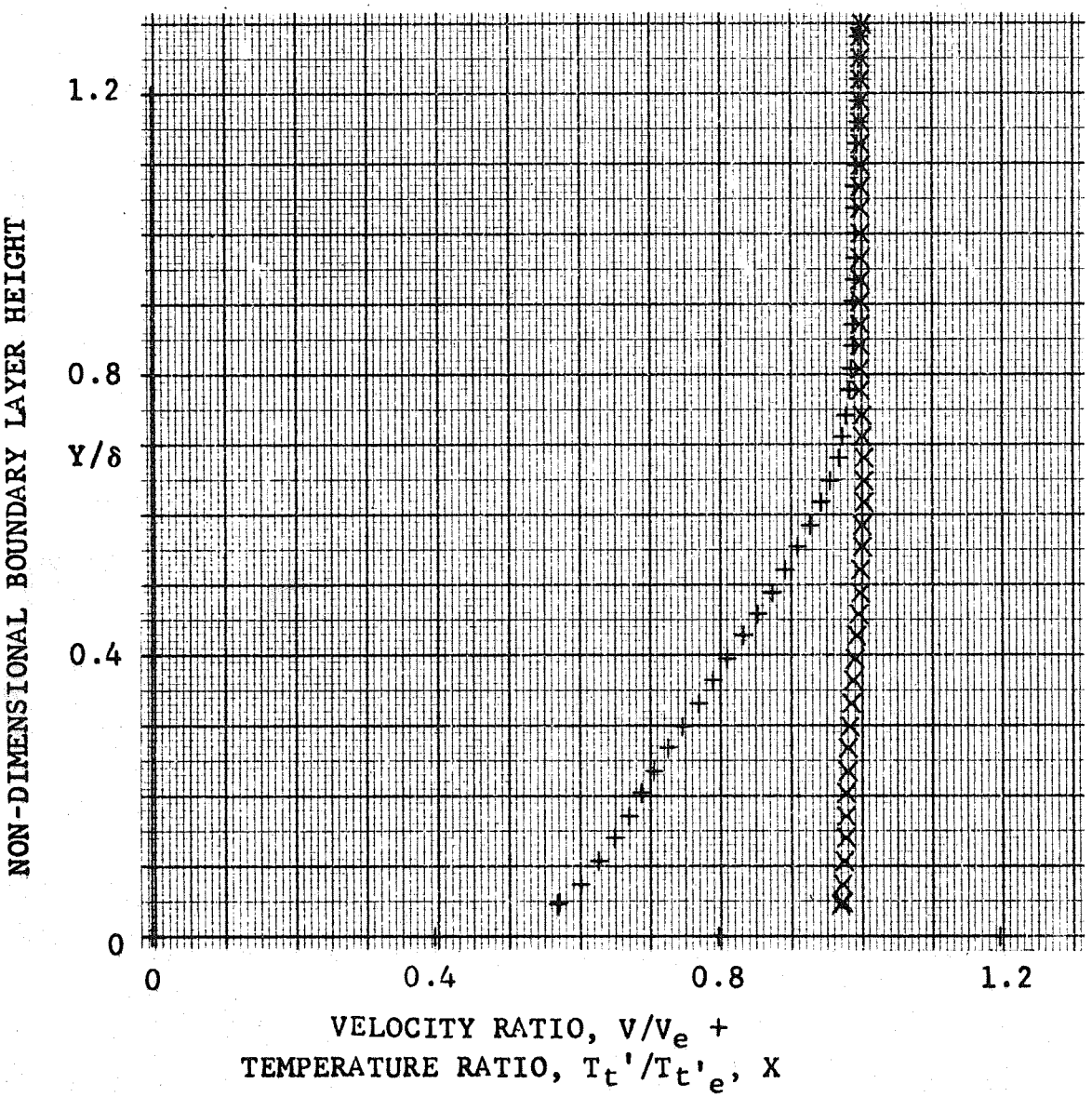

FIGURE 22.-NON-DIMENSIONAL VELOCITY AND TEMPERATURE PROFILES (INTERACTION REGION)

M_o 3.18 RE/1 14.5×10^6 per ft. RUN 8

T_w/T_{to} 0.96 T_{to} 543 ^oR

Wedge Configuration W_6^5

Probe Station XP(2) = 36.00 inches

$\delta = 0.473$ inches $T_{t'_e} = 531$ ^oR $M_e = 2.64$

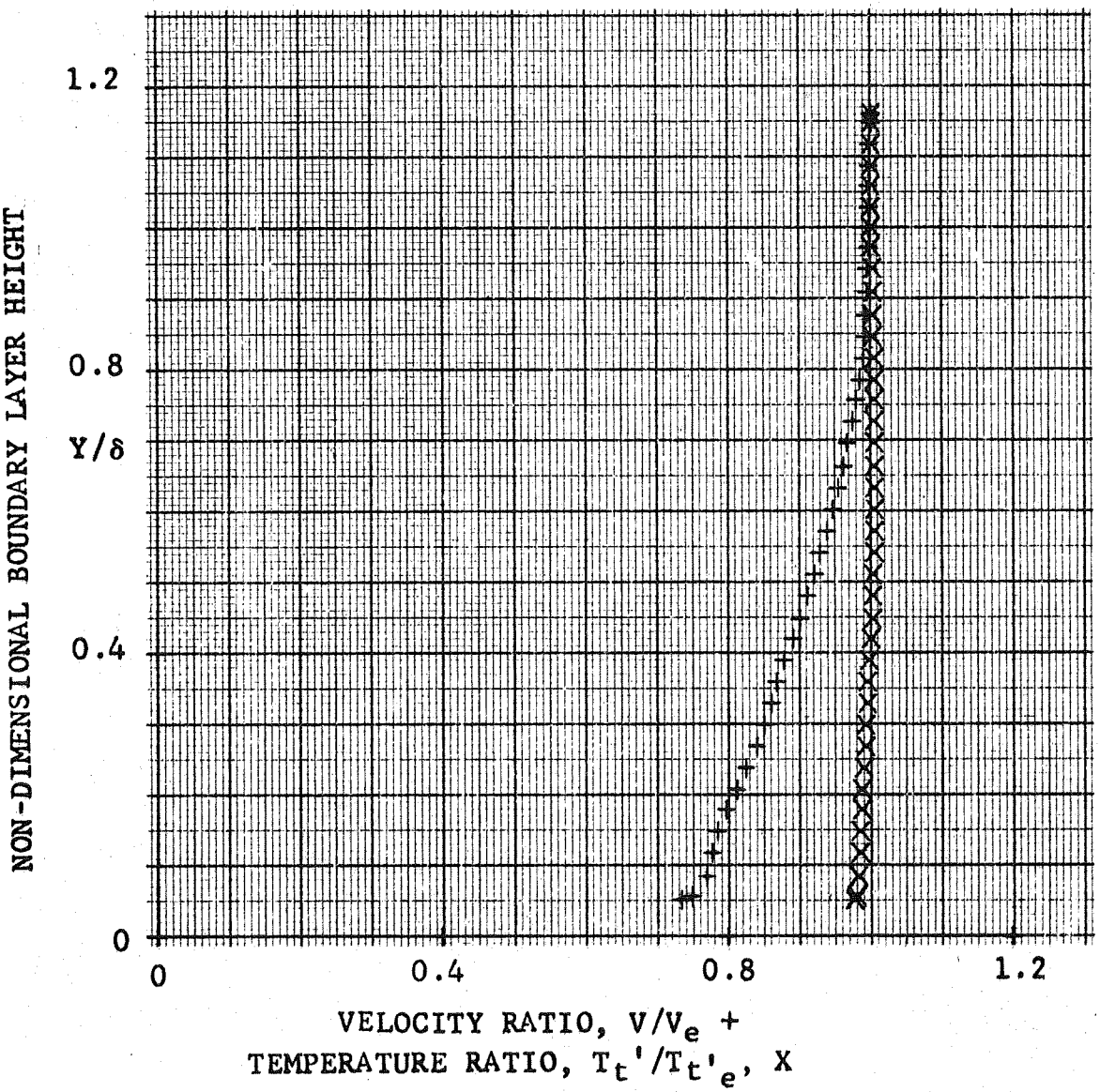

FIGURE 23.-NON-DIMENSIONAL VELOCITY AND TEMPERATURE PROFILES (DOWNSTREAM OF INTERACTION)

M_o 3.18 RE/1 14.5×10^6 per ft. RUN 10

T_w/T_{to} 0.96 T_{to} 536 ^oR

Wedge Configuration W_8^6

Probe Station XP(1) = 31.25 inches

δ = 0.424 inches $T_{t'_e}$ = 522 ^oR M_e = 2.40

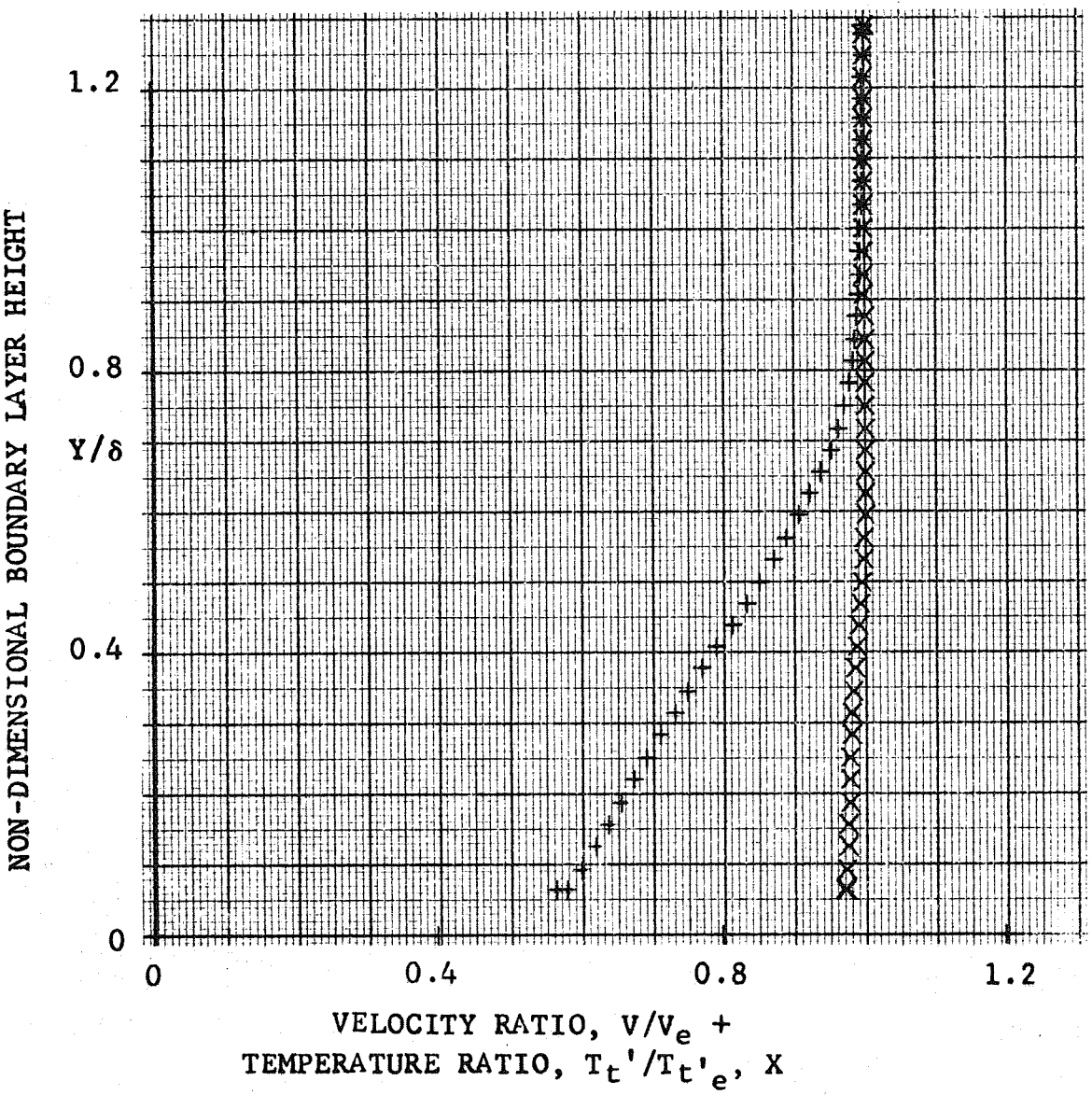

FIGURE 24.- NON-DIMENSIONAL VELOCITY AND TEMPERATURE PROFILES (INTERACTION REGION)

M_o 3.18 RE/1 14.5×10^6 per ft. RUN 9

T_w/T_{to} 0.96 T_{to} 537 ^oR

Wedge Configuration $W_8{}^6$

Probe Station XP(2) = 36.00 inches

δ = 0.552 inches $T_{t'_e}$ = 527 ^oR M_e = 2.43

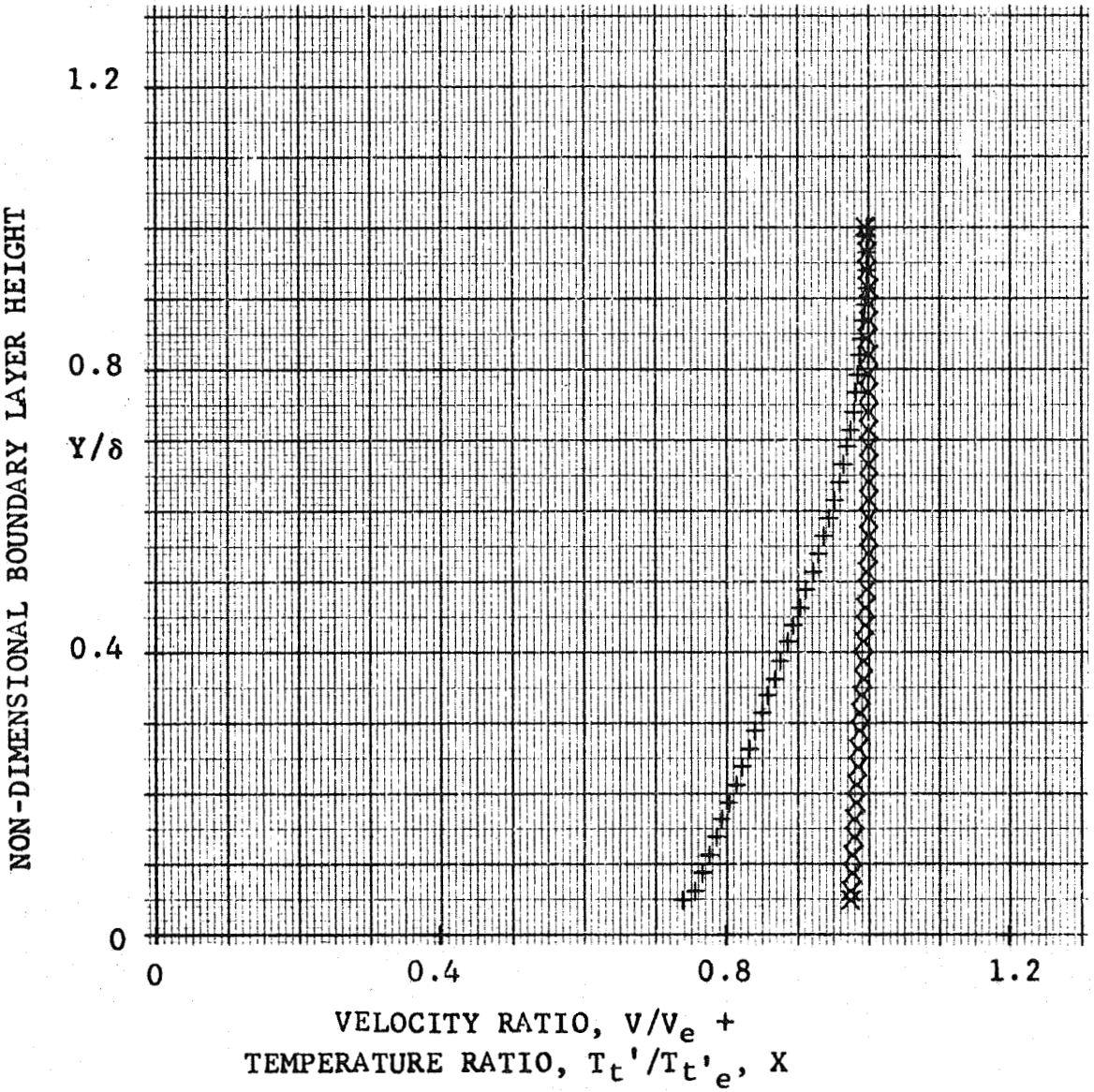

FIGURE 25.- NON-DIMENSIONAL VELOCITY AND TEMPERATURE PROFILES (DOWNSTREAM OF INTERACTION)

M_o 3.18 RE/1 14.5×10^6 per ft. RUN 22

T_w/T_{to} 0.30 T_{to} 540 ^oR

Probe Station XP(0) = 27.00 inches

$\delta = 0.408$ inches $T_{t'_e} = 530\ ^oR$ $M_e = 3.22$

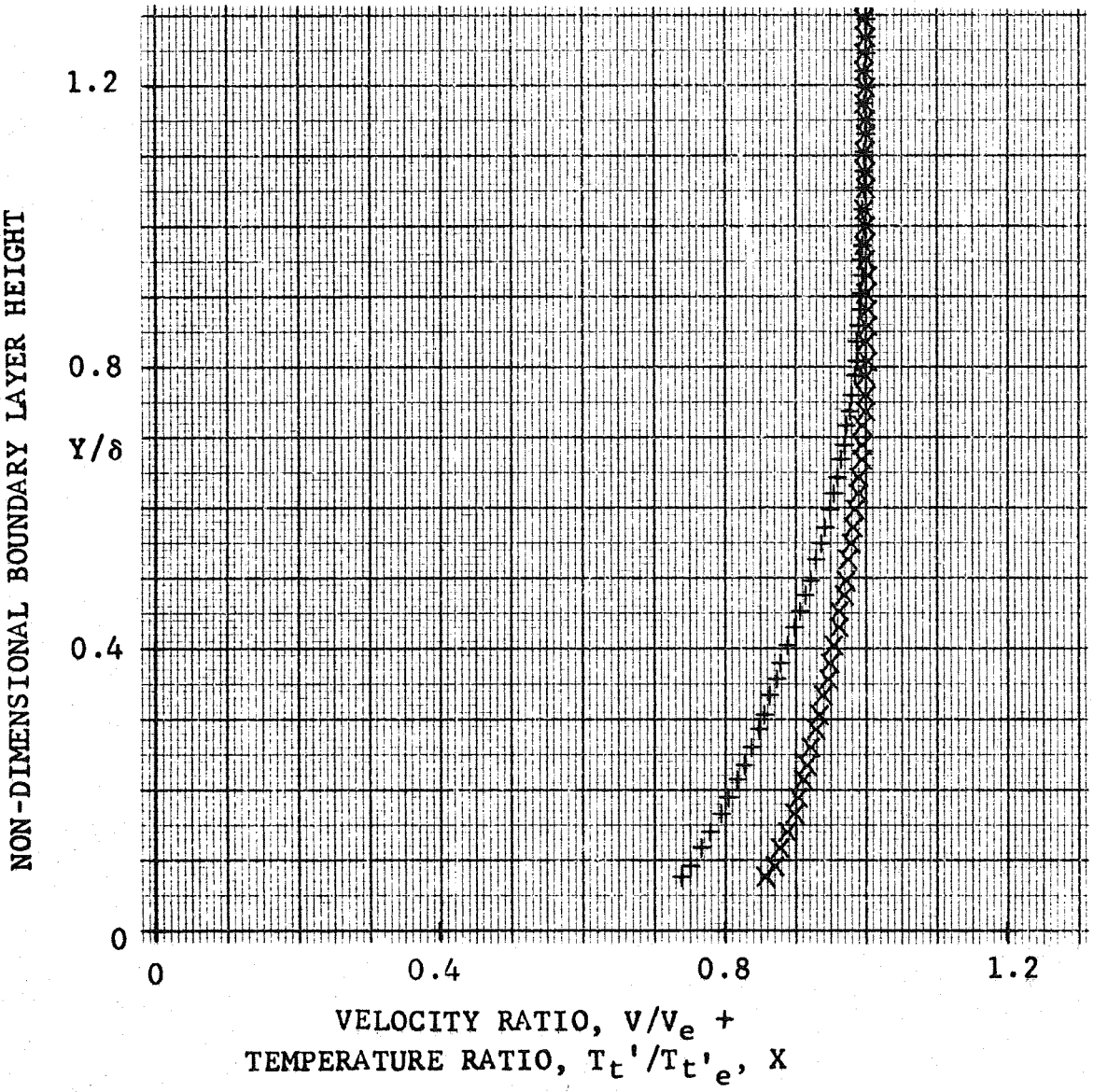

FIGURE 26.- NON-DIMENSIONAL VELOCITY AND TEMPERATURE PROFILES (UPSTREAM OF INTERACTION)

M_o 3.18 RE/1 14.5×10^6 per ft. RUN 29

T_w/T_{to} 0.30 T_{to} 543 ^oR

Wedge Configuration W_6^5

Probe Station XP(1) = 31.25 inches

δ = 0.376 inches $T_{t'_e}$ = 536 ^oR M_e = 2.68

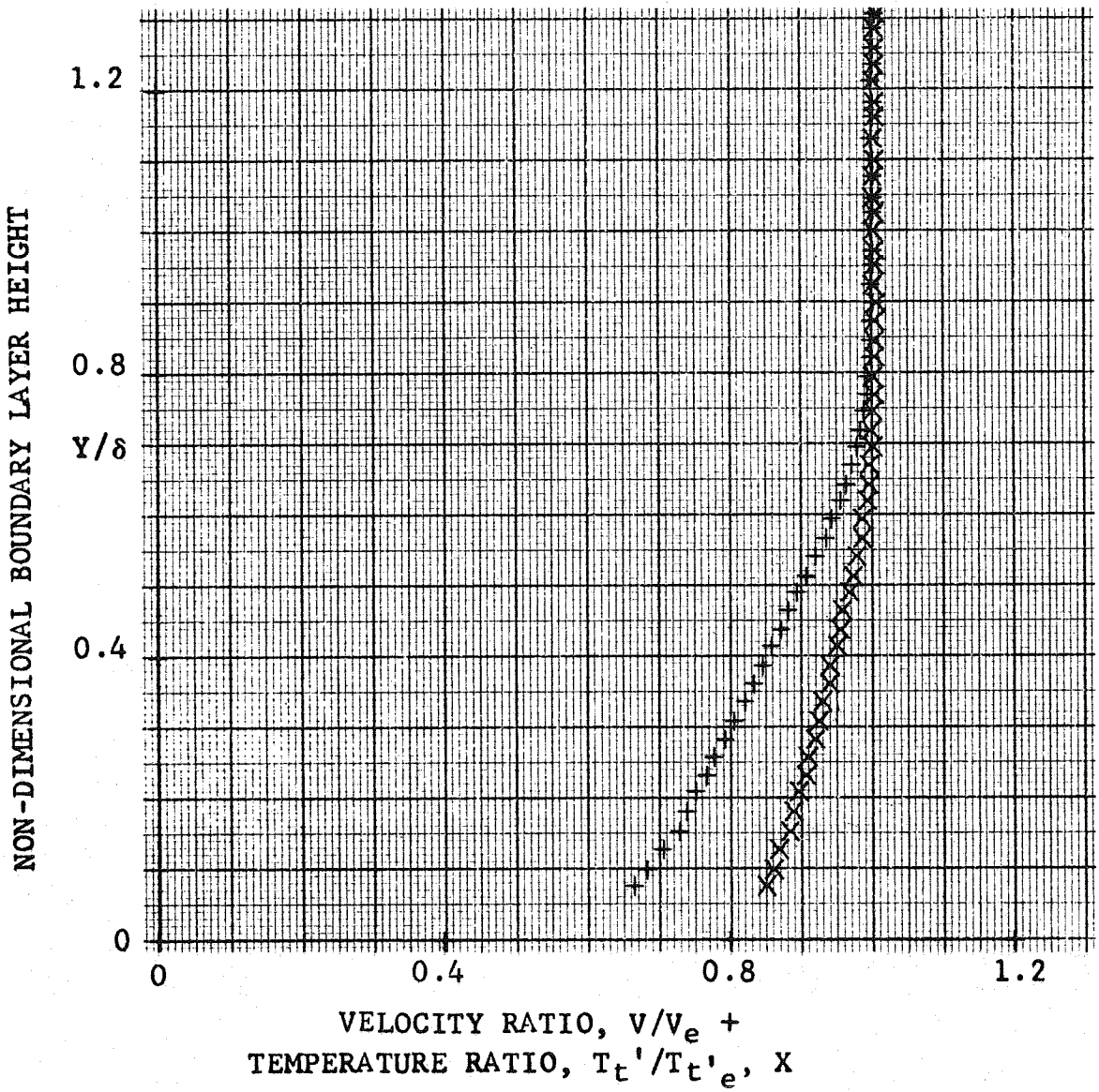

FIGURE 27.-NON-DIMENSIONAL VELOCITY AND TEMPERATURE PROFILES (INTERACTION REGION)

M_o 3.18 RE/1 14.5×10^6 per ft. RUN 21

T_w/T_{to} 0.30 T_{to} 542 ^oR

Wedge Configuration $W_6{}^5$

Probe Station XP(2) = 36.00 inches

$\delta = 0.469$ inches $T_t'_e = 534\ ^oR$ $M_e = 2.65$

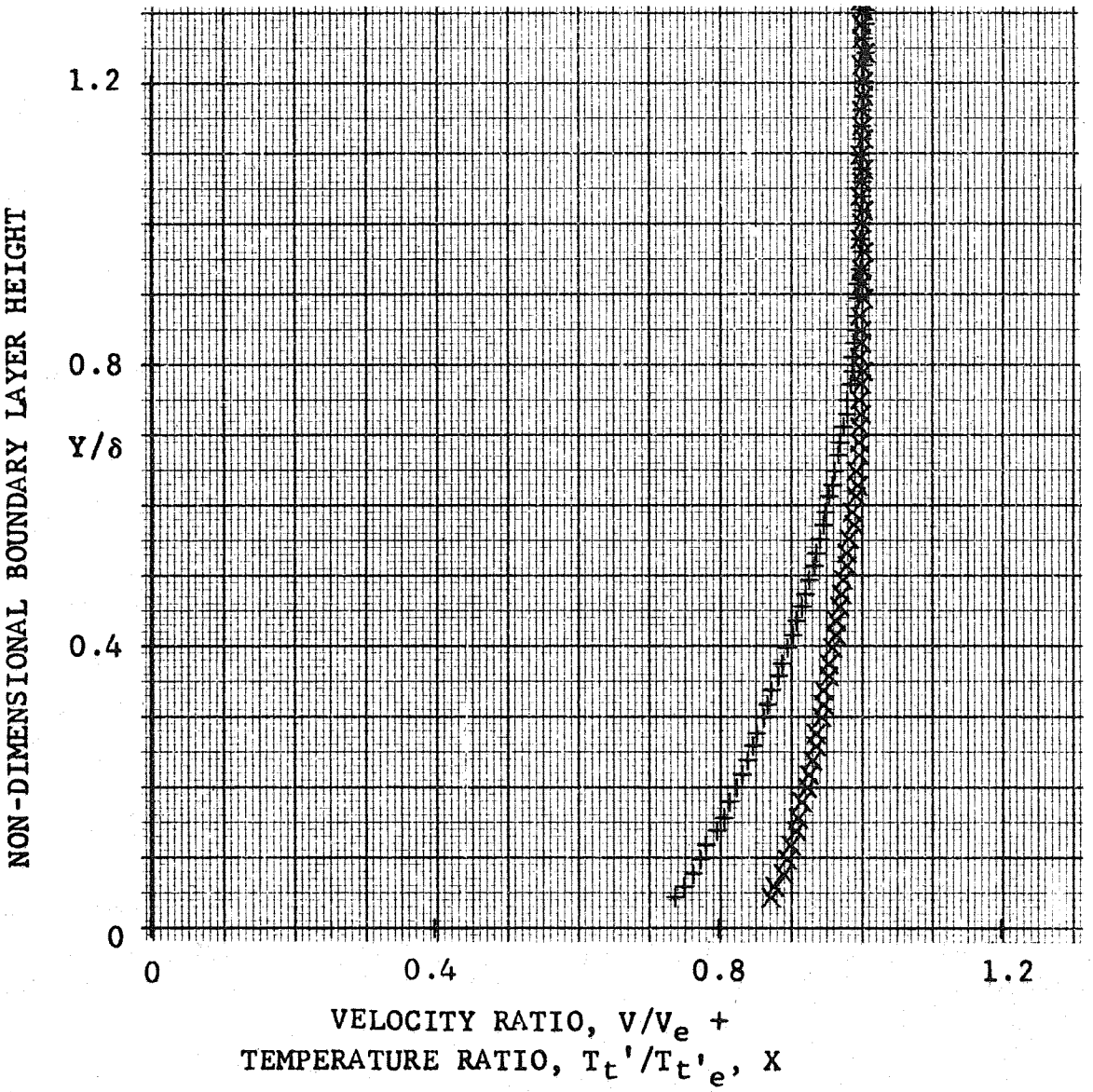

FIGURE 28.- NON-DIMENSIONAL VELOCITY AND TEMPERATURE PROFILES (DOWNSTREAM OF INTERACTION)

M_o 3.18 RE/1 14.5×10^6 per ft. RUN 28

T_w/T_{to} 0.30 T_{to} 542 ^oR

Wedge Configuration W_8^6

Probe Station XP(1) = 31.25 inches

δ = 0.385 inches $T_{t'e}$ = 535 ^oR M_e = 2.43

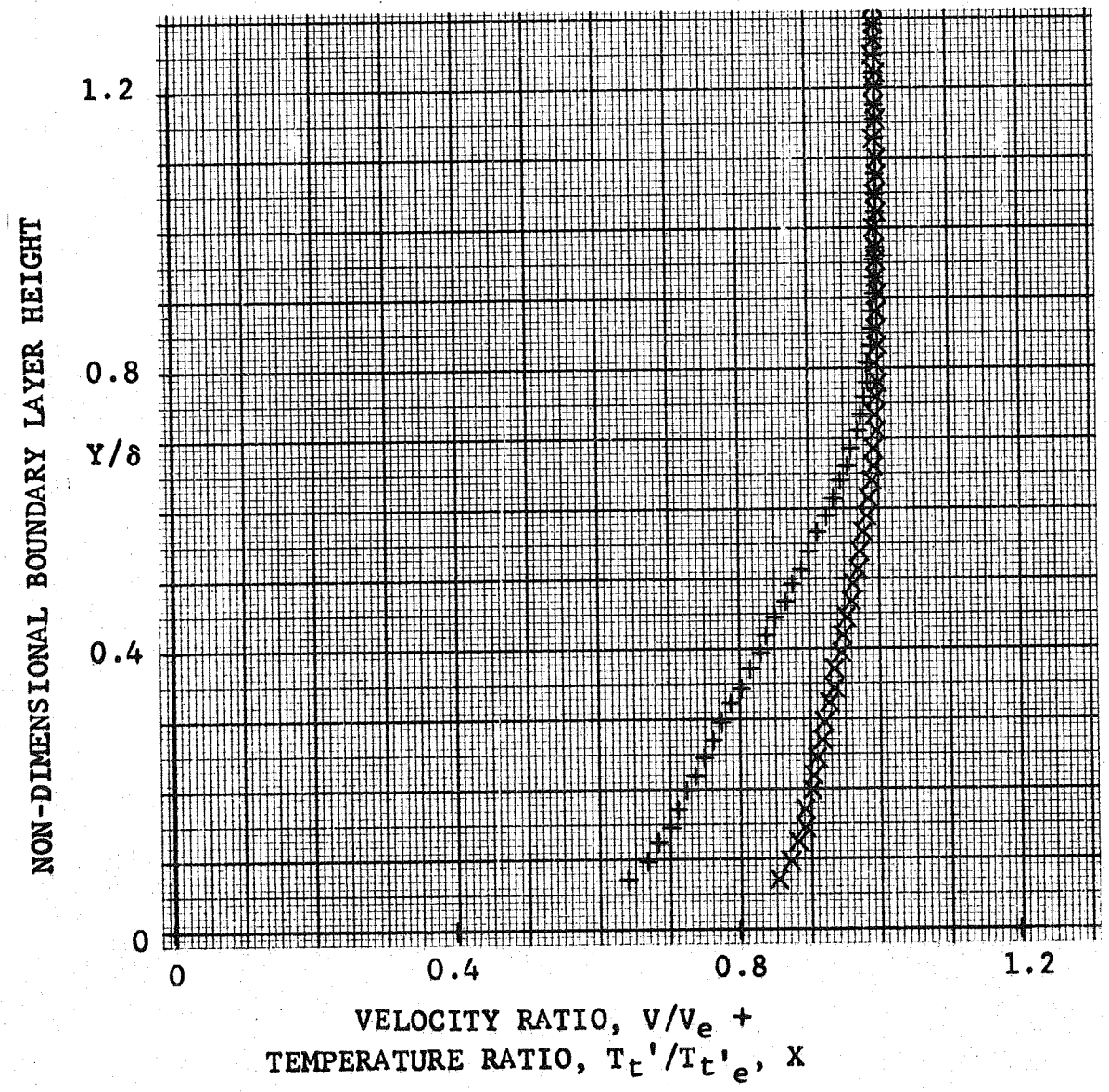

FIGURE29.- NON-DIMENSIONAL VELOCITY AND TEMPERATURE PROFILES (INTERACTION REGION)

M_o 3.18 RE/1 14.5×10^6 per ft. RUN 20

T_w/T_{to} 0.30 T_{to} 549 ^oR

Wedge Configuration W_8^6

Probe Station XP(2) = 36.00 inches

δ = 0.529 inches $T_{t'_e}$ = 545 ^oR M_e = 2.47

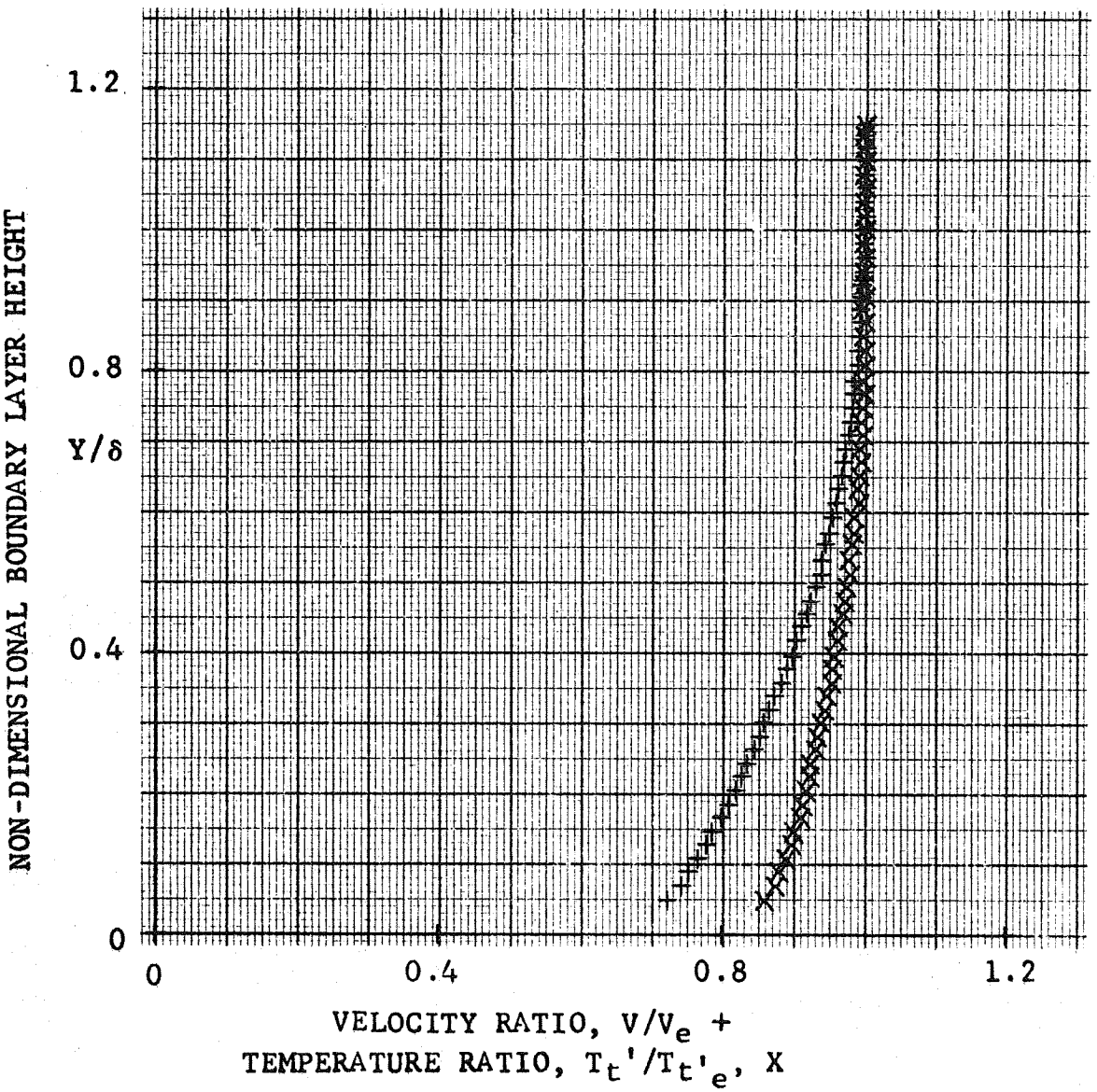

FIGURE 30.-NON-DIMENSIONAL VELOCITY AND TEMPERATURE PROFILES (DOWNSTREAM OF INTERACTION)

M_o 3.18 RE/1 11.5 x 10^6 per ft. RUN 23

T_w/T_{to} 0.31 T_{to} 543 ^oR

Probe Station XP(0) = 27.00 inches

δ = 0.378 inches $T_{t'e}$ = 536 ^oR M_e = 3.37

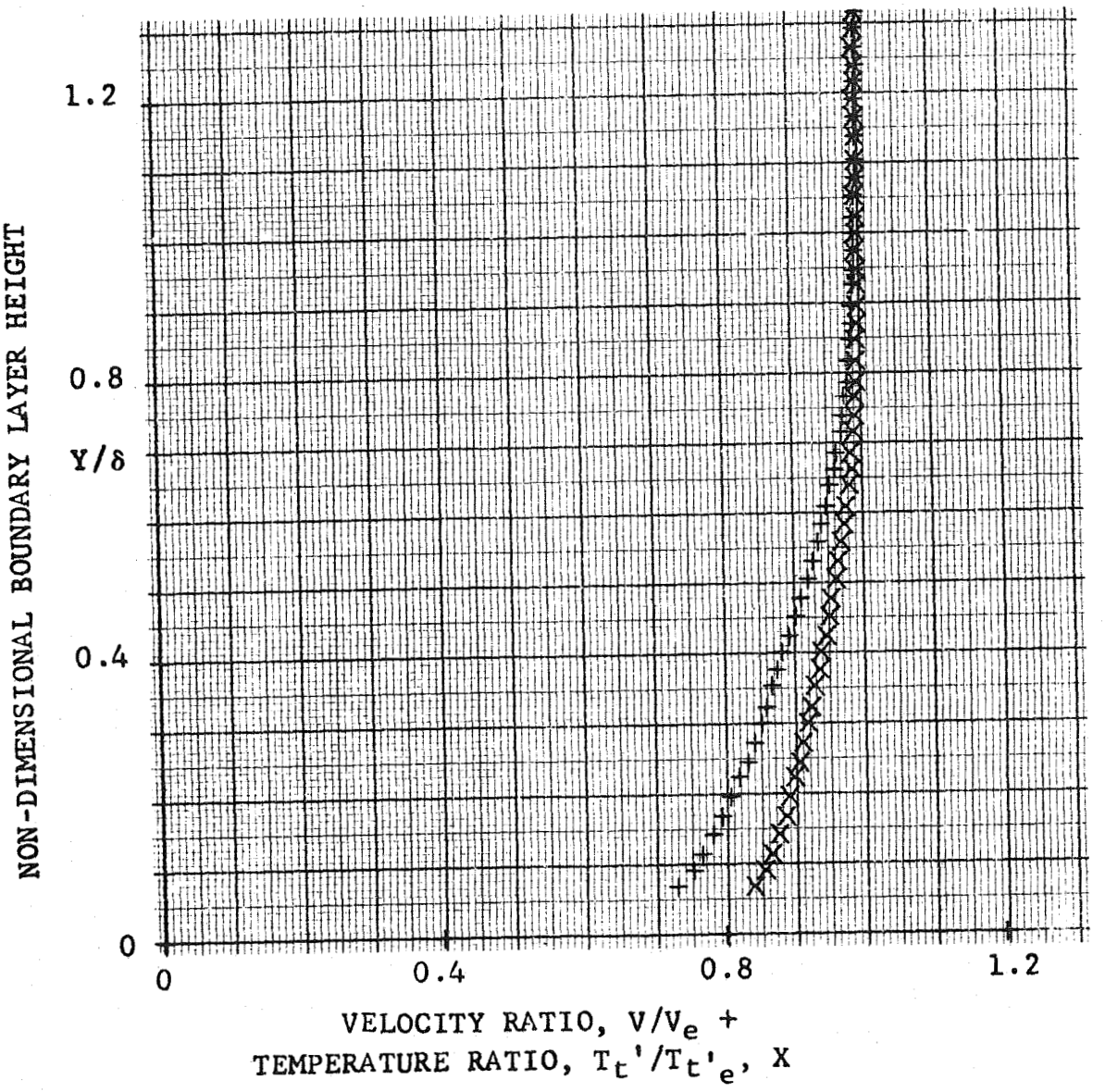

FIGURE 31.- NON-DIMENSIONAL VELOCITY AND TEMPERATURE PROFILES (UPSTREAM OF INTERACTION)

M_o 3.18 RE/1 11.5 x 10^6 per ft. RUN 30

T_w/T_{to} 0.31 T_{to} 541 ^oR

Wedge Configuration W_6^5

Probe Station XP(1) = 31.25 inches

δ = 0.374 inches $T_{t'_e}$ = 535 ^oR M_e = 2.64

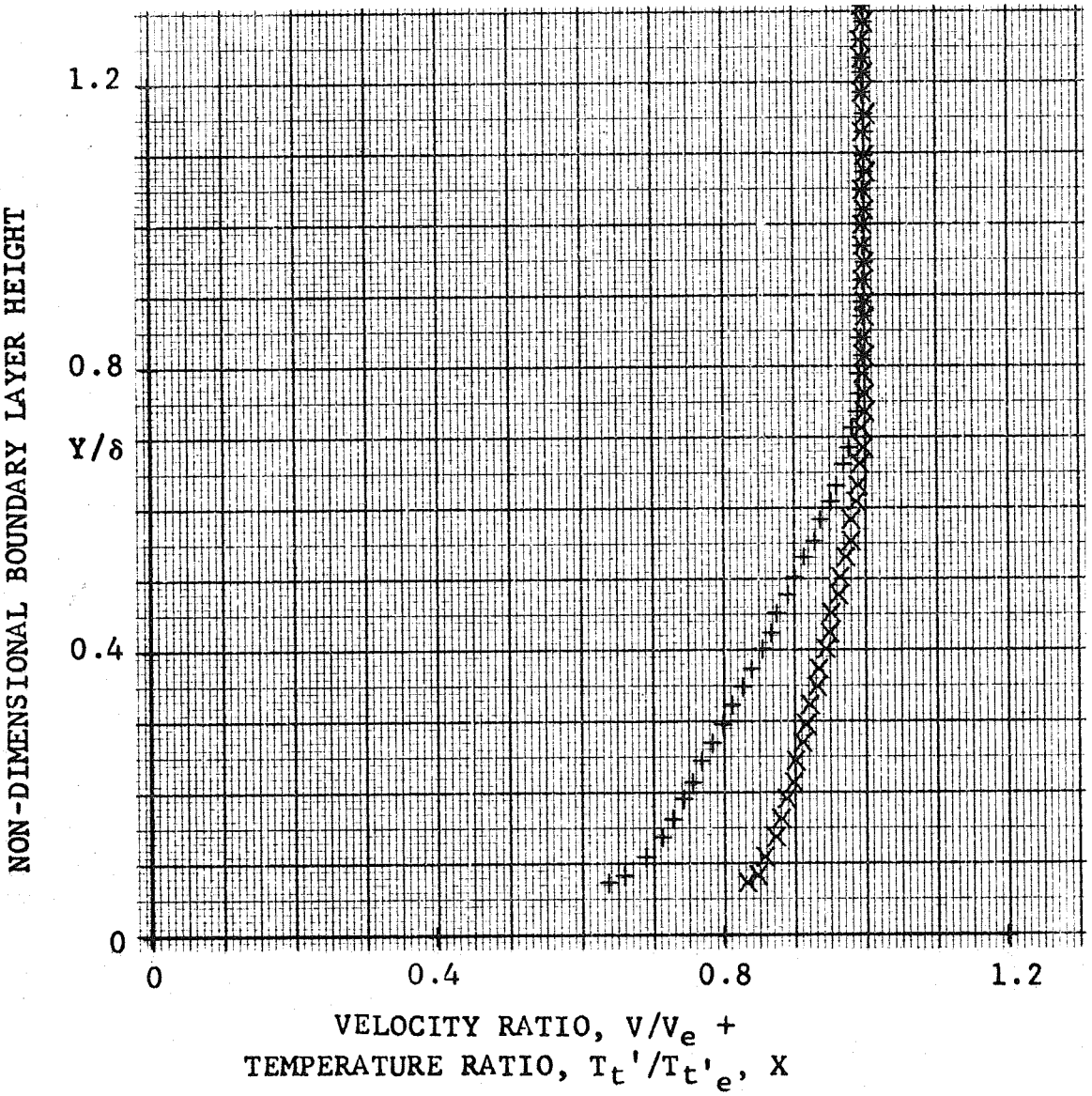

FIGURE 32.- NON-DIMENSIONAL VELOCITY AND TEMPERATURE PROFILES (INTERACTION REGION)

M_o 3.18 RE/1 11.5×10^6 per ft. RUN 14

T_w/T_{to} 0.31 T_{to} 534 ^oR

Wedge Configuration W_6^5

Probe Station XP(2) = 36.00 inches

δ = 0.446 inches $T_t'_e$ = 523 ^oR M_e = 2.61

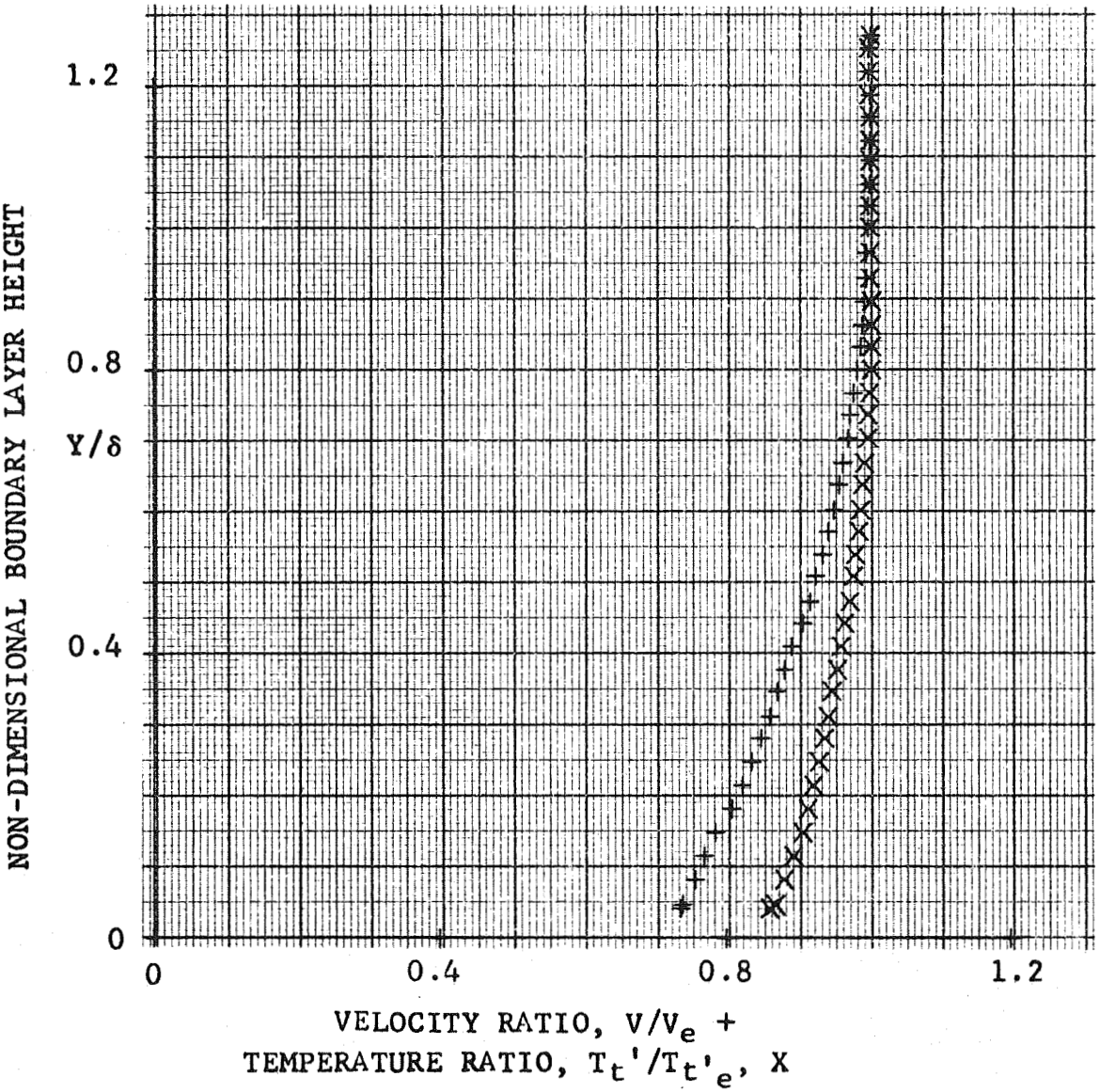

FIGURE 33.- NON-DIMENSIONAL VELOCITY AND TEMPERATURE PROFILES (DOWNSTREAM OF INTERACTION)

M_o 3.18 RE/1 11.5×10^6 per ft. RUN 27

T_w/T_{to} 0.31 T_{to} 541 ^oR

Wedge Configuration W_8^6

Probe Station XP(1) = 31.25 inches

δ = 0.381 inches $T_{t'_e}$ = 535 ^oR M_e = 2.43

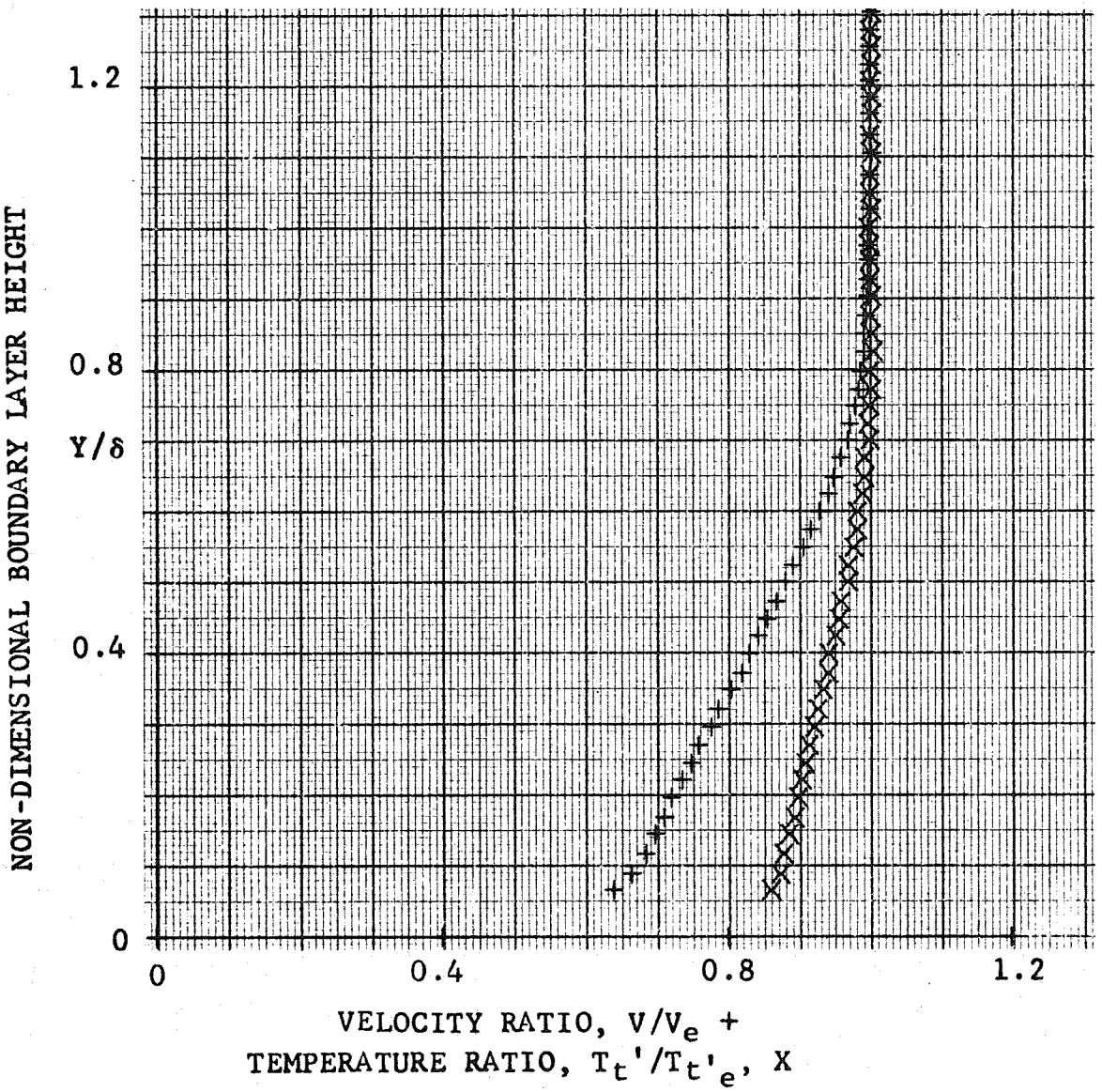

FIGURE 34.- NON-DIMENSIONAL VELOCITY AND TEMPERATURE PROFILES (INTERACTION REGION)

M_o 3.18 RE/1 11.5×10^6 per ft. RUN 19

T_w/T_{to} 0.31 T_{to} 544 ^oR

Wedge Configuration W_8^6

Probe Station XP(2) = 36.00 inches

δ = 0.509 inches $T_{t'_e}$ = 541 ^oR M_e = 2.42

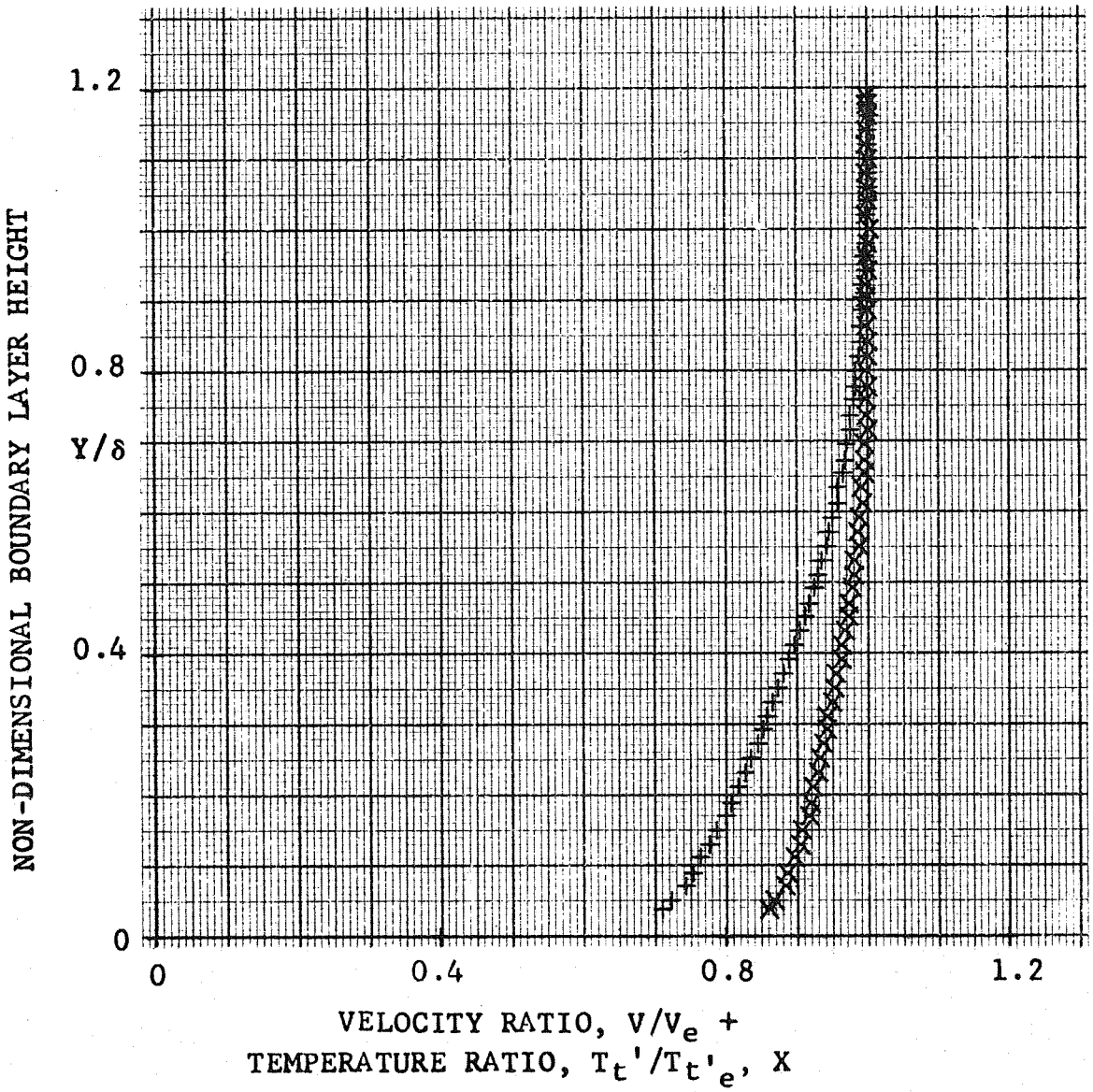

FIGURE 35.- NON-DIMENSIONAL VELOCITY AND TEMPERATURE PROFILES (DOWNSTREAM OF INTERACTION)

M_o 3.18 RE/1 10.3 x 10^6 per ft. RUN 25

T_w/T_{to} 0.31 T_{to} 544 ^oR

Probe Station XP(0) = 27.00 inches

δ = 0.407 inches $T_{t'_e}$ = 538 ^oR M_e = 3.31

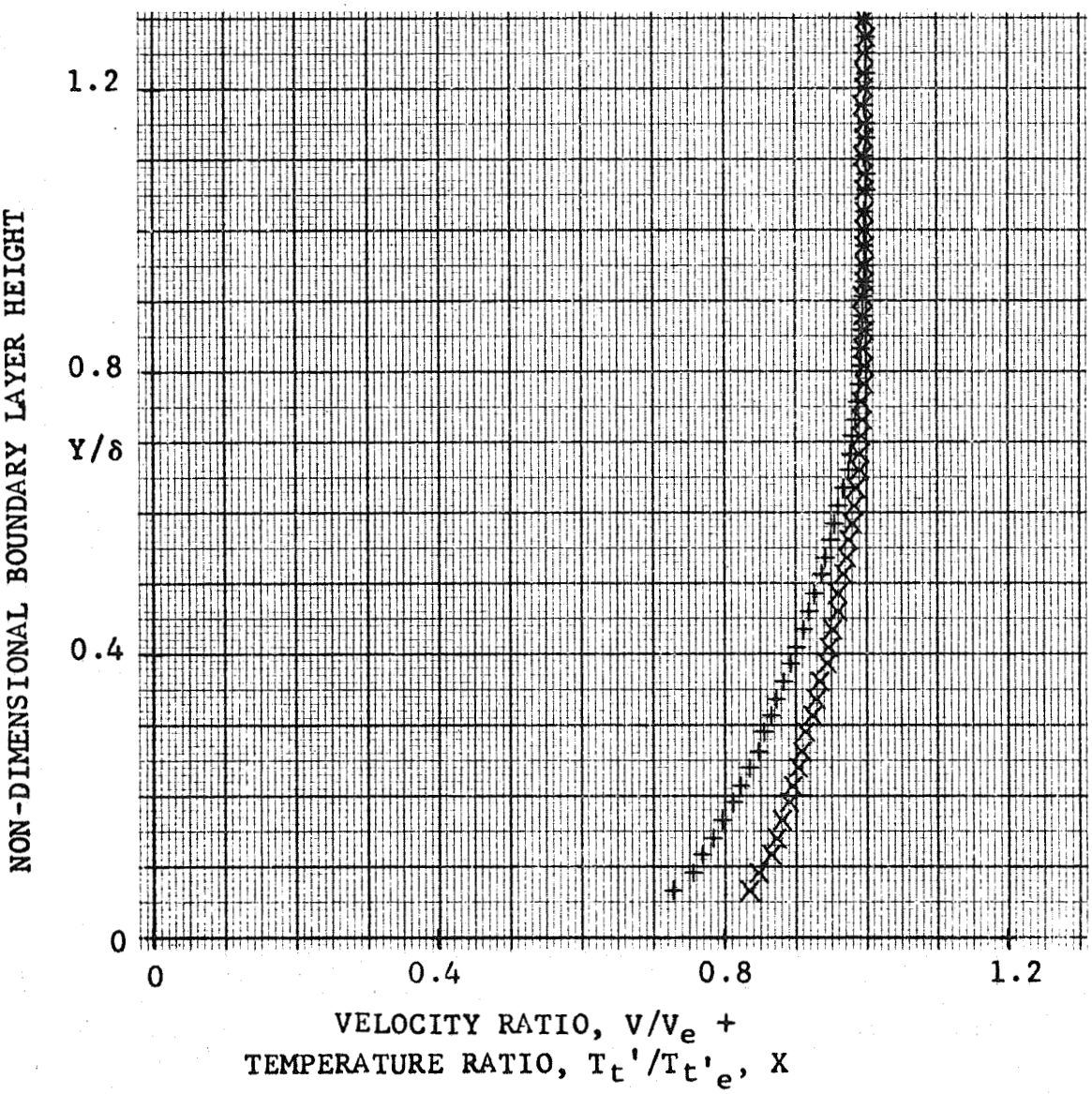

FIGURE36.- NON-DIMENSIONAL VELOCITY AND TEMPERATURE PROFILES (UPSTREAM OF INTERACTION)

M_o 3.18 RE/1 10.3×10^6 per ft. RUN 31

T_w/T_{to} 0.31 T_{to} 537 ^oR

Wedge Configuration W_6^5

Probe Station XP(1) = 31.25 inches

δ = 0.350 inches $T_{t'_e}$ = 530 ^oR M_e = 2.64

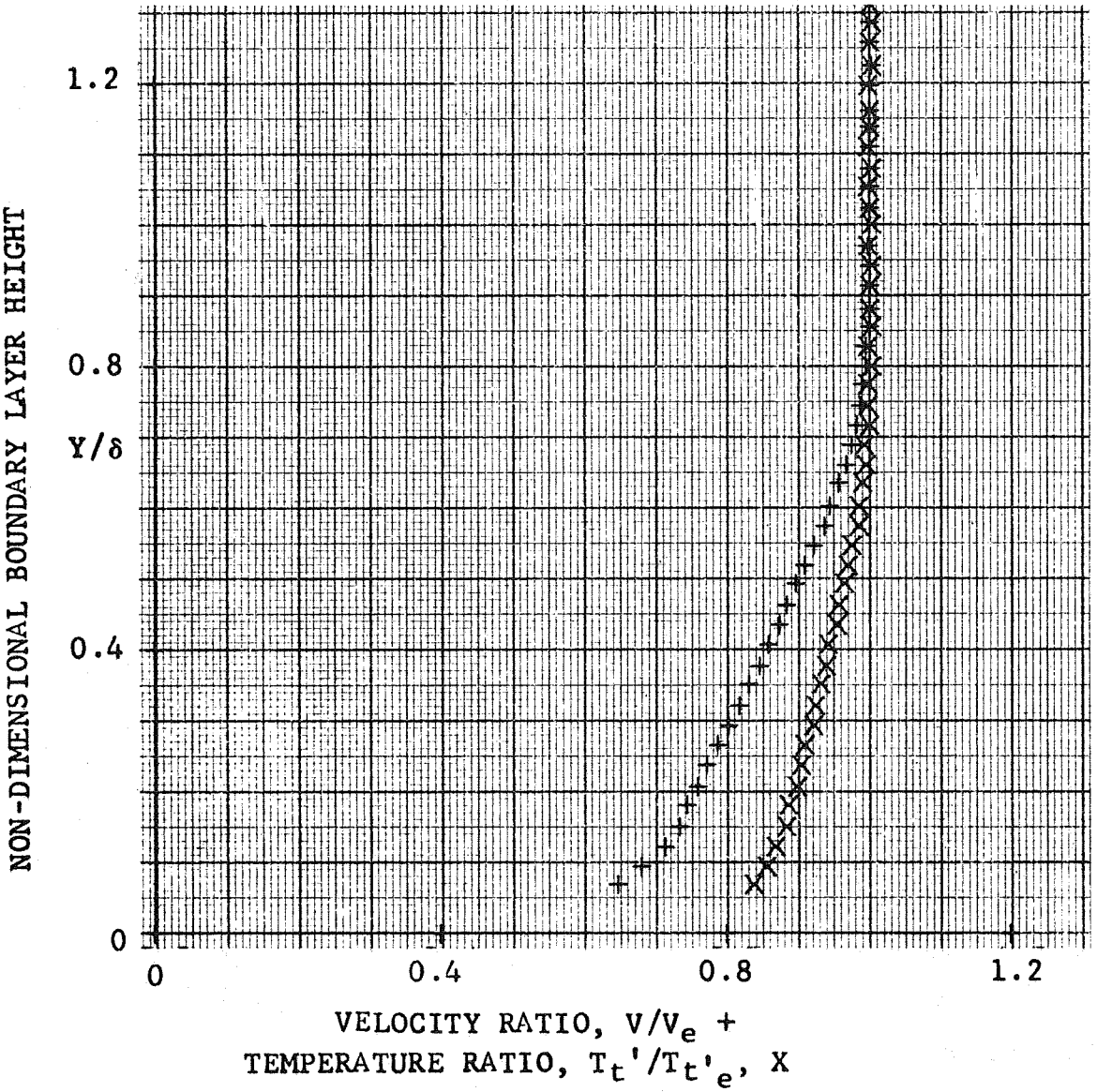

FIGURE37.- NON-DIMENSIONAL VELOCITY AND TEMPERATURE PROFILES (INTERACTION REGION)

M_o 3.18 RE/1 10.3 x 10^6 per ft. RUN 17

T_w/T_{to} 0.31 T_{to} 545 ^oR

Wedge Configuration W_6^5

Probe Station XP(2) = 36.00 inches

δ = 0.450 inches $T_{t'e}$ = 540 ^oR M_e = 2.68

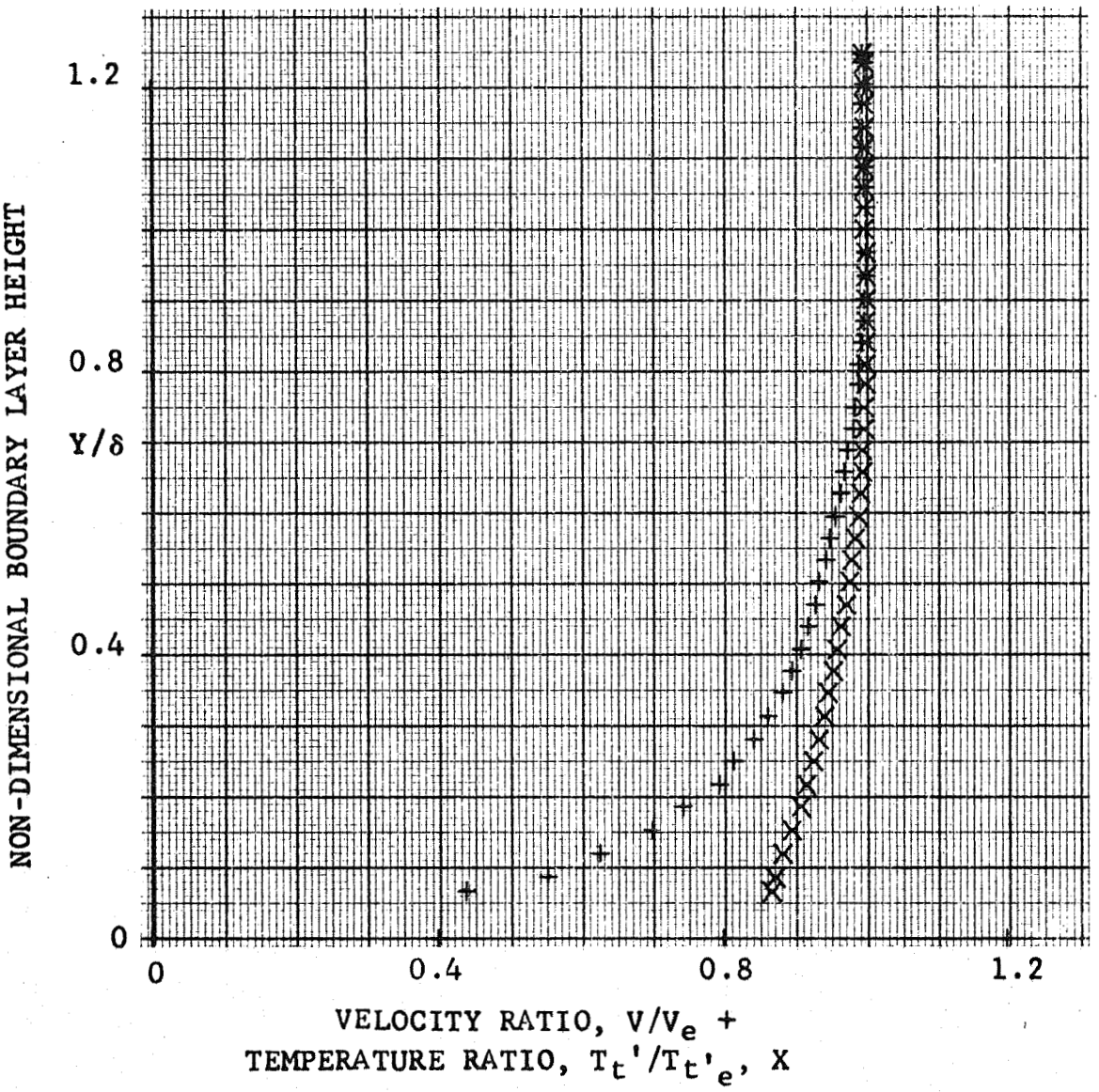

FIGURE 38.- NON-DIMENSIONAL VELOCITY AND TEMPERATURE PROFILES (DOWNSTREAM OF INTERACTION)

M_o 3.18 RE/1 10.3×10^6 per ft. RUN 26

T_w/T_{to} 0.31 T_{to} 544 ^oR

Wedge Configuration W_8^6

Probe Station XP(1) = 31.25 inches

δ = 0.368 inches $T_{t'_e}$ = 537 ^oR M_e = 2.42

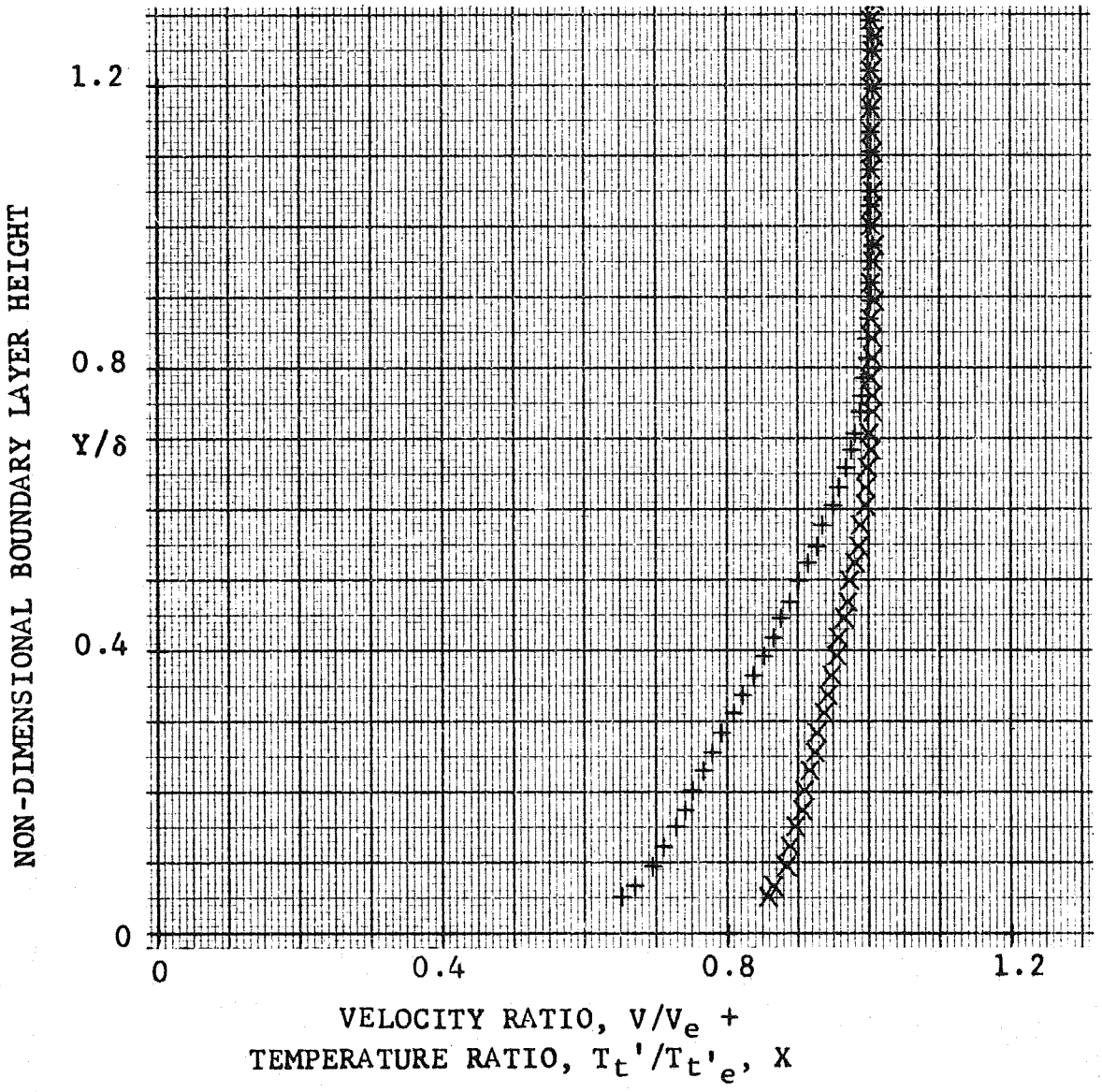

FIGURE 39.- NON-DIMENSIONAL VELOCITY AND TEMPERATURE PROFILES (INTERACTION REGION)

M_o 3.18 RE/1 10.3×10^6 per ft. RUN 18

T_w/T_{to} 0.31 T_{to} 545 ^oR

Wedge Configuration W_8^6

Probe Station XP(2) = 36.00 inches

δ = 0.505 inches $T_{t'_e}$ = 541 ^oR M_e = 2.50

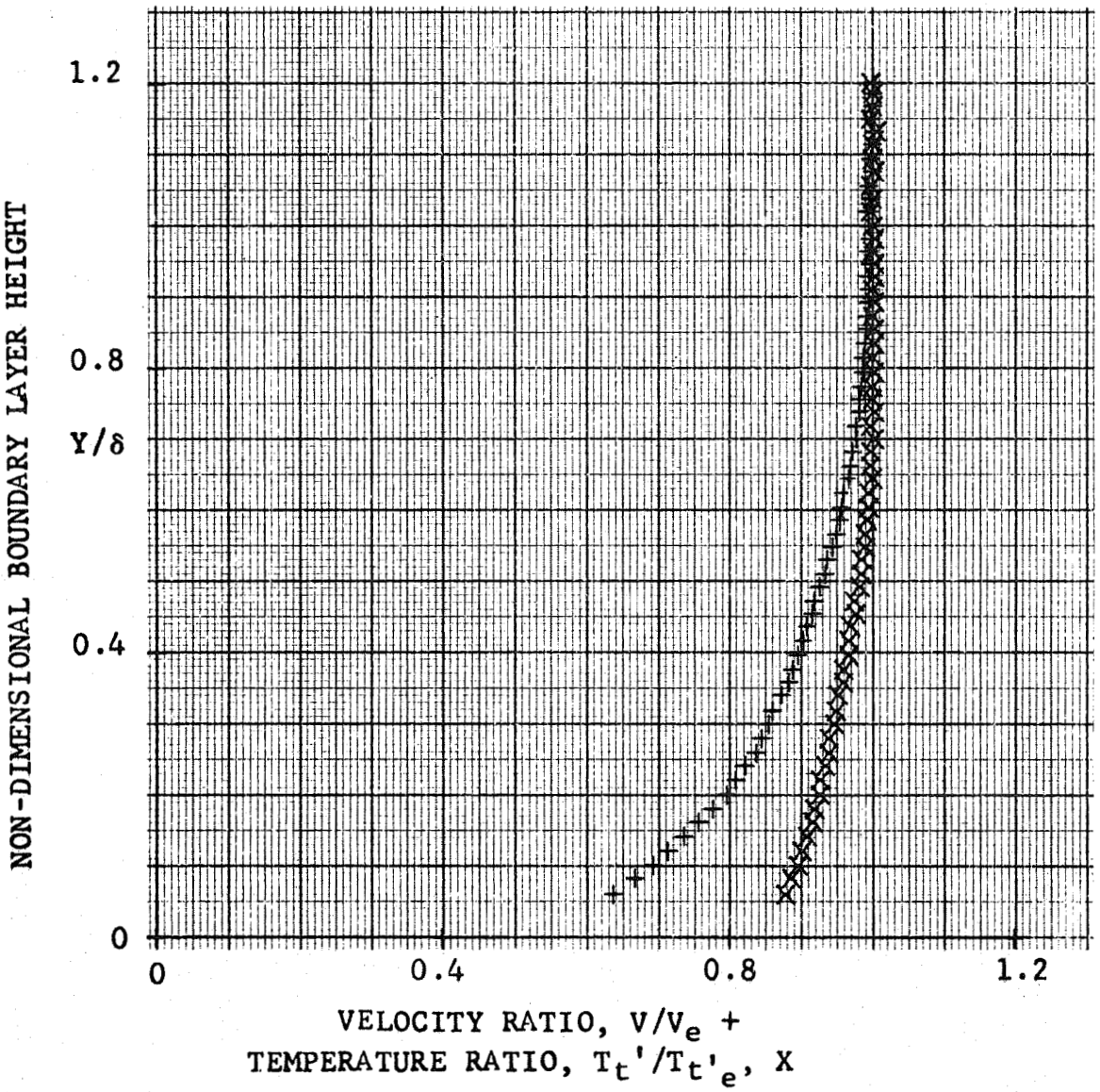

FIGURE 40.- NON-DIMENSIONAL VELOCITY AND TEMPERATURE PROFILES (DOWNSTREAM OF INTERACTION)

M_o 2.01 RE/1 12.2×10^6 per ft. RUN 32

T_w/T_{to} 0.34 T_{to} 524 ^oR

Wedge Configuration W_6^7

Probe Station XP(2) = 36.00inches

δ = 0.528 inches $T_t'_e$ = 521 ^oR M_e = 1.58

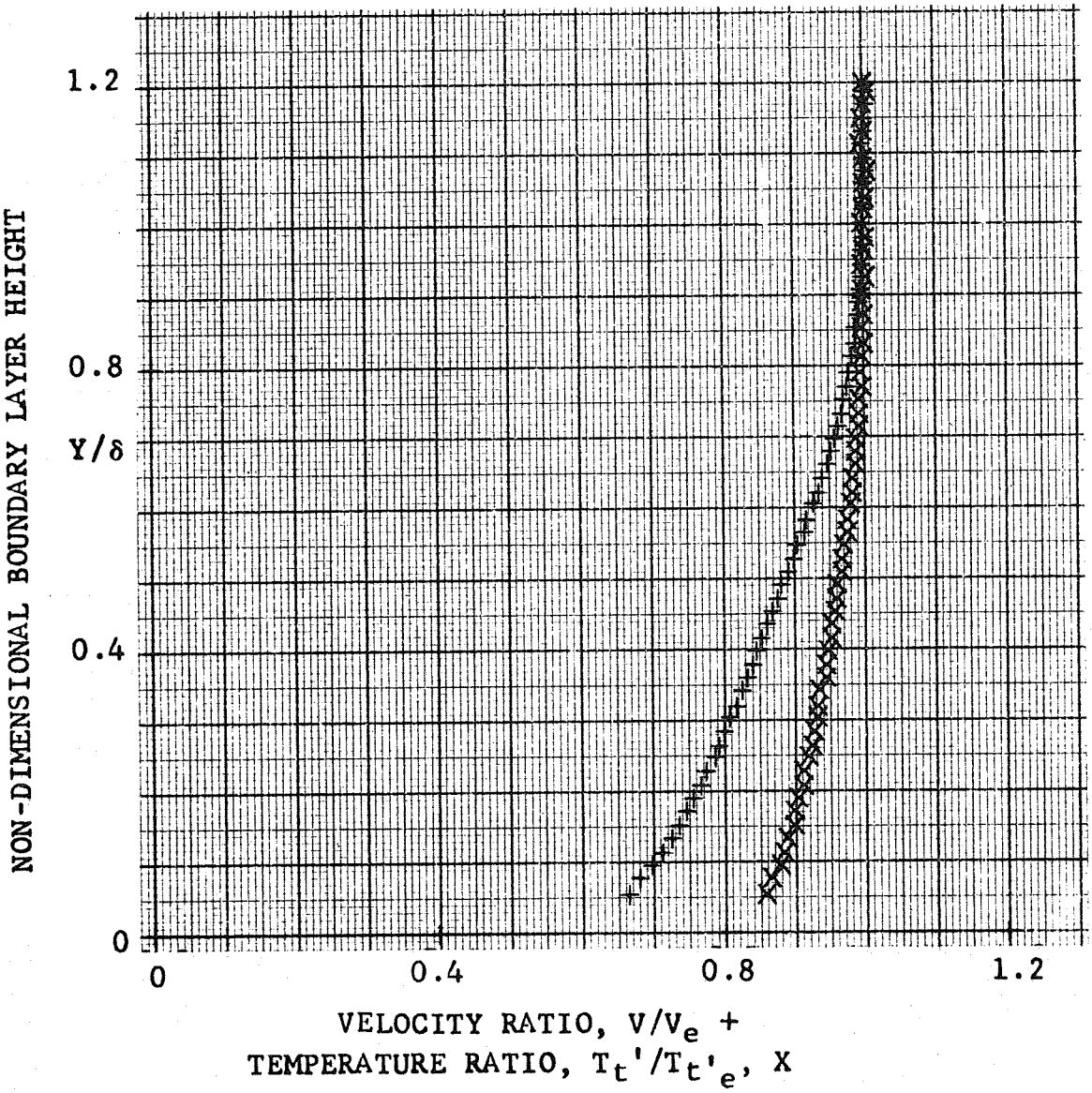

FIGURE 41.- NON-DIMENSIONAL VELOCITY AND TEMPERATURE PROFILES (DOWNSTREAM OF INTERACTION)

M_o 2.01 RE/1 12.2×10^6 per ft. RUN 36

T_w/T_{to} 0.34 T_{to} 528 ^oR

Wedge Configuration W_8^8

Probe Station XP(2) = 36.00 inches

δ = 0.613 inches $T_{t'_e}$ = 526 ^oR M_e = 1.41

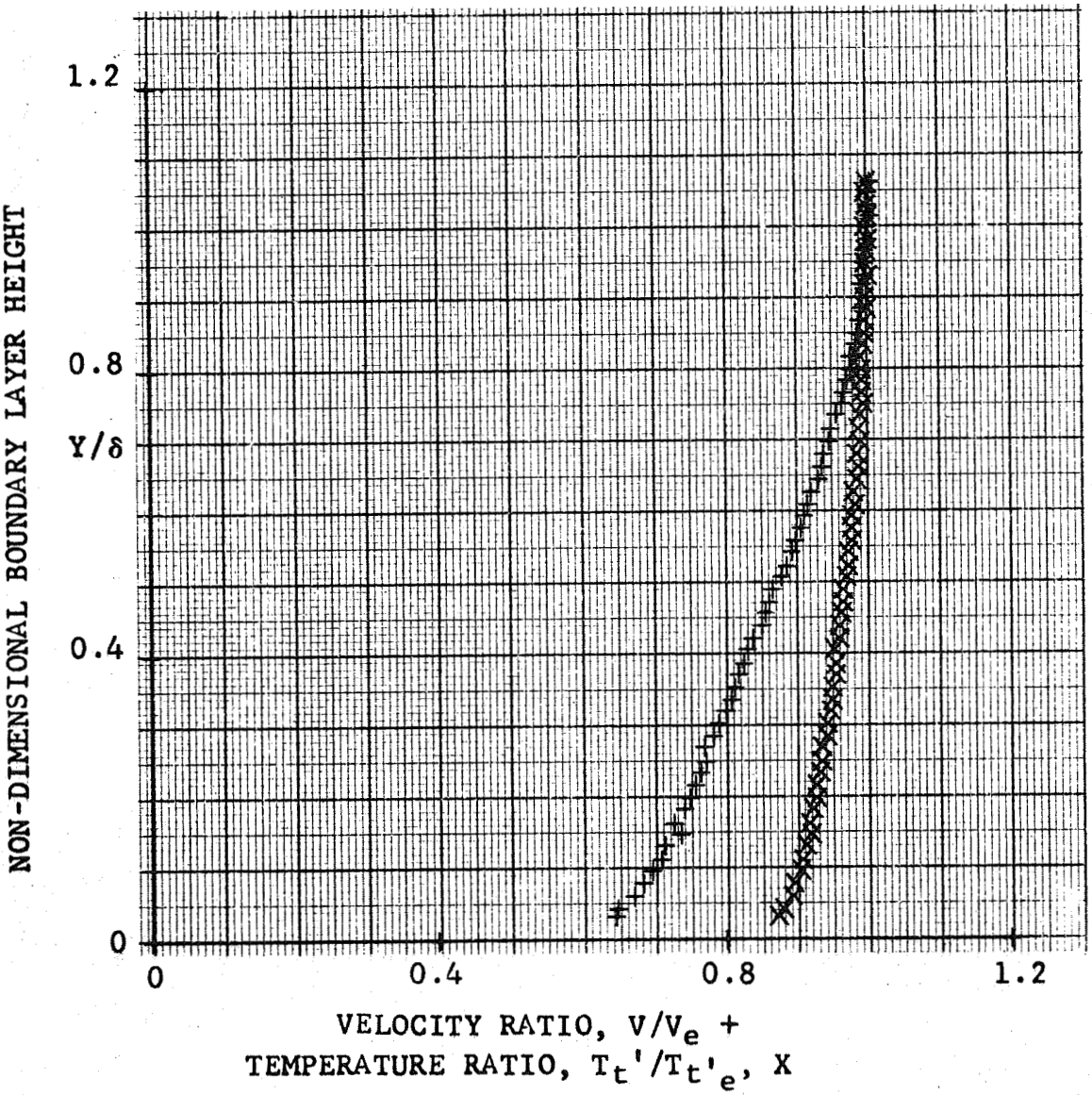

FIGURE 42.- NON-DIMENSIONAL VELOCITY AND TEMPERATURE PROFILES (DOWNSTREAM OF INTERACTION)

M_o 2.01 RE/1 6.4×10^6 per ft. RUN 33

T_w/T_{to} 0.32 T_{to} 537 ^oR

Wedge Configuration W_6^7

Probe Station XP(2) = 36.00 inches

δ = 0.532 inches $T_{t'_e}$ = 553 ^oR M_e = 1.57

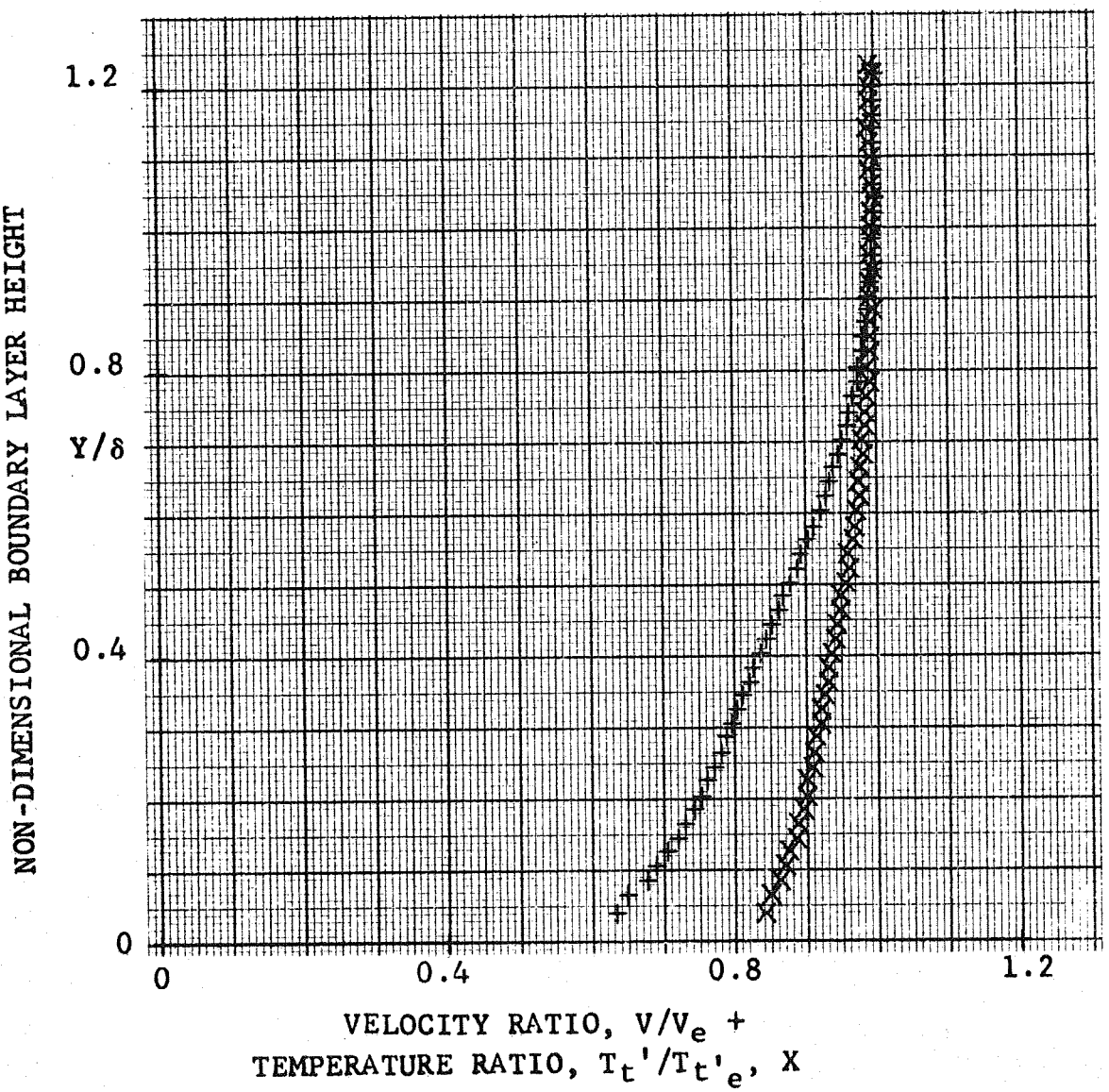

FIGURE 43.- NON-DIMENSIONAL VELOCITY AND TEMPERATURE PROFILES (DOWNSTREAM OF INTERACTION)

M_o 2.01 RE/1 6.4×10^6 per ft. RUN 34

T_w/T_{to} 0;32 T_{to} 529 ^oR

Wedge Configuration W_8^8

Probe Station XP(2) = 36.00 inches

$\delta = 0.620$ inches $T_{t'_e} = 522\ ^oR$ $M_e = 1.39$

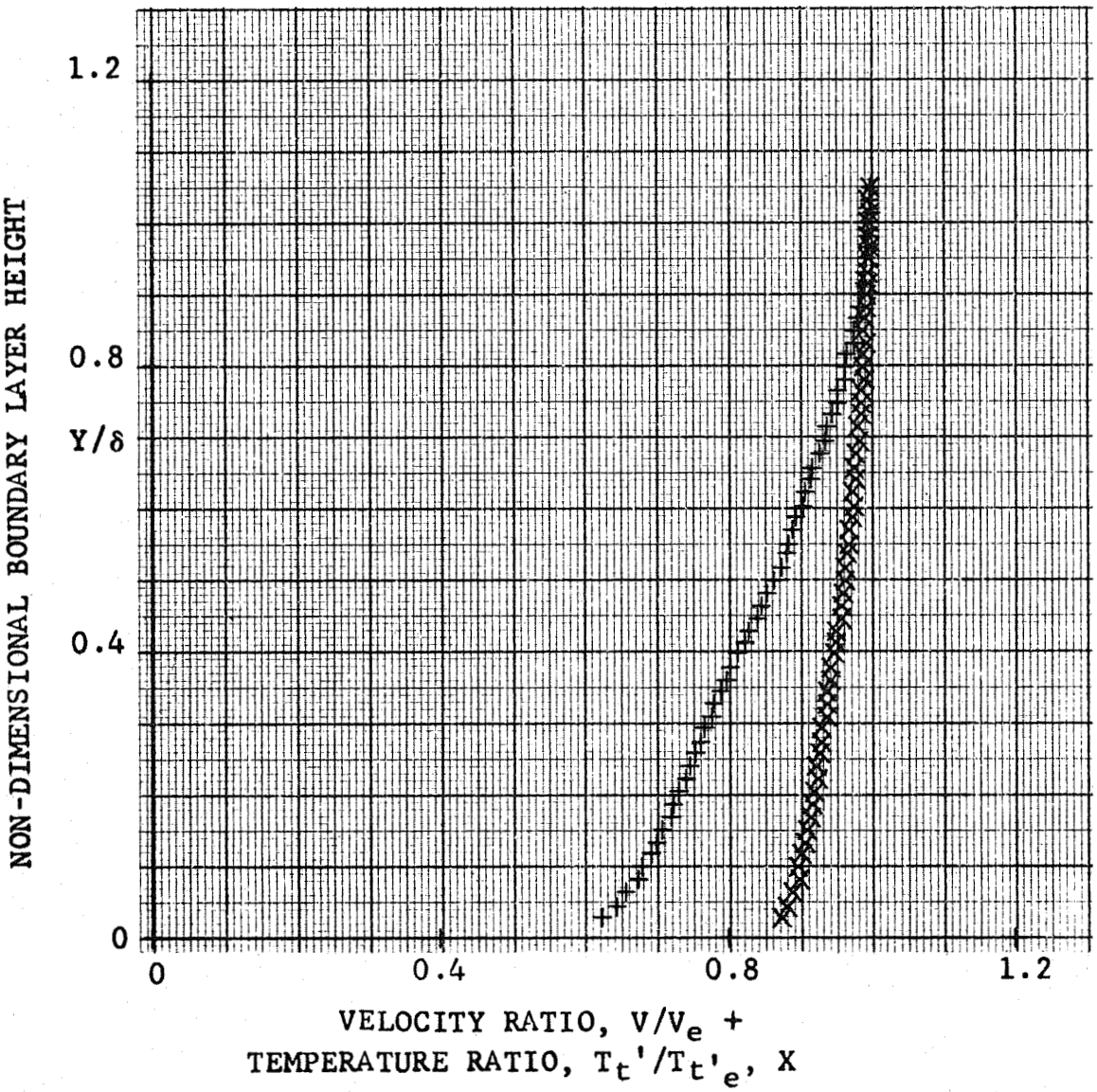

FIGURE 44.- NON-DIMENSIONAL VELOCITY AND TEMPERATURE PROFILES (DOWNSTREAM OF INTERACTION)

M_o 4.2 RE/1 20.2 x 10^6 per ft. RUN 43

T_w/T_{to} 0.32 T_{to} 529 ^oR

Wedge Configuration W_8^3

Probe Station XP(2) = 33.00 inches

δ = 0.268 inches $T_{t'e}$ = 504 ^oR M_e = 3.08

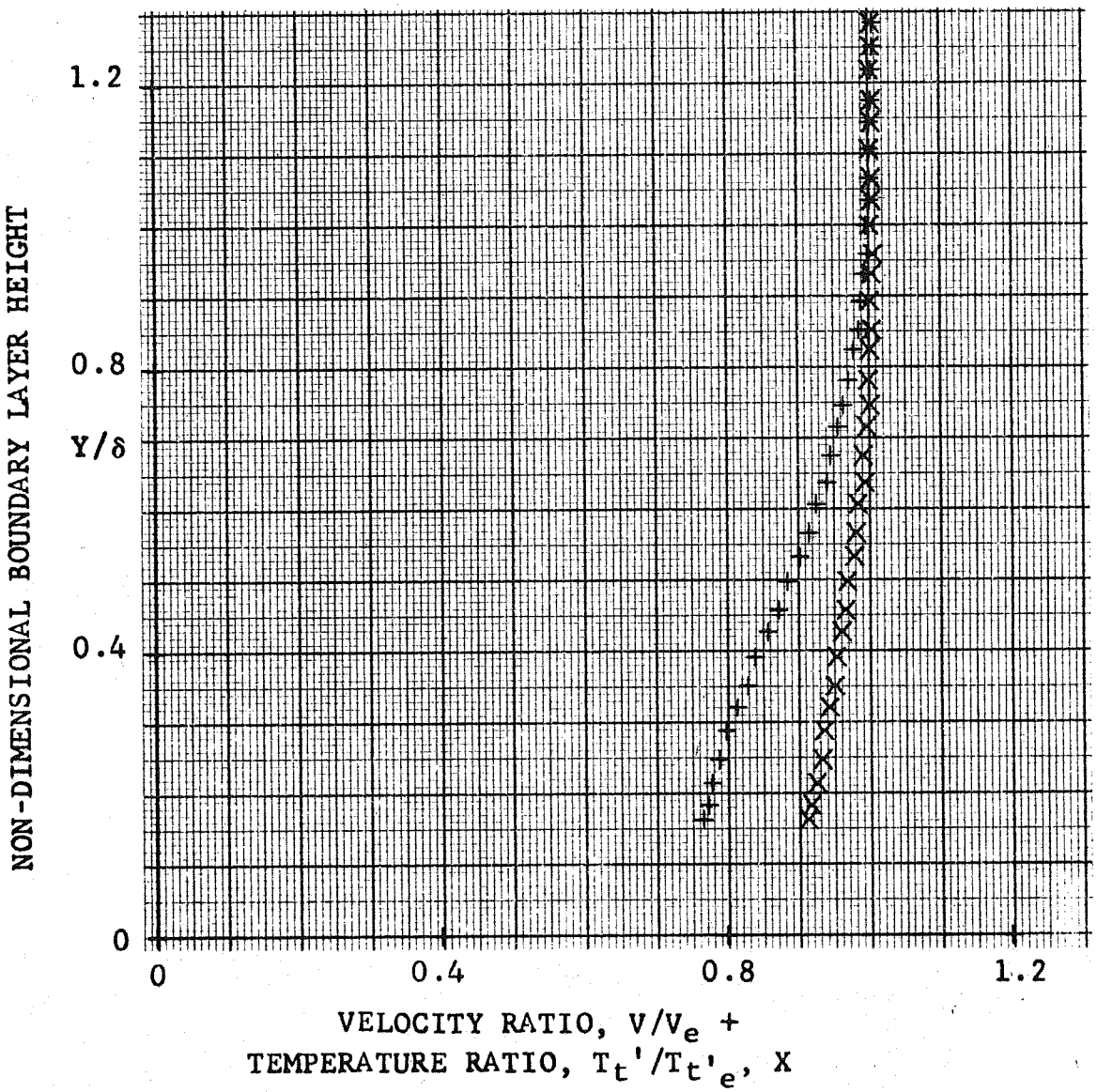

FIGURE 45.- NON-DIMENSIONAL VELOCITY AND TEMPERATURE PROFILES (DOWNSTREAM OF INTERACTION)

M_o 4.2 RE/1 14.5 x 10^6 per ft. RUN 46

T_w/T_{to} 0.32 T_{to} 523 ^oR

Wedge Configuration W_6^2

Probe Station XP(2) = 33.00 inches

δ = 0.361 inches $T_t'_e$ = 505 ^oR M_e = 3.46

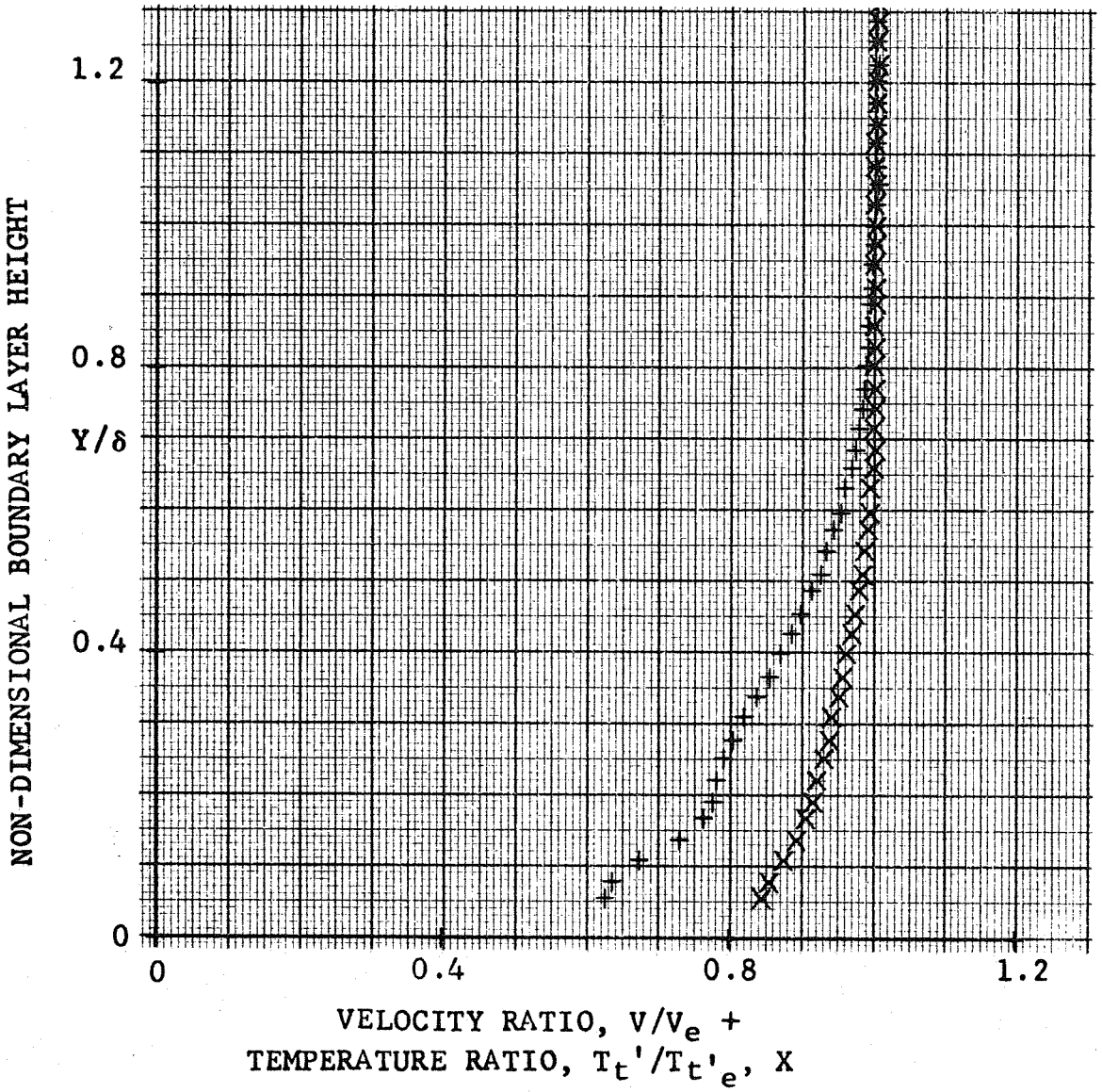

FIGURE 46.- NON-DIMENSIONAL VELOCITY AND TEMPERATURE PROFILES (DOWNSTREAM OF INTERACTION)

M_o 4.2 RE/1 14.5 x 10^6 per ft. RUN 44

T_w/T_{to} 0.32 T_{to} 531 ^oR

Wedge Configuration $W_8{}^3$

Probe Station XP(2) = 33.00 inches

δ = 0.313 inches $T_{t'_e}$ = 516 ^oR M_e = 3.15

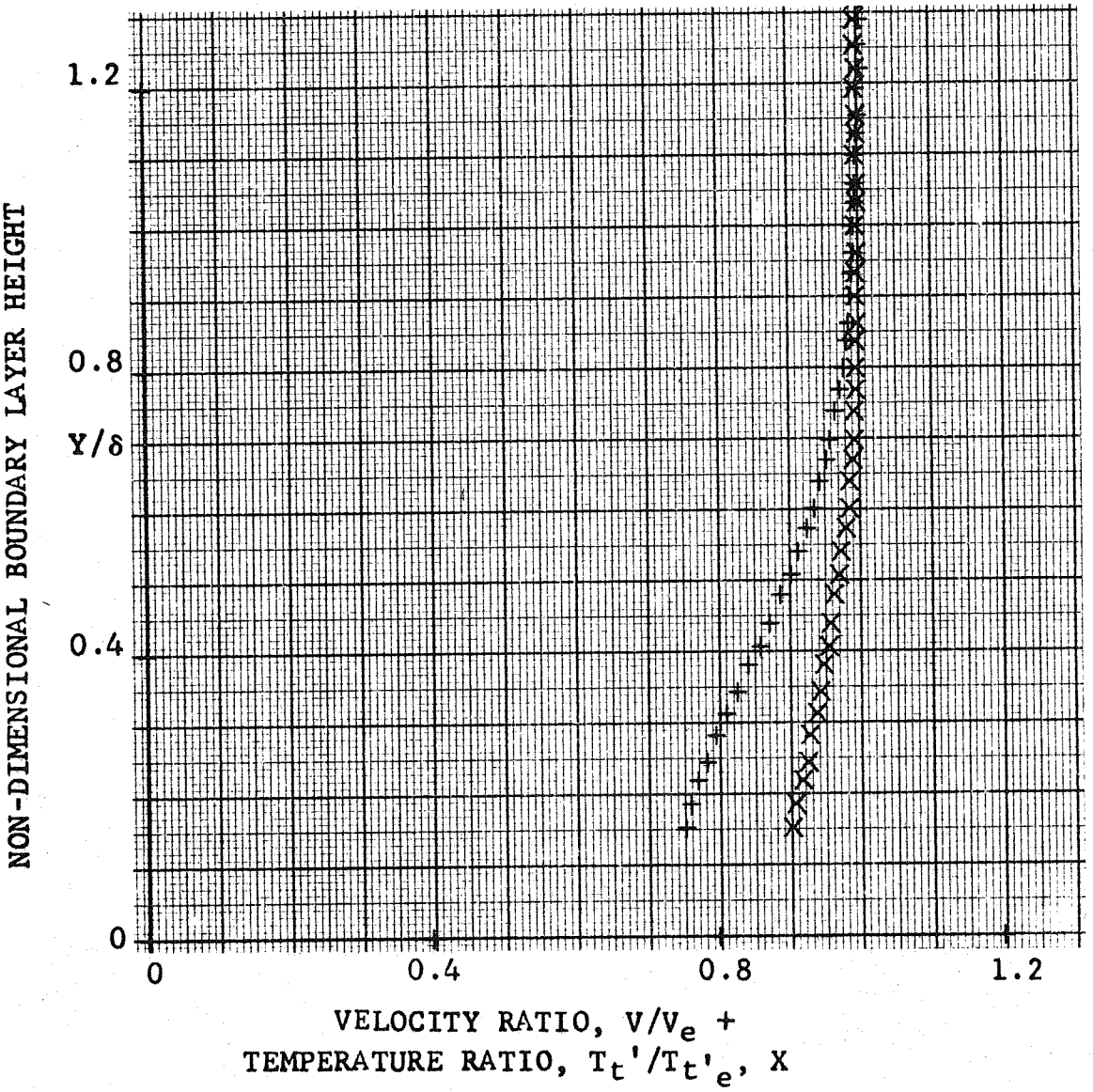

FIGURE 47.- NON-DIMENSIONAL VELOCITY AND TEMPERATURE PROFILES (DOWNSTREAM OF INTERACTION)